Supplementary Information (SI) for Sustainable Energy & Fuels.
This journal is © The Royal Society of Chemistry 2026

## Supporting Information for

# Decarbonization pathways for liquid fuels: A multi-sector energy system perspective

Jun Wen Law[1], Bryan K. Mignone[2], Dharik S. Mallapragada[3*]

1. MIT Energy Initiative, Massachusetts Institute of Technology, Cambridge, MA 02139

2. ExxonMobil Technology and Engineering Company, Annandale, NJ 08801

3. Chemical and Biomolecular Engineering Department, Tandon School of Engineering, New York University, Brooklyn, NY 11201

*Correspondence: Dharik S. Mallapragada

**Email:** dharik.mallapragada@nyu.edu

**Keywords:** Multi-sector optimization; Sector-coupling; Biofuels; Synthetic fuels; Carbon capture and utilization; Biomass availability

**Summary:** This supporting information contains 74 pages, 37 figures, 48 tables, and 51 equations.

## Table of Contents

## S1. Additional results

### S1.1 Default case scenario sets

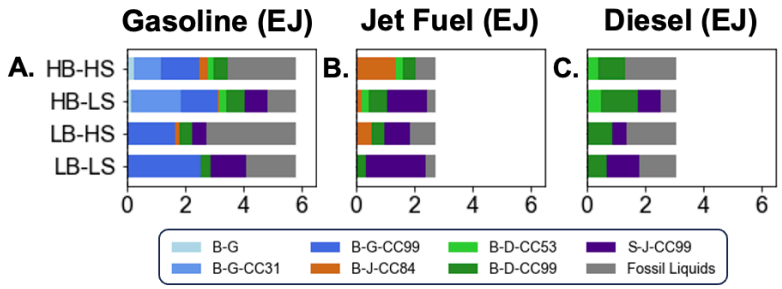


Figure S1. A) Gasoline production pathways, B) Jet fuel production pathways, and C) Diesel production pathways across the core scenarios as described in Figure 3A under default "IA-PF" modeling assumptions as described in Figure 3B, and default demand distribution in Figure 2A. Liquid fuels production technology labels follow Table 1.

Table S1. $CO_2$ marginal abatement cost (defined as the dual value of the $CO_2$ emission policy constraint as described in Eq. S51 in Section S5.5), and total levelized system cost (defined as total system cost divided by total exogenous energy demand of 11385 TWh) of core scenarios described in Figure 3A of the main text, under default "IA-PF" modeling assumptions as described in Figure 3B, and default demand distribution as described in Figure 2A.

| Scenarios | HB-HS | HB-LS | LB-HS | LB-LS |
|---|---|---|---|---|
| $CO_2$ marginal abatement cost ($/tonne) | 119.23 | 298.56 | 548.48 | 663.55 |
| Total levelized system cost ($/MWh) | 57.96 | 62.14 | 67.89 | 75.29 |

Table S2. Disposition of atmospheric $CO_2$ uptake, which includes biomass $CO_2$ content and $CO_2$ captured from DAC across core scenarios described in Figure 3A, under default "IA-PF" modeling assumptions as described in Figure 3B, and default demand distribution as described in Figure 2A. Converted to fuels = carbon content in biofuels and synthetic fuels, sequestered = percentage of atmospheric carbon that is captured and sequestered in geological storage, emitted = carbon vented in biofuel processes as a result of lower $CO_2$ capture (CC) rates.

| Scenarios | HB-HS | HB-LS | LB-HS | LB-LS |
|---|---|---|---|---|
| Converted to fuels (%) | 33% | 49% | 32% | 63% |
| Sequestered (%) | 51% | 30% | 66% | 36% |
| Emitted (%) | 16% | 21% | 2% | 1% |

Table S3. System average fuel production costs calculated using commodity shadow prices of energy system results, (detailed method described in Section S2.1) across the core scenarios as described in Figure 3A, under default "IA-PF" modeling assumptions as described in Figure 3B, and default demand distribution as described in Figure 2A. Liquid fuels production technology labels follow Table 1.

| Fuel production cost ($/GJ) | B-G | B-G-CC31 | B-G-CC99 | B-D | B-D-CC53 | B-D-CC99 | B-J-CC75 | B-J-CC84 | B-J-CC99 | S-J | S-J-CC99 |
|---|---|---|---|---|---|---|---|---|---|---|---|
| HB-HS | 38.76 | 37.34 | 36.48 | 42.29 | 38.53 | 38.29 | 42.21 | 34.54 | 40.93 | 43.15 | 42.44 |
| HB-LS | 53.75 | 52.22 | 51.63 | 54.88 | 50.97 | 50.86 | 58.81 | 47.41 | 57.55 | 46.29 | 45.70 |
| LB-HS | 126.06 | 106.94 | 67.66 | 109.25 | 85.55 | 67.94 | 91.56 | 71.44 | 73.34 | 87.47 | 64.94 |
| LB-LS | 141.54 | 120.18 | 76.25 | 121.69 | 95.46 | 75.76 | 102.62 | 79.92 | 82.30 | 95.03 | 69.74 |

## S1.2 Equal demand distribution case (E-D)

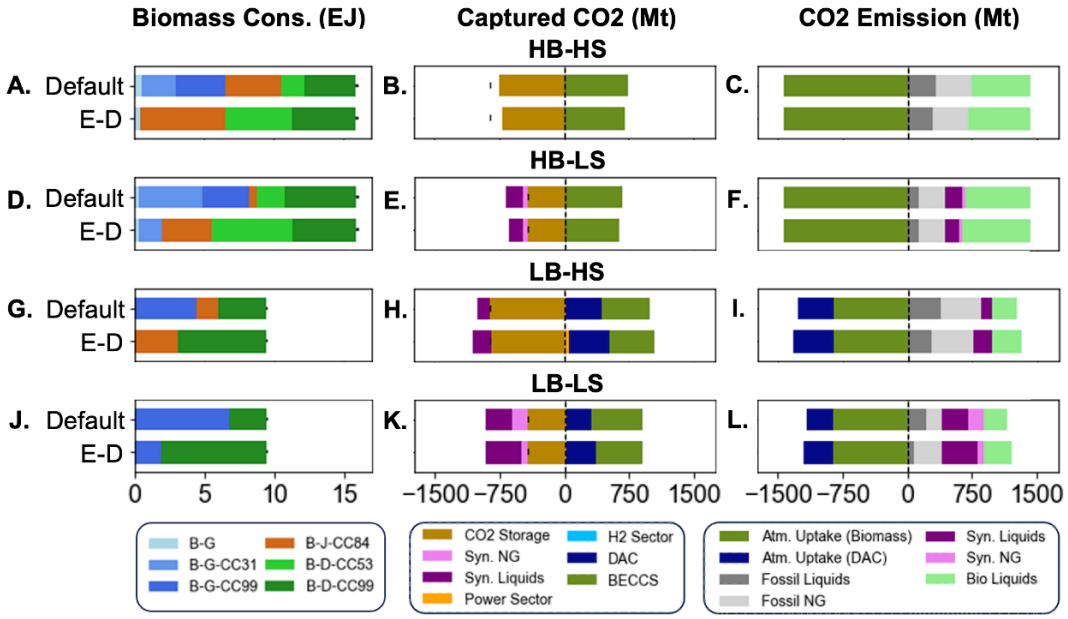


Figure S2. Biomass consumption by technologies (Panels A, D, G, J), captured $CO_2$ balance (Panels B, E, H, K), and $CO_2$ emission balance (Panels C, F, I, L) results across the core scenarios as described in Figure 3A under default "IA-PF" modeling assumptions as described in Figure 3B, and both default and "E-D" demand distribution as described in Figure 2A. Liquid fuels production technology labels follow Table 1. The resource limit of biomass and $CO_2$ sequestration are indicated by the bars in their respective plots.

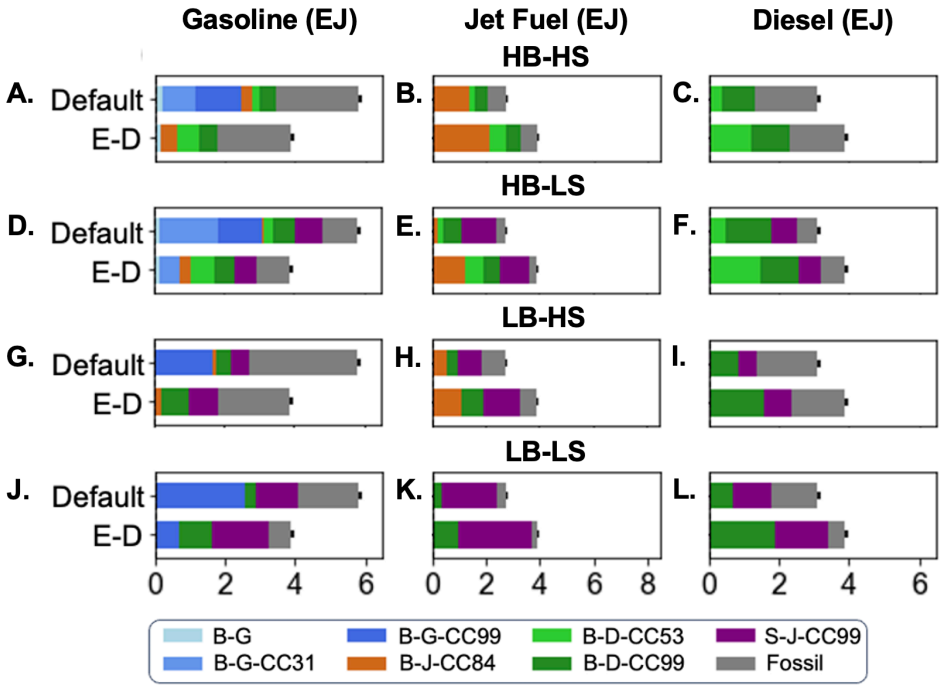


Figure S3. Gasoline, jet fuel, and diesel production pathways across the core scenarios as described in Figure 3A under default "IA-PF" modeling assumptions as described in Figure 3B, and both default and "E-D" demand distribution as described in Figure 2A. Liquid fuels production technology labels follow Table 1.

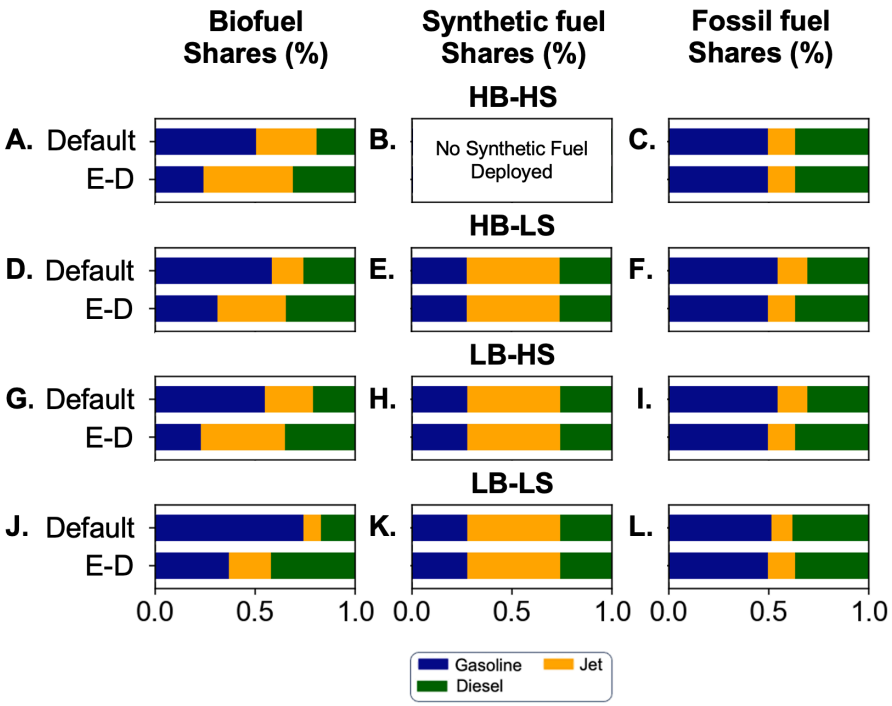


Figure S4. Shares of gasoline, jet fuel, and diesel within total biofuel, synthetic fuel, and fossil fuel production across the core scenarios as described in Figure 3A under default "IA-PF" modeling assumptions as described in Figure 3B, and both default and "E-D" demand distribution as described in Figure 2A. Liquid fuels production technology labels follow Table 1.

Table S4. Disposition of atmospheric carbon uptake from biofuel processes and direct air capture across the core scenarios as described in Figure 3A under default "IA-PF" modeling assumptions as described in Figure 3B, and "E-D" demand distribution as described in Figure 2A.

| E-D scenarios | HB-HS | HB-LS | LB-HS | LB-LS |
|---|---|---|---|---|
| Converted to fuels (%) | 36% | 49% | 39% | 65% |
| Sequestered (%) | 49% | 30% | 58% | 34% |
| Emitted (%) | 15% | 20% | 3% | 1% |

## Shadow prices comparison

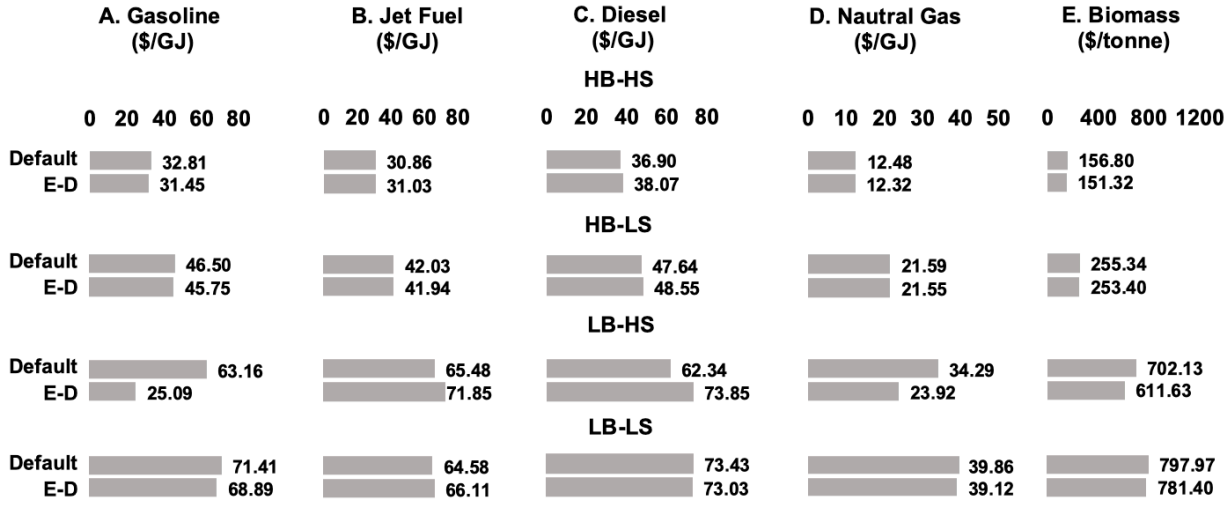


Figure S5. System average shadow prices for A) gasoline, B) jet fuel, C) diesel, D) natural gas, and E) biomass across the core scenarios as described in Figure 3A under default "IA-PF" modeling assumptions as described in Figure 3B, and both default and "E-D" demand distribution as described in Figure 2A. Shadow prices of commodities represent the dual value of the supply-balance constraints of the respective commodities in MACRO, and system average shadow prices are calculated according to Eq. S1 in Section S2.1.

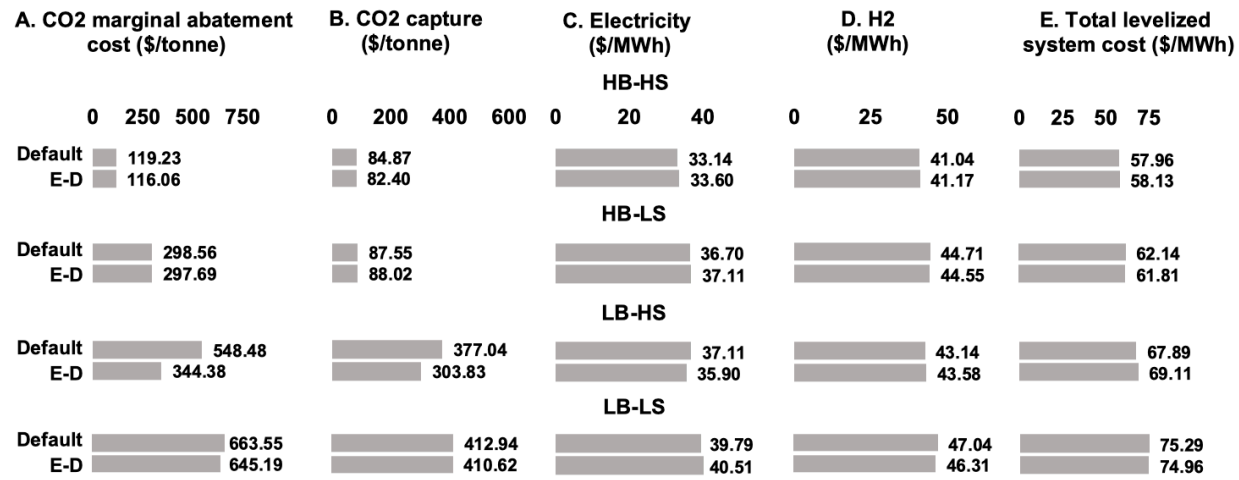


Figure S6. A) $CO_2$ marginal abatement cost, B) system average $CO_2$ capture price, C) system average electricity shadow price, D) system average H2 shadow price, E) Total levelized system cost across the core scenarios as described in Figure 3A under default "IA-PF" modeling assumptions as described in Figure 3B, and both default and "E-D" demand distribution as described in Figure 2A. Shadow prices of commodities represent the dual value of the supply-balance constraints of the respective commodities in MACRO, and system average shadow prices are calculated according to Eq. S1 in Section S2.1. $CO_2$ marginal abatement cost = dual value of the $CO_2$ emission policy constraint as described in Eq. S51 in Section S5.5. System average $CO_2$ capture price = $CO_2$ marginal abatement cost – system average dual value of the captured $CO_2$ balance constraint. This represents the value of avoided $CO_2$ emission, which is cost of utilization and sequestration of captured $CO_2$. Total levelized system cost = total system cost divided by total exogenous energy demand of 11385 TWh.

## S1.3 Other flexibility assumption cases (Default demand distribution)

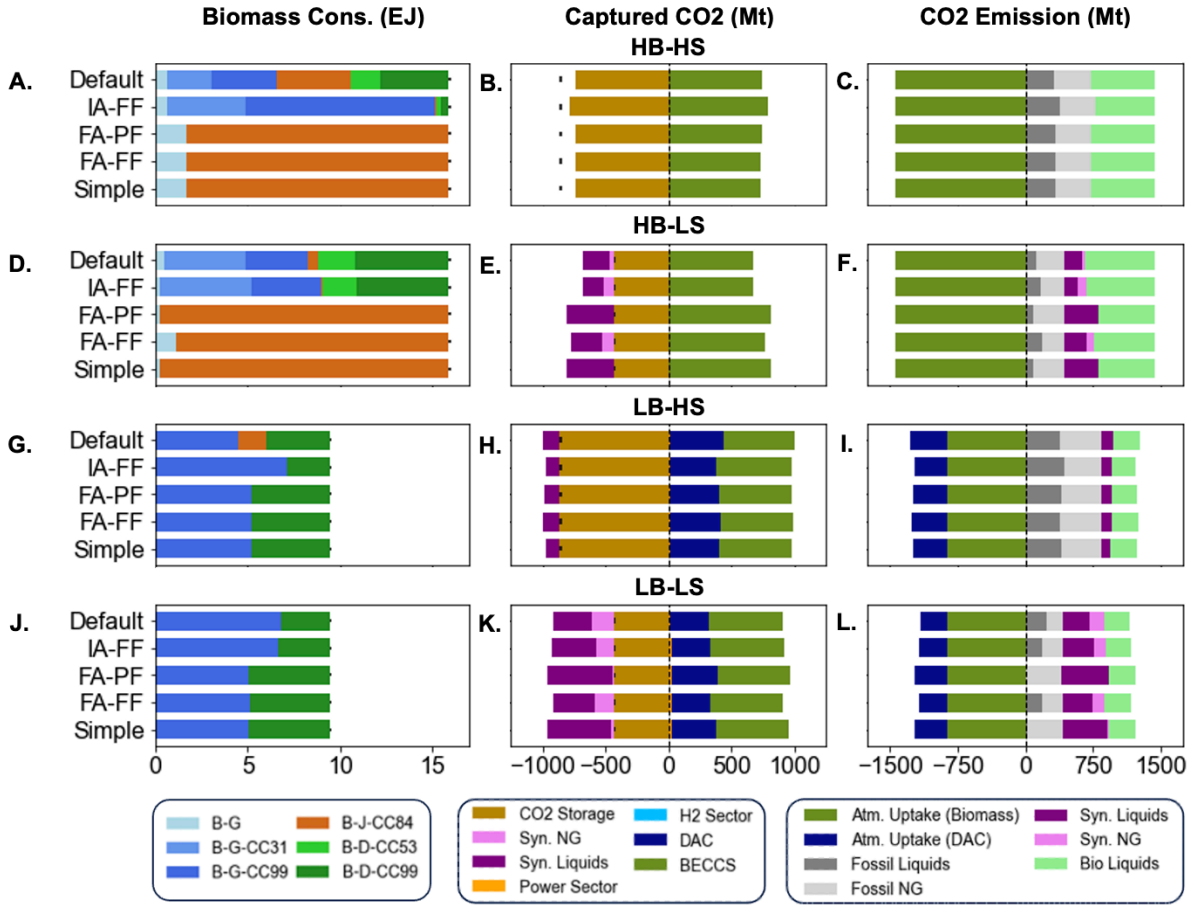


Figure S7. Effect of liquid fuel flexibility modeling assumptions on biomass consumption by technologies (Panels A, D, G, J), captured CO2 balance (Panels B, E, H, K), and CO2 emission balance (Panels C, F, I, L) across the core scenarios as described in Figure 3A, under default demand distribution as described in Figure 2A. Each row compares the five flexibility modeling assumptions as described in Figure 3B. Liquid fuels production technology labels follow Table 1, and the resource limit of biomass and CO2 sequestration are indicated by the bars in their respective plots.

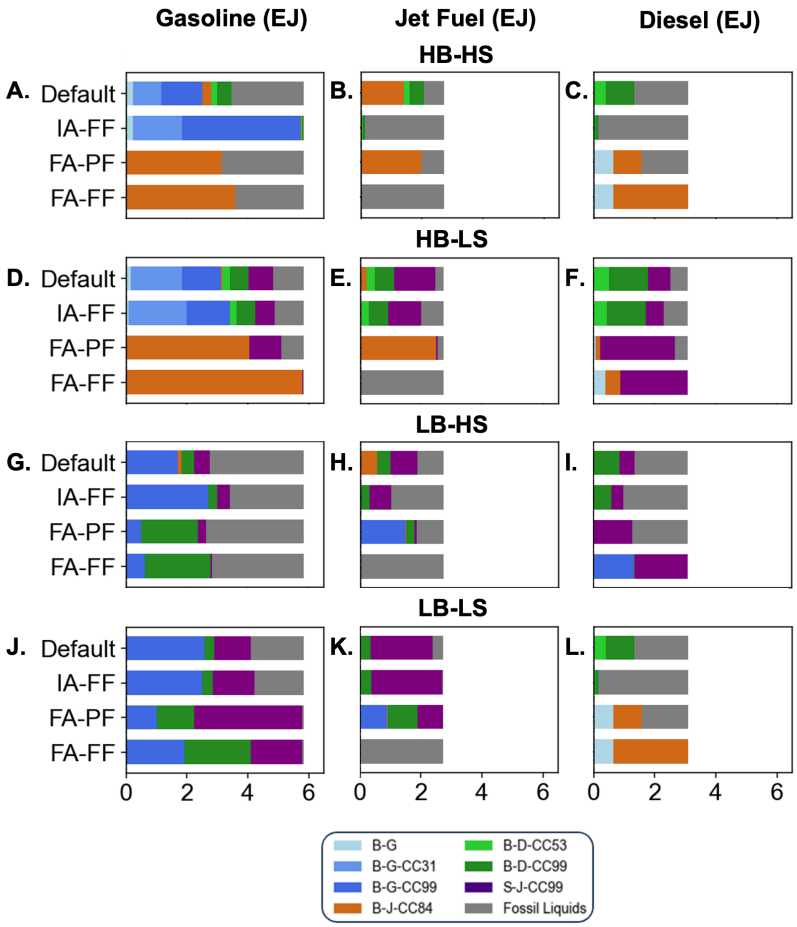


Figure S8. Effect of liquid fuel flexibility modeling assumptions on gasoline, jet fuel, and diesel production pathways across the core scenarios as described in Figure 3A, under default demand distribution as described in Figure 2A. Each row compares the five flexibility modeling assumptions as described in Figure 3B. Liquid fuels production technology labels follow Table 1.

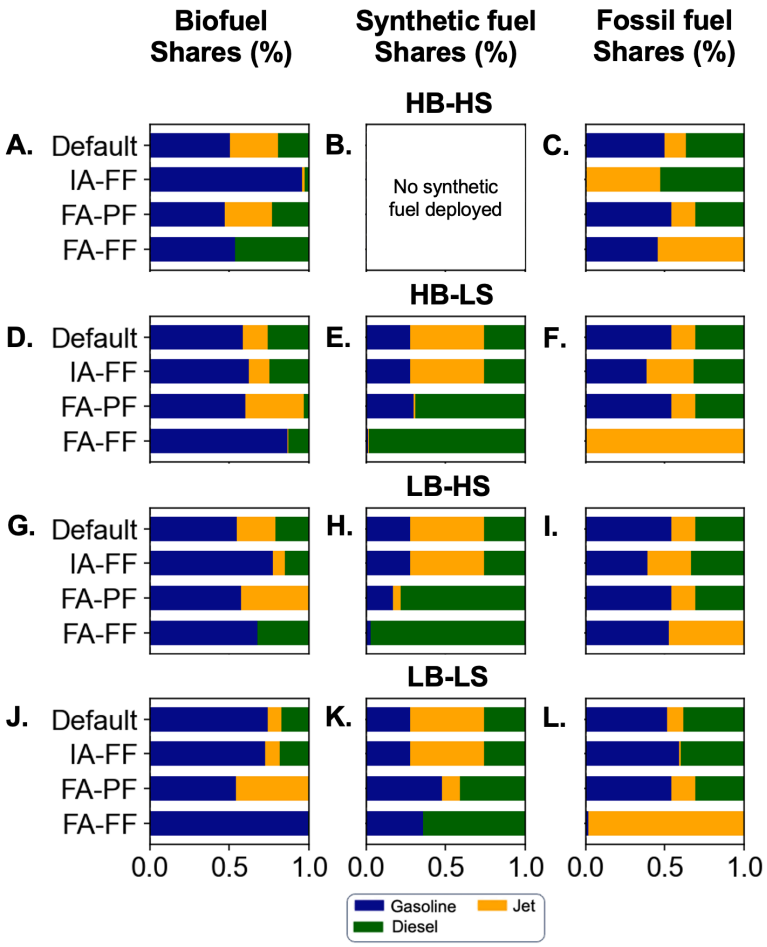


Figure S9. Shares of gasoline, jet fuel, and diesel within total biofuel, synthetic fuel, and fossil fuel production across the core scenarios as described in Figure 3A, under default demand distribution as described in Figure 2A. Each row compares the five flexibility modeling assumptions as described in Figure 3B. Liquid fuels production technology labels follow Table 1.

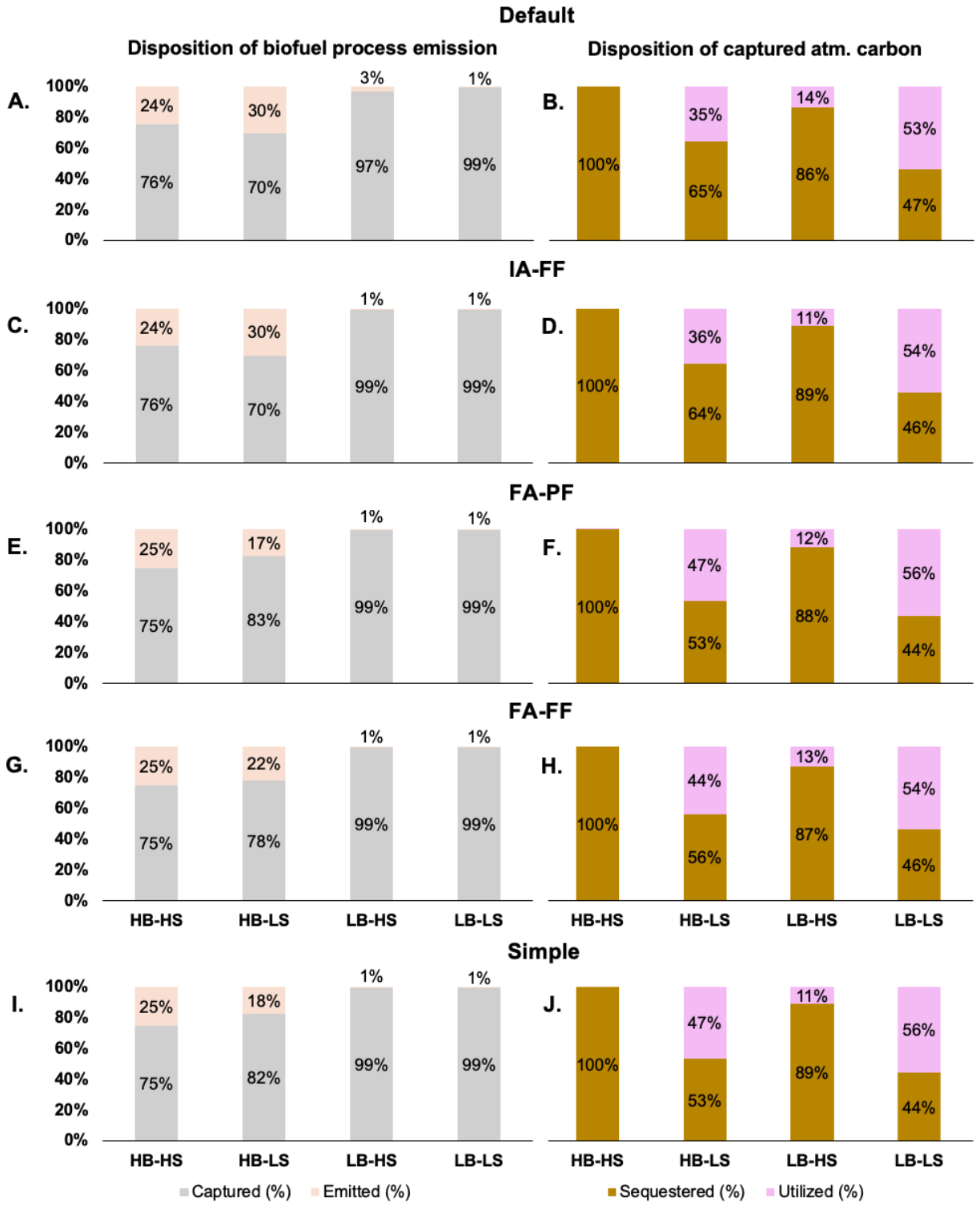


Figure S10. A,C,E,G,I) Disposition of biofuel production carbon emissions (excludes the carbon content in biofuel products), B,D,F,H,J) Disposition of captured atmospheric carbon from biofuel processes and direct air capture across the core scenarios described in Figure 3A under default demand distribution as described in Figure 2A, for the five flexibility modeling assumptions as described in Figure 3B: "Default" (Panels A,B), "IA-FF" (Panels C,D), "FA-PF" (Panels E,F), "FA-FF" (Panels G,H), "Simple" (Panels I,J).

Table S5. Disposition of atmospheric carbon uptake from biofuel processes and direct air capture across the core scenarios as described in Figure 3A under “IA-FF” modeling assumptions as described in Figure 3B, and default demand distribution as described in Figure 2A.

| IA-FF scenarios | HB-HS | HB-LS | LB-HS | LB-LS |
|---|---|---|---|---|
| Converted to fuels (%) | 29% | 49% | 30% | 64% |
| Sequestered (%) | 54% | 30% | 70% | 35% |
| Emitted (%) | 17% | 21% | 0% | 1% |

Table S6. Disposition of atmospheric carbon uptake from biofuel processes and direct air capture across the core scenarios as described in Figure 3A under “FA-PF” modeling assumptions as described in Figure 3B, and default demand distribution as described in Figure 2A.

| FA-PF scenarios | HB-HS | HB-LS | LB-HS | LB-LS |
|---|---|---|---|---|
| Converted to fuels (%) | 32% | 49% | 32% | 66% |
| Sequestered (%) | 51% | 30% | 68% | 34% |
| Emitted (%) | 17% | 21% | 0% | 1% |

Table S7. Disposition of atmospheric carbon uptake from biofuel processes and direct air capture across the core scenarios as described in Figure 3A under “FA-FF” modeling assumptions as described in Figure 3B, and default demand distribution as described in Figure 2A.

| FA-FF scenarios | HB-HS | HB-LS | LB-HS | LB-LS |
|---|---|---|---|---|
| Converted to fuels (%) | 32% | 48% | 32% | 64% |
| Sequestered (%) | 51% | 30% | 67% | 35% |
| Emitted (%) | 17% | 22% | 0% | 1% |

Table S8. Disposition of atmospheric carbon uptake from biofuel processes and direct air capture across the core scenarios as described in Figure 3A under “Simple” modeling assumptions as described in Figure 3B, and default demand distribution as described in Figure 2A.

| Simple model scenarios | HB-HS | HB-LS | LB-HS | LB-LS |
|---|---|---|---|---|
| Converted to fuels (%) | 32% | 49% | 31% | 65% |
| Sequestered (%) | 51% | 30% | 68% | 34% |
| Emitted (%) | 17% | 21% | 0% | 1% |

## Shadow prices comparison

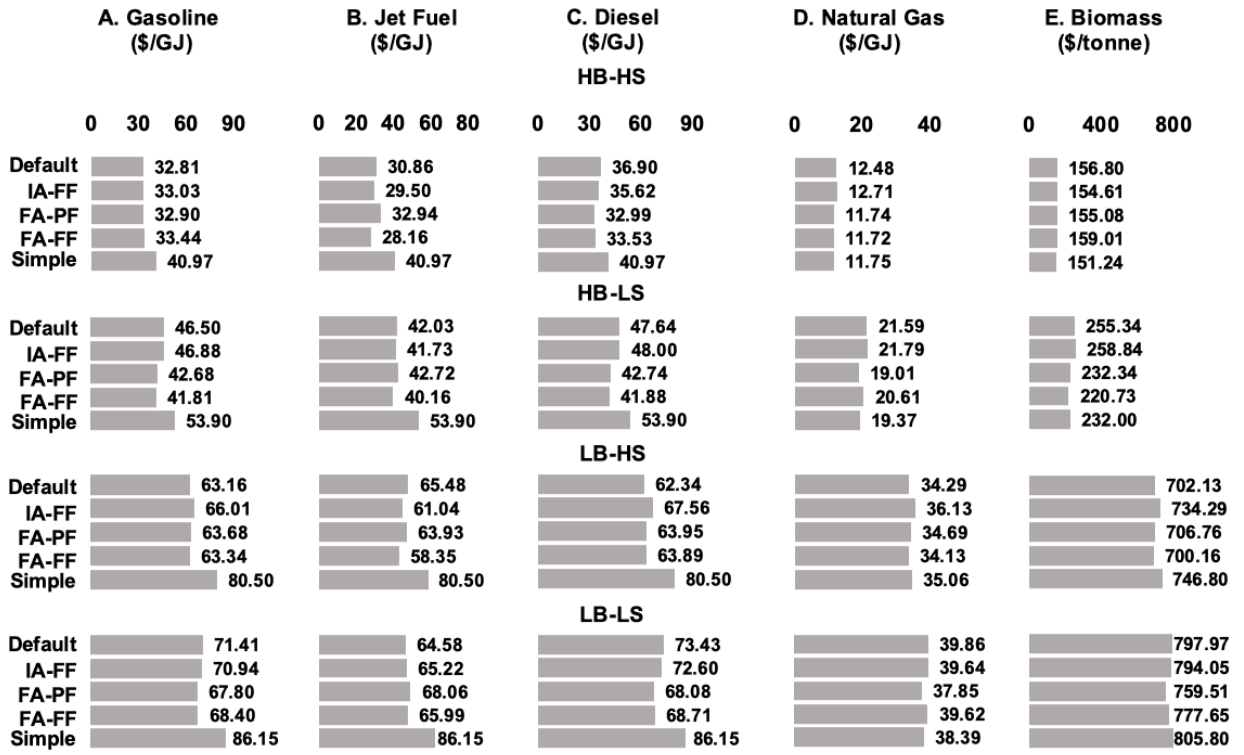


Figure S11. System average shadow prices for A) gasoline, B) jet fuel, C) diesel, D) natural gas, and E) biomass across the core scenarios as described in Figure 3A. Each row compares five flexibility modeling assumptions as described in Figure 3B under default demand distribution as described in Figure 2A.

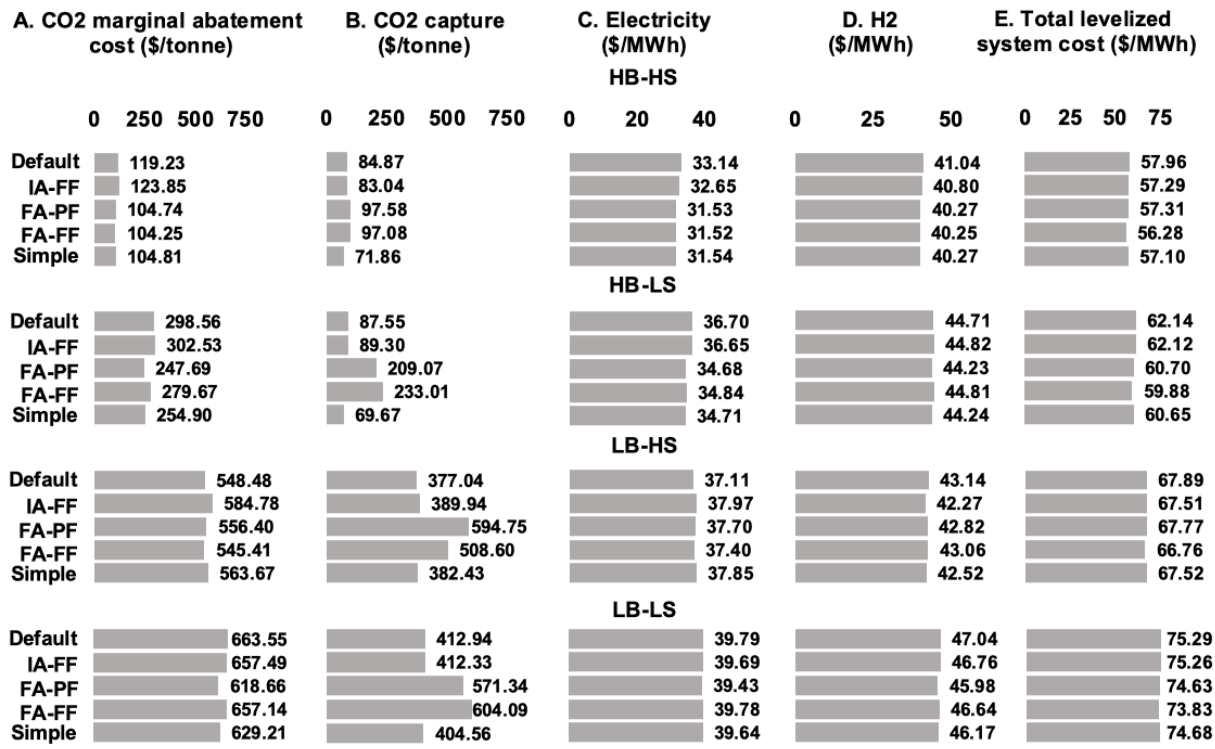


Figure S12. A) $CO_2$ marginal abatement cost, B) system average $CO_2$ capture price, C) system average electricity shadow price, D) system average $H_2$ shadow price, E) Total levelized system cost across the core scenarios as described in Figure 3A. Each row compares five flexibility modeling assumptions as described in Figure 3B under default demand distribution as described in Figure 2A.

## S1.4 Other flexibility assumption cases (E-D demand distribution)

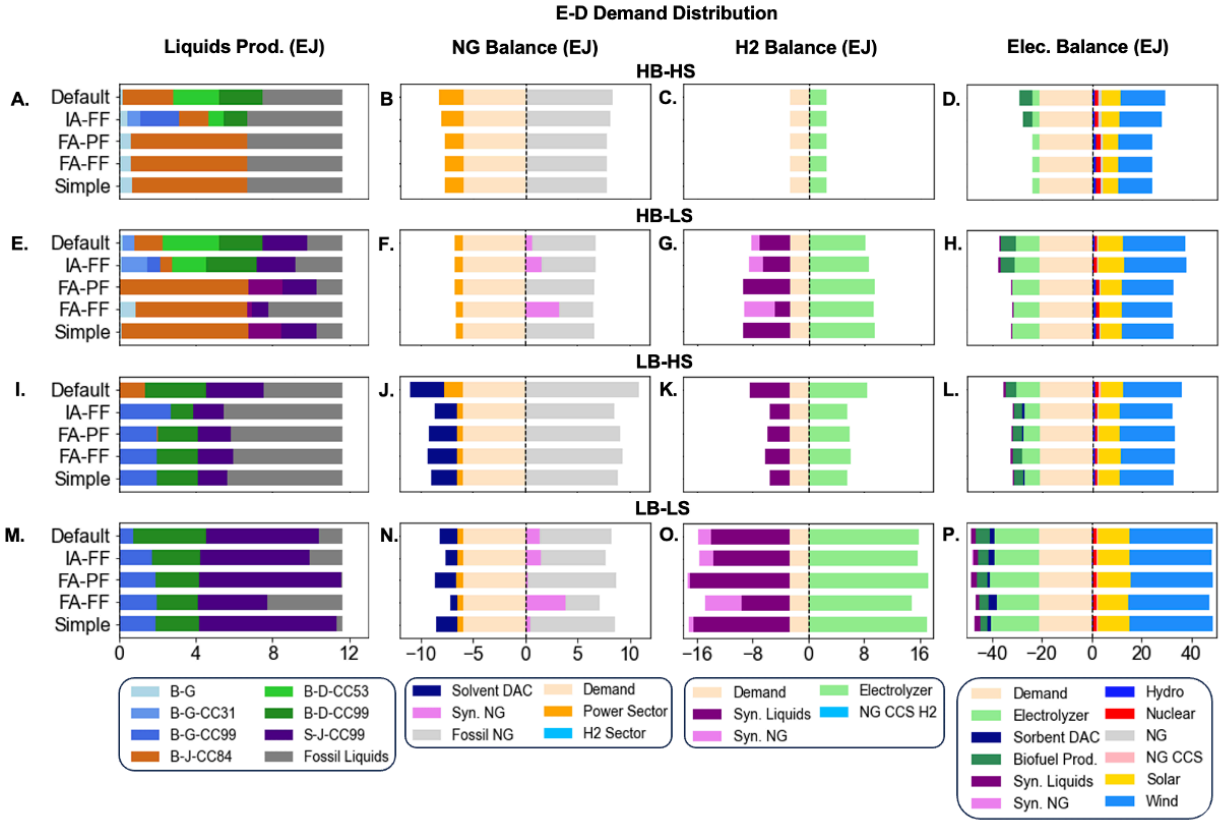


Figure S13. Effect of liquid fuel flexibility modeling assumptions on energy system outcomes: Liquid fuels production by pathway (Panels A,E,I,M), NG balance (Panels B,F,J,N), $H_2$ balance (Panels C,G,K,O), and electricity balance (Panels D,H,L,P) across the core scenarios as described in Figure 3A, under "E-D" demand distribution as described in Figure 2A. Each row compares the five flexibility modeling assumptions as described in Figure 3B. Liquid fuels production technology labels follow Table 1.

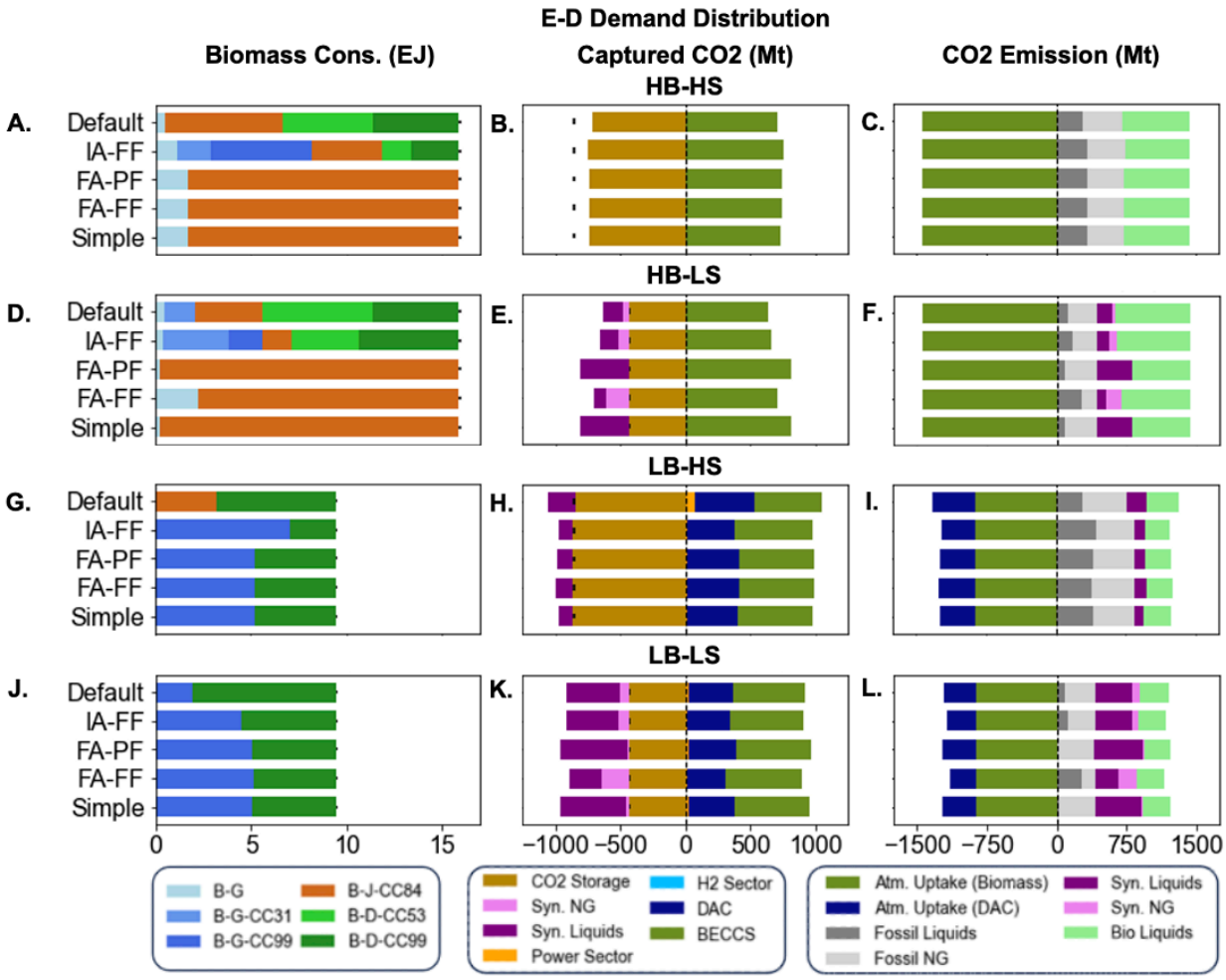


Figure S14. Effect of liquid fuel flexibility modeling assumptions on biomass consumption by technologies (Panels A, D, G, J), captured $CO_2$ balance (Panels B, E, H, K), and $CO_2$ emission balance (Panels C, F, I, L) results across the core scenarios as described in Figure 3A, under "E-D" demand distribution as described in Figure 2A. Each row compares the five flexibility modeling assumptions as described in Figure 3B. Liquid fuels production technology labels follow Table 1, and the resource limit of biomass and $CO_2$ sequestration are indicated by the bars in their respective plots.

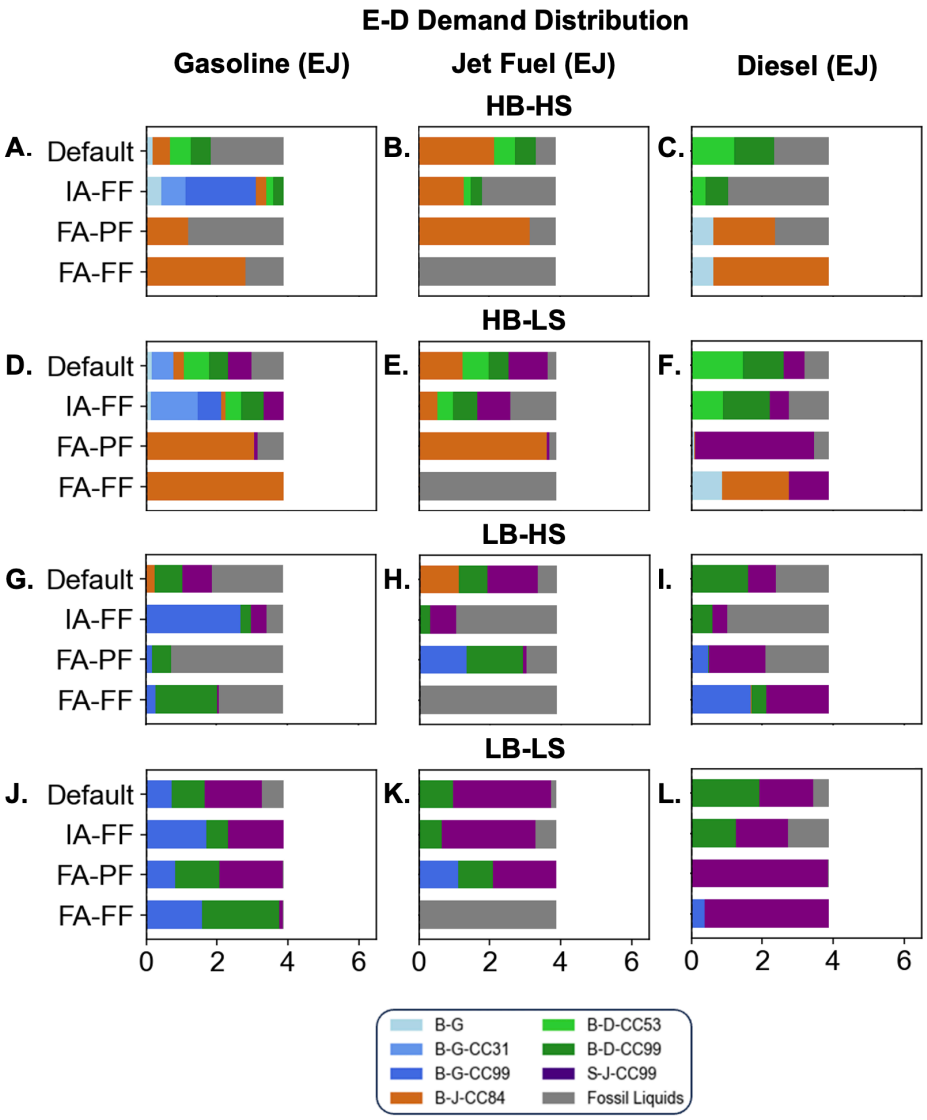


Figure S15. Effect of liquid fuel flexibility modeling assumptions on gasoline, jet fuel, and diesel production pathways across the core scenarios as described in Figure 3A across the five flexibility modeling assumptions as described in Figure 3B, and “E-D” demand distribution as described in Figure 2A. Liquid fuels production technology labels follow Table 1.

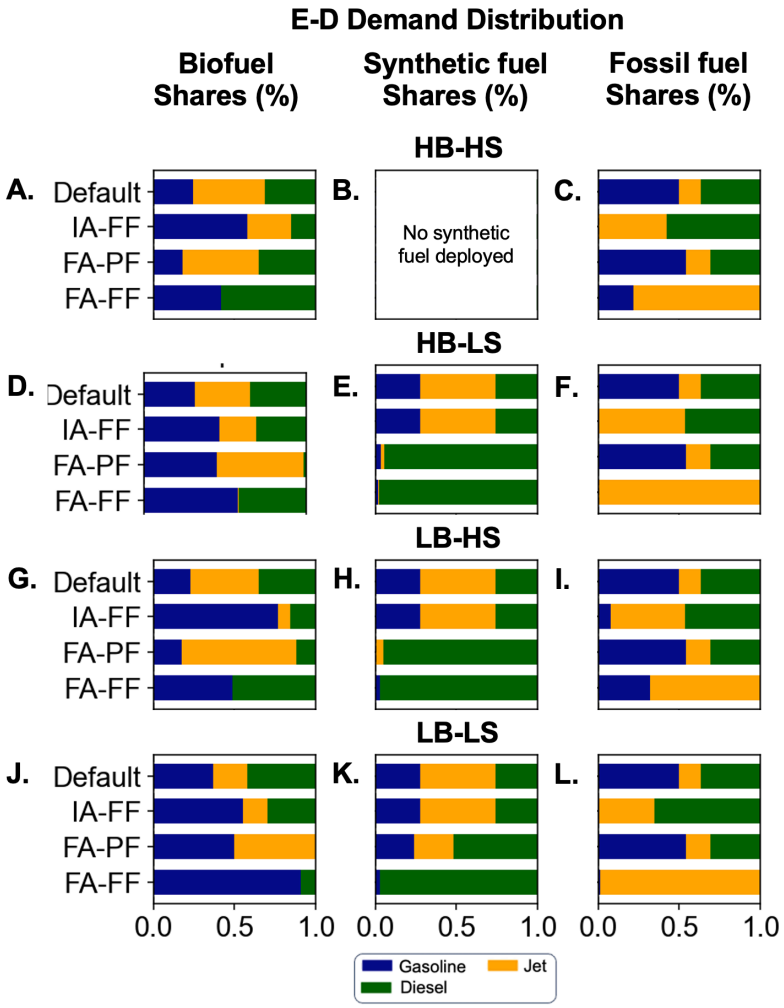


Figure S16. Effect of liquid fuel flexibility modeling assumptions on shares of gasoline, jet fuel, and diesel within total biofuel, synthetic fuel, and fossil fuel production across the core scenarios as described in Figure 3A across the five flexibility modeling assumptions as described in Figure 3B, and "E-D" demand distribution as described in Figure 2A. Liquid fuels production technology labels follow Table 1.

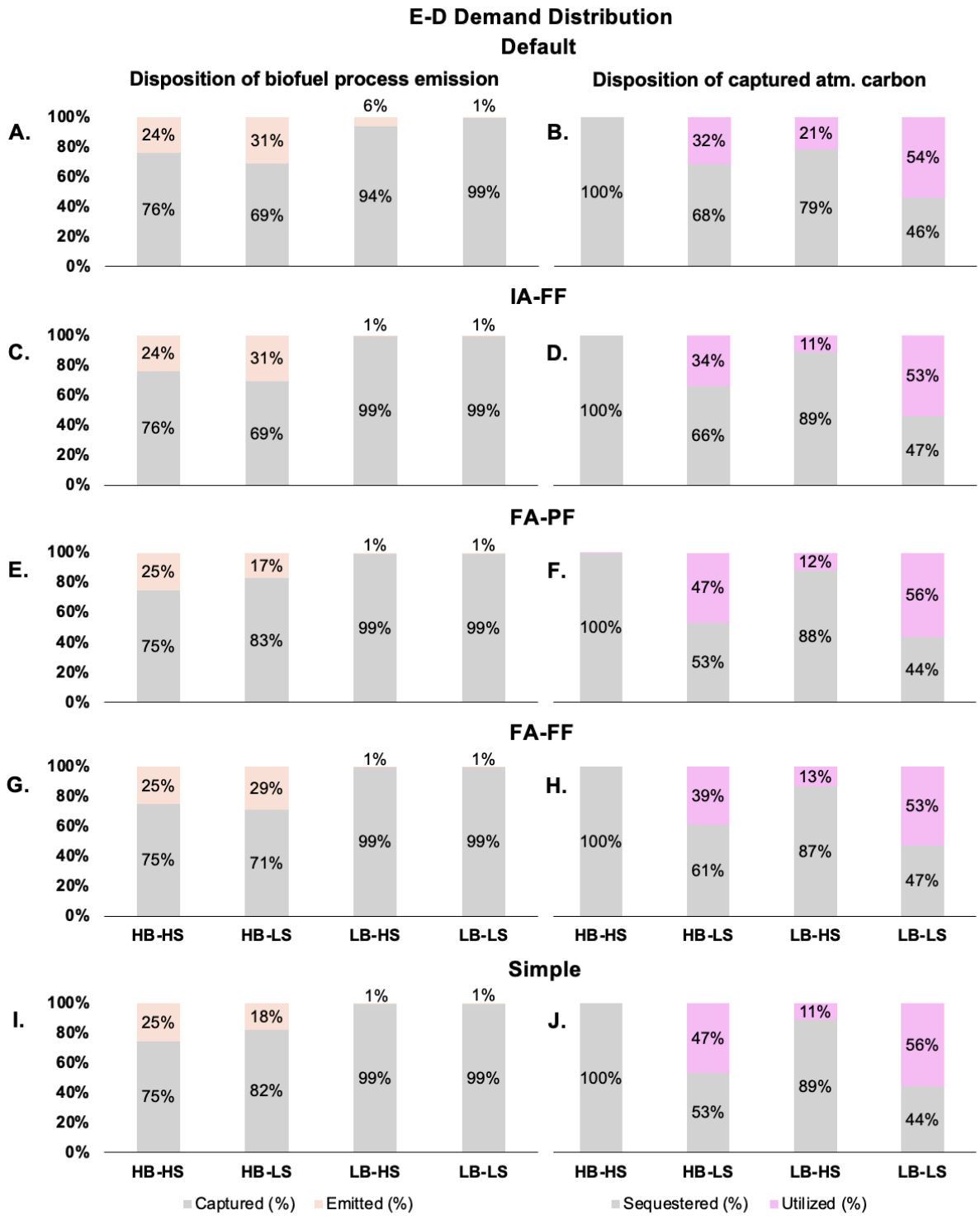


Figure S17. Panels A,C,E,G,I) Disposition of biofuel production carbon emissions (excludes the carbon content in biofuel products), panels B,D,F,H,J) Disposition of captured atmospheric carbon from biofuel processes and direct air capture across the core scenarios described in Figure 3A under "E-D" demand distribution as described in Figure 2A, for the five flexibility modeling assumptions as described in Figure 3B: "Default" (Panels A,B), "IA-FF" (Panels C,D), "FA-PF" (Panels E,F), "FA-FF" (Panels G,H), "Simple" (Panels I,J).

## S1.5 Cost sensitivity cases

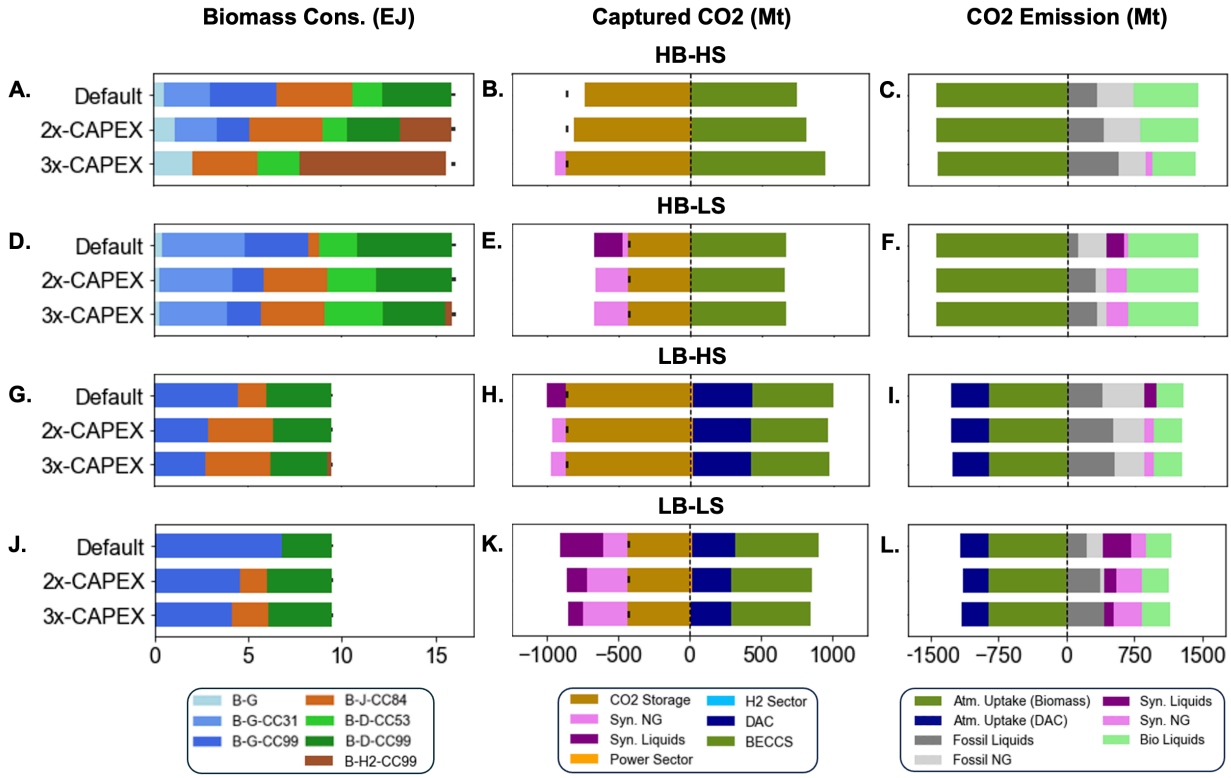


Figure S18. Additional energy system outcomes: Biomass consumption by technologies (Panels A, D, G, J), captured $CO_2$ balance (Panels B, E, H, K), and $CO_2$ emission balance (Panels C, F, I, L) across various capital cost assumptions across core scenarios as described in Figure 3A for "IA-PF" modeling assumptions as described in Figure 3B under default demand distribution as described in Figure 2A. The resource limit of biomass and $CO_2$ sequestration are indicated by the bars in their respective plots.

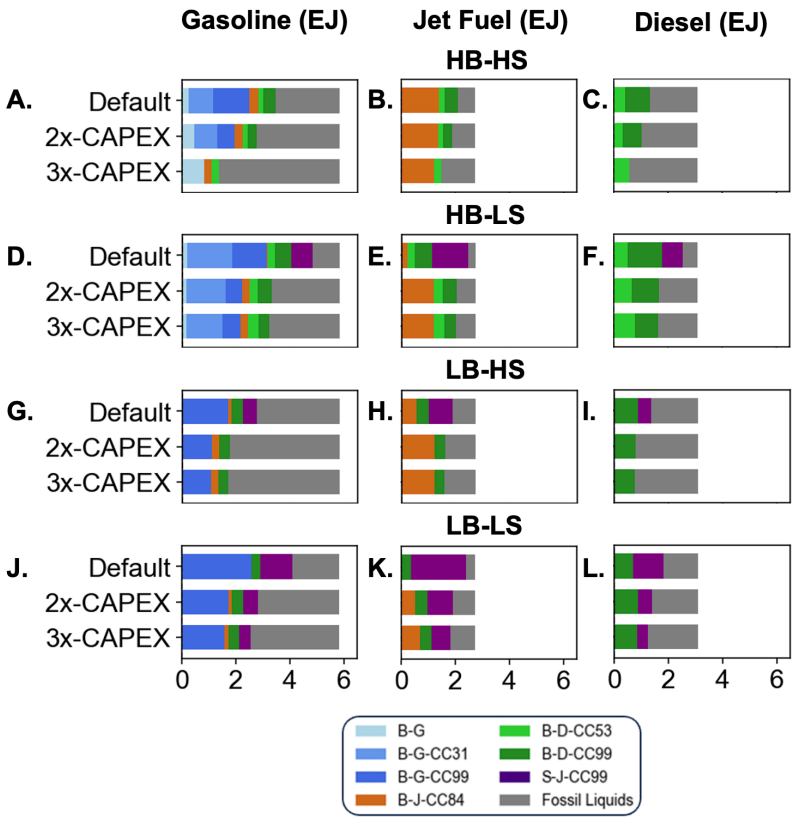


Figure S19. Effect of capital cost assumptions on gasoline, jet fuel, and diesel production pathways across core scenarios as described in Figure 3A for "IA-PF" modeling assumptions as described in Figure 3B under default demand distribution as described in Figure 2A. Liquid fuels production technology labels follow Table 1. "2x-CAPEX" = Doubled capital costs for bio and synthetic liquid fuels production technologies, "3x-CAPEX" = Tripled capital costs for bio and synthetic liquid fuels production technologies.

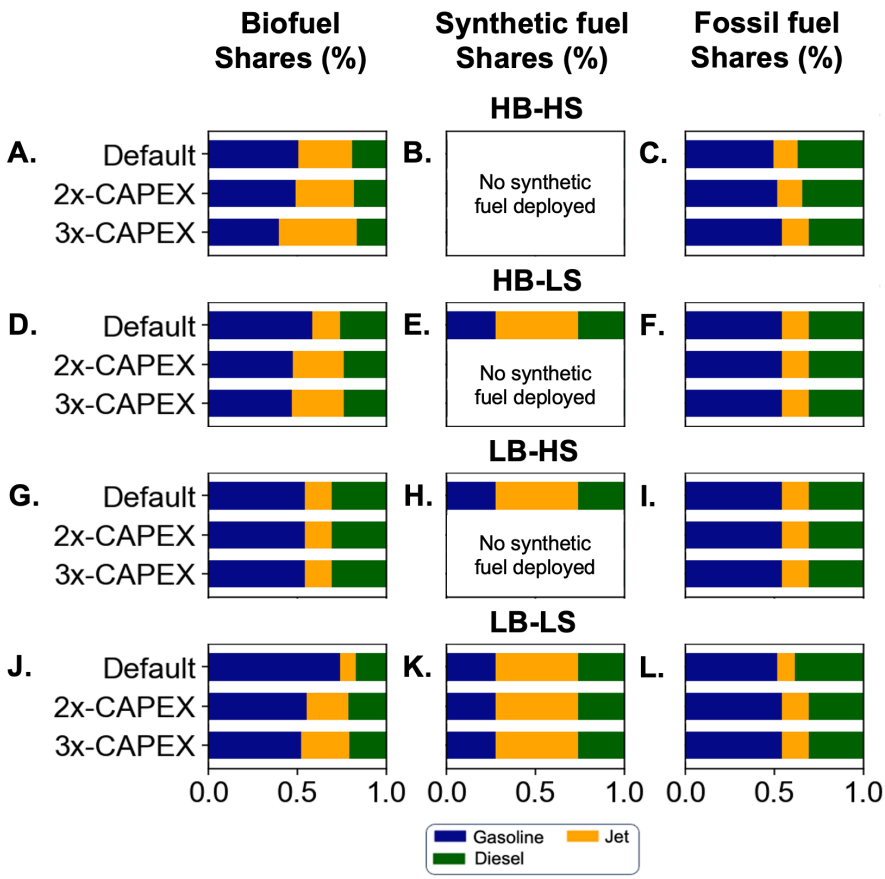


Figure S20. Effect of capital cost assumptions on shares of gasoline, jet fuel, and diesel within total biofuel, synthetic fuel, and fossil fuel production across core scenarios as described in Figure 3A for "IA-PF" modeling assumptions as described in Figure 3B under default demand distribution as described in Figure 2A.

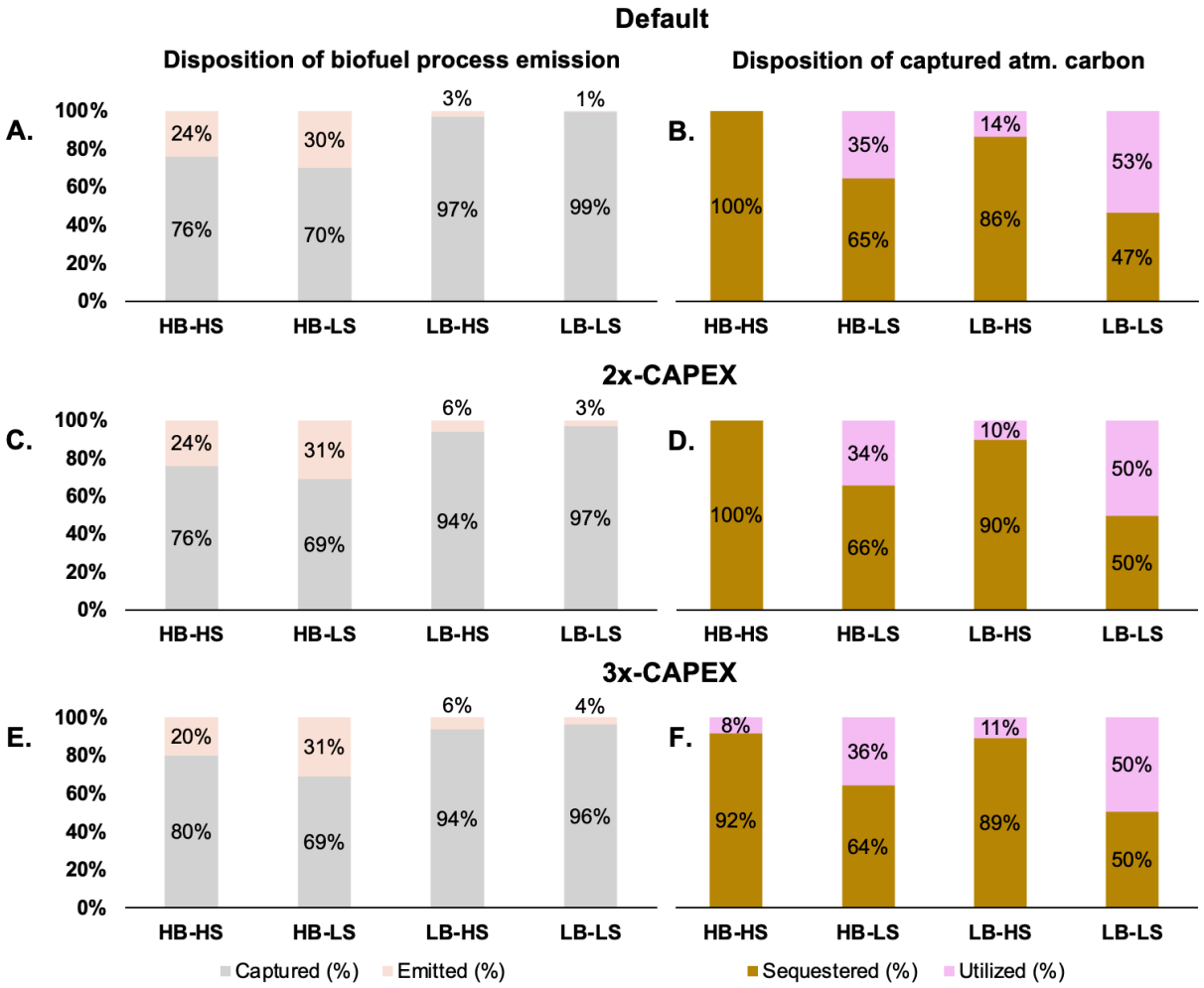


Figure S21. A,C,E) Disposition of biofuel production carbon emissions (excludes the carbon content in biofuel products), B,D,F) Disposition of captured atmospheric carbon from biofuel processes and direct air capture for various cost assumptions: Default (panel A,B), "2x-CAPEX" (panel C,D), and "3x-CAPEX" (panel E,F) as described in Section 3.6 across the core scenarios as described in Figure 3A, under default "IA-PF" modeling assumption as described in Figure 3B and default demand distribution as described in Figure 2A.

Table S9. Disposition of atmospheric carbon uptake from biofuel processes and direct air capture across the core scenarios as described in Figure 3A with "2x-CAPEX" cost assumptions, under default "IA-PF" modeling assumptions as described in Figure 3B, and default demand distribution as described in Figure 2A.

| 2x-CAPEX scenarios | HB-HS | HB-LS | LB-HS | LB-LS |
|---|---|---|---|---|
| Converted to fuels (%) | 27% | 48% | 30% | 61% |
| Sequestered (%) | 55% | 30% | 67% | 37% |
| Emitted (%) | 18% | 21% | 3% | 3% |

Table S10. Disposition of atmospheric carbon uptake from biofuel processes and direct air capture across the core scenarios as described in Figure 3A with “3x-CAPEX” cost assumptions, under default “IA-PF” modeling assumptions as described in Figure 3B, and default demand distribution as described in Figure 2A.

| 3x-CAPEX scenarios | HB-HS | HB-LS | LB-HS | LB-LS |
|---|---|---|---|---|
| Converted to fuels (%) | 22% | 49% | 30% | 60% |
| Sequestered (%) | 61% | 30% | 67% | 37% |
| Emitted (%) | 17% | 22% | 3% | 3% |

## Shadow prices comparison

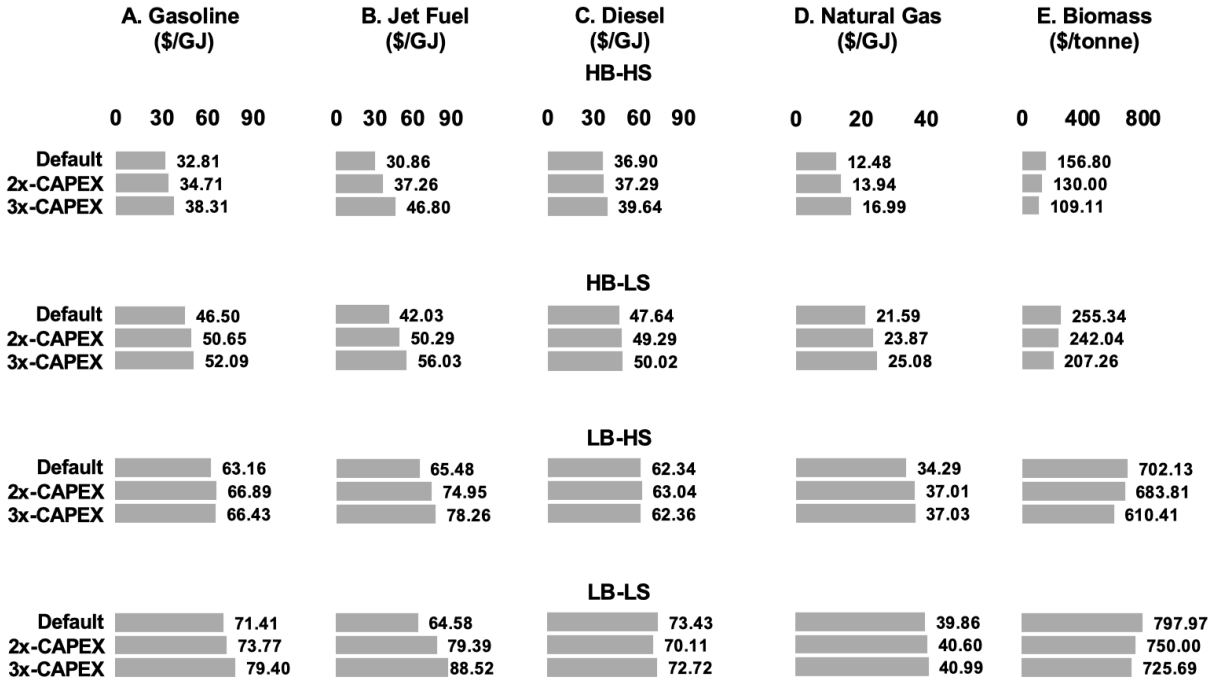


Figure S22. System average shadow prices for A) gasoline, B) jet fuel, C) diesel, D) natural gas, and E) biomass calculated according to Eq. S1 across the core scenarios as described in Figure 3A for various cost assumptions described in Section 3.6, under default “IA-PF” modeling assumptions as described in Figure 3B, and default demand distribution as described in Figure 2A.

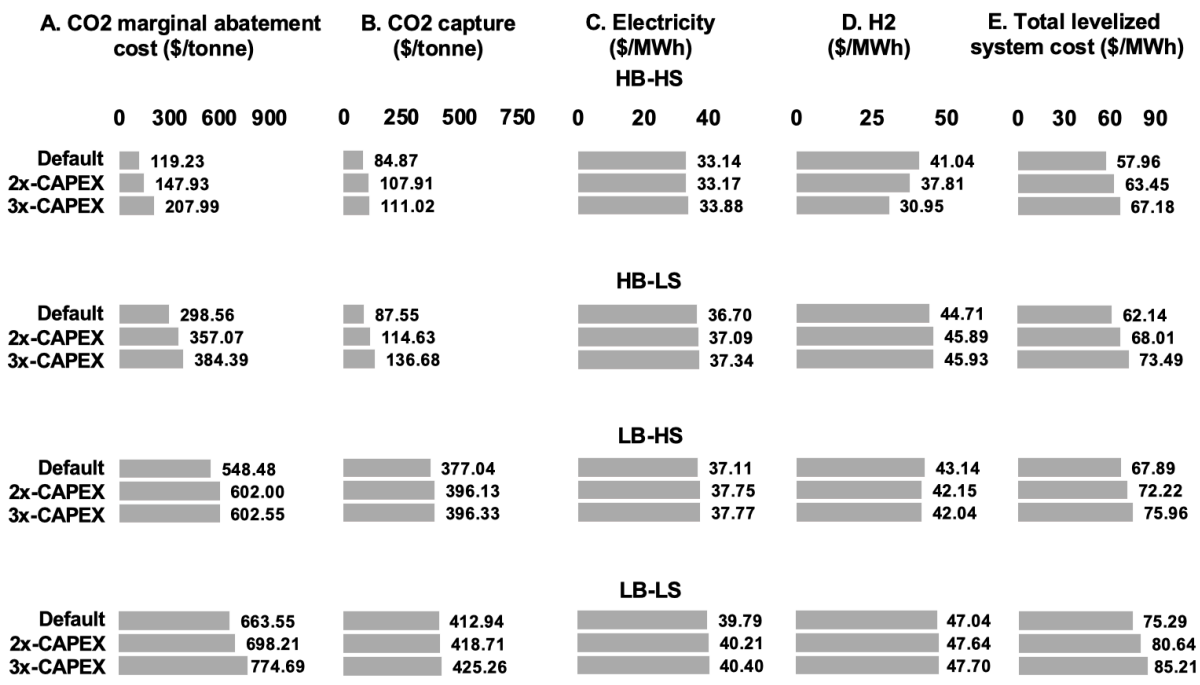


Figure S23. A) $CO_2$ marginal abatement cost, B) system average $CO_2$ capture price, C) system average electricity shadow price, D) system average $H_2$ shadow price, E) Total levelized system cost across the core scenarios as described in Figure 3A for various cost assumptions described in Section 3.6, under default "IA-PF" modeling assumptions as described in Figure 3B, and default demand distribution as described in Figure 2A.

## S2. Methods

### S2.1. Energy system shadow prices

#### Method of calculating system average shadow prices

Liquid fuels shadow prices represent system-level prices as the supply demand balance constraints are enforced at system-level (Eq. S15– S17). System average shadow prices of other resource $\overline{\lambda_r}$ with supply-demand balance constraints enforced at the regional level such as electricity, hydrogen, and natural gas are calculated using Eq. S1:

$$\overline{\lambda_r} = \frac{\sum_{t=1}^{T}\sum_{z=1}^{Z} \omega_t \cdot \lambda_{t,r,z}}{\sum_{t=1}^{T} \omega_t} \quad (\text{Eq. S1})$$

Where $\lambda_{t,r,z}$ is the shadow price of each resource in region z in time t, and $\omega_t$ is the time weight of each time t.

#### Method of calculating system average liquid fuels production cost

The system average liquid fuels production cost for each production resource i ($\overline{C_{prod,i}}$) presented in Section 3.3 is calculated according to Eq. S2:

$$\overline{C_{prod,i}} = \frac{\sum_{z=1}^{Z} C_{prod,i,z} \cdot LF_{prod,z}}{\sum_{z=1}^{Z} LF_{prod,z}} \quad (\text{Eq. S2})$$

Where,

$C_{prod,i,z}$ = Liquid fuels production cost for resource i in region z calculated according to Eq. S3 – S4

$LF_{prod,z}$ = Total liquid fuels produced in region z

For biofuel production resource i:

$$C_{prod,i,z} = \text{Fixed Cost}_i + VOM_i + \overline{\lambda_{Bio}} \cdot \theta_{Bio,i} + \overline{\lambda_{electricity,z}} \cdot \xi_{elec,i} - \overline{\lambda_{CO2\ Capt,z}} \cdot \theta_{CO2\ Capt,i} \quad (\text{Eq. S3})$$

For synthetic fuels production resource i:

$$C_{prod,i,z} = \text{Fixed Cost}_i + VOM_i + \overline{\lambda_{electricity,z}} \cdot \xi_{elec,i} + \overline{\lambda_{H2,z}} \cdot \xi_{H2,i} + \overline{\lambda_{CO2\ Capt,z}} \cdot \xi_{,CO2\ in,i} \quad (\text{Eq. S4})$$

Where,

$\text{Fixed Cost}_i$ = CAPEX + Fixed maintenance and operation (FOM) costs ($/GJ)

$VOM_i$ = Variable maintenance and operation costs ($/GJ)

$\theta_{CO2\ Capt,i}$ = $CO_2$ captured by the biofuel process (tonne $CO_2$ captured/GJ)

$\theta_{Bio,i}$ = biomass input (tonne biomass/GJ) for biofuel production

$\xi_{elec,i}$ = electricity consumption (MWh/GJ)

$\xi_{H2,i}$ = hydrogen consumption (MWh/GJ)

$\xi_{CO2\ in,i}$ = captured $CO_2$ input (tonne $CO_2$/GJ) for synthetic fuel production

$\overline{\lambda_{CO2\ Capt,z}}$ = average regional $CO_2$ capture price ($/tonne $CO_2$ captured) = $CO_2$ marginal abatement cost – dual value of the captured $CO_2$ balance constraint. This represents the value avoided $CO_2$ emission, which is cost of utilization and sequestration of captured $CO_2$.

For electricity, hydrogen, and biomass, $\overline{\lambda_{r,z}} = \frac{\sum_{t=1}^{T} \omega_t \cdot \lambda_{t,r,z}}{\sum_{t=1}^{T} \omega_t}$, where $\lambda_{tz}$ is the shadow price of each resource in region z in time t, and $\omega_t$ is the time weight of each time t.

## S2.2 Standardized approximation method for estimating $CO_2$ capture costs and energy requirements

This section presents an approximation methodology for estimating the costs and energy requirements of retrofitting $CO_2$ capture units onto fuel production processes that were originally designed without $CO_2$ capture in their respective reference TEAs. This approach enables the representation of a wide variety of $CO_2$ capture rates for biofuels and synthetic fuels processes in this study.

The method described in this section involves systematically identifying major $CO_2$ emission streams from published process flow diagrams and mass balances in reference TEAs of fuel production processes, then matching those streams to analogous industrial processes with established post-combustion capture technologies. Cost and energy penalty estimates are derived from the U.S. National Energy Technology Laboratory (NETL) TEAs of $CO_2$ capture in industrial point sources and power plants [1], [2] as shown in Table S11. By mapping emission streams to comparable industrial sources based on flue gas composition, this framework enables consistent estimation of $CO_2$ capture system costs and energy requirements across process types. It preserves the integrity of the original process design and energy conversion, while enabling evaluation of $CO_2$ capture configurations not modeled in existing literature.

For each identified $CO_2$ emission stream from published process flow diagrams in reference TEAs, the selection of appropriate $CO_2$ capture technology is based on the concentration of $CO_2$ in each emission stream. Assumptions were made to the concentration in each emission stream when the data is unavailable. For example, industrial process flue gas emissions were assumed to be 10-20% wt. $CO_2$, while natural gas related flue gas emissions were assumed to be <4% wt. $CO_2$. The framework employs a systematic approach to match emission streams based on their $CO_2$ concentrations to representative $CO_2$ capture processes in NETL TEAs:

- High-Concentration $CO_2$ Streams (~100% wt. $CO_2$): For streams with nearly pure $CO_2$, such as those from syngas cleaning in gasification processes, ethanol plant $CO_2$ compression parameters are assumed with 100% CC rate [1].

- Medium-Concentration $CO_2$ Streams (10-20% wt. $CO_2$): Emission streams with moderate $CO_2$ concentrations are matched to cement plant $CO_2$ capture parameters with 99% CC rate [1].

- Low-Concentration $CO_2$ Streams (<4% wt. $CO_2$): Dilute $CO_2$ streams, are mapped to $CO_2$ capture parameters of natural gas combined cycle (NGCC) Power Plant with 95% CC rate [2].

The NETL TEAs provide breakdowns of capital expenditures (CAPEX), operating expenditures (OPEX), and energy penalties associated with different $CO_2$ capture technologies and configurations (see Table S11). We assumed that all thermal energy input requirements for the capture process are met through electricity. Assuming both the cost and energy requirements of $CO_2$ capture systems scale linearly with the input $CO_2$ mass flow rate, we adapt NETL's reference $CO_2$ capture data to the specific scale and $CO_2$ emission characteristics of the various emission streams of fuel production technologies in this study using the following steps:

1. The costs and energy requirements of the $CO_2$ capture processes from NETL TEAs are normalized to a per-tonne $CO_2$ mass inflow basis.

2. These normalized costs and energy requirements are scaled to match the targeted $CO_2$ emission streams of the fuel production technologies based on their respective reference TEAs, and then scaled to a per-unit biomass input basis for biofuel production processes, and per-unit $CO_2$ feedstock input basis for synthetic fuels processes.

3. The scaled $CO_2$ capture costs and energy requirements are added to the original plant input parameters and used as inputs for MACRO.

4. Finally, the overall CC rate of the fuel production technology is calculated as the ratio of the sum of captured $CO_2$ from all streams to the sum of original $CO_2$ emission streams and used as inputs for MACRO.

The pathways characterized using this method are included in Table S33, Table S34, and Table S37, and Section S4 shows carbon balance diagrams of various variants of biofuels and synthetic fuels production technologies including those parameterized using the above-mentioned approximation method.

Table S11. Costs and energy requirements of $CO_2$ capture technology used in the approximation method to develop variants of biofuel and synthetic fuels technologies with various $CO_2$ capture rates. Cost assumptions are scaled according to per tonne CO2 input basis and converted to 2022 dollars, a technology lifetime of 30 years and discount rate of 4.5% is used to annualize investment costs.

| Industrial $CO_2$ capture | Input $CO_2$ concentration range (% wt.) | $CO_2$ capture rate (%) | CAPEX ($/(tonne $CO_2$ input/h)) | Annualized CAPEX ($/(tonne $CO_2$ input/h)/y) | FOM ($/(tonne $CO_2$ input/h)/y) | VOM ($/tonne $CO_2$ input) | Electricity input (MWh/tonne $CO_2$ input) |
|---|---|---|---|---|---|---|---|
| Ethanol plant $CO_2$ capture | ~ 100% | 100.0 | 1,384,619 | 85,004 | 76,359 | 1.66 | 0.11 |
| Cement plant 99% $CO_2$ capture | 10 - 20 % | 99.0 | 2,746,462 | 168,610 | 87,115 | 5.54 | 1.14 |
| NGCC 95% $CO_2$ capture | <4 % | 95.0 | 2,233,695 | 137,130 | 74,912 | 6.36 | 0.91 |

## S2.3. Harmonization of carbon and energy balances for fuels production technologies

This section details the methodology used to harmonize the carbon and energy balances of various fuels production processes in this study obtained from techno-economic analyses (TEAs) in the literature, including the additional variants with various $CO_2$ capture rates described in Section S2.2. This harmonization allows for the application of user-defined carbon content for biomass and fuels in the model while preserving the original process's energy conversion and product distribution as reported in their respective TEAs, and ensuring the balance of carbon and energy balances in the inputs and outputs of the processes.

### Harmonization of energy balance for biofuel production in MACRO

The following steps are involved to obtain harmonized biofuel energy conversion parameters for MACRO across the biofuel technologies modeled in this study.

1. Determining biomass energy converted to biofuels for MACRO biofuel modeling (Eq. S8 – S10)

   As we modeled energy conversion of biofuel processes based on higher heating value (HHV) efficiency, defined as fraction of input biomass energy converted into fuels in MACRO, these values are directly utilized if reported in the technology's reference TEA, or calculated from using available data within the reference. Any assumptions to infer energy content of fuels were obtained from the GREET 2023 database. For example, if the reference TEA only reported the volume of fuels produced, GREET 2023 database is used to estimate the energy content of the fuels product, and the process energy efficiency is calculated by dividing the energy content of the products by the energy content of the original input biomass [3]. Any necessary conversions from lower heating value (LHV) to HHV are performed using appropriate assumptions. This allows MACRO to model biofuel technology for biomass types with unique energy contents, reflecting differences in fuel output yields per unit mass of biomass across different biomass types. For example, a biomass type with higher energy content will produce more fuel products per tonne of purchased biomass.

2. Determining the fraction of individual fuel products

   For biofuel processes yielding multiple fuel products, the distribution is required in MACRO (Eq. S8 – S10). The energy distribution ratios of individual fuels according to HHV energy content are directly utilized if the reference provides them. However, if only mass ratios are available in the reference, the energy ratios are calculated using GREET 2023 energy content data [3].

3. Assumptions used for harmonizing biofuel energy modeling in MACRO

   1) Process energy efficiency and fuel product distribution remain constant regardless of the biomass type.
   2) Costs are assumed to be based on a per-unit biomass mass input and remain consistent irrespective of the biomass type.
   3) Any electricity inputs are also assumed to be on a per-unit biomass mass input basis and remain constant regardless of the biomass type (see Eq. S22)
   4) The cost and energy requirements of the plant are assumed to scale linearly with the input biomass input.

## Harmonization of carbon balance for biofuel production in MACRO

The carbon balance modeling for biofuel processes in MACRO is described in Eq. S13 – S14, where the amount of vented $CO_2$ emissions and captured $CO_2$ are calculated according to user defined 1) biomass carbon content and 2) $CO_2$ capture (CC) rates for various processes. Eq. S13 and S14 ensure that any carbon content not in biofuel products are either emitted into the atmosphere (see Eq. S51), or captured for utilization or sequestration (see Eq. S50). As such, this ensures that no carbon is unaccounted for in the energy system.

The carbon content in the biofuels is calculated by applying emission factors obtained from the GREET 2023 database shown in Table S31 to the fuel product outputs of the biofuel production processes (see Eq. S8 – S10). This allows the carbon balance to be complete in MACRO with the user providing input parameters on 1) biomass carbon content and 2) CC rates for various processes.

## Harmonization of carbon and energy balance for synthetic fuels production in MACRO

As compared to biofuels where different feedstocks have unique carbon and energy content, synthetic fuels production is scaled to per unit $CO_2$ feedstock inputs, and we can directly utilize the production yield of various fuels product per unit $CO_2$ feedstock input from the reference in the literature, as modeled in Eq. S5 – S7 in MACRO. Similarly, the electricity and $H_2$ input requirements are scaled to per unit $CO_2$ feedstock input and can be directly utilized from the original reference, as modeled in Eq. S22 – S23 in MACRO. Nonetheless, the amount of vented $CO_2$ emissions and captured $CO_2$ of the synthetic fuels process are calculated in MACRO according to user defined $CO_2$ capture (CC) rates as shown in Eq. S11 – S12. This ensures that any carbon content not in the synthetic fuel products are either emitted into the atmosphere (see Eq. S51), or captured for utilization or sequestration (see Eq. S50), with all carbon accounted for in the energy system.

## S3. Modeling input assumptions

### S3.1. Energy demand across sectors

Table S12. Annual energy demand for various commodities in this study: Power, $H_2$, natural gas, and liquid fuels (gasoline, jet fuel, diesel). Hourly power demand profiles were obtained from projected 2050 state-level data from Princeton University's Net-Zero America low electrification scenario [4]. Annual $H_2$, natural gas, and liquid fuels demands were obtained from projected 2050 state-level end-uses likewise from Net-Zero America low electrification scenario, with the assumption of constant hourly demand in creating hourly demand profiles. State-level demands were then aggregated into respective regions based on the states within each region. Electricity, $H_2$, and natural gas supply-balance constraints are modeled based on hourly regional resolution in MACRO, while liquid fuels are modeled as a systemwide supply-demand constraint as shown in Eq. S15 – S17 to reflect the low cost of liquid fuels transportation, using the "Total" column of this table. "CA" = California, "NW" = Northwest, "SW" = Southwest, "TX" = Texas, "NCEN" = North Central, "CEN" = Central, "SE" = Southeast, "MIDAT" = Mid-Atlantic, "NE" = Northeast.

| Energy Demand | CA | NW | SW | TX | NCEN | CEN | SE | MIDAT | NE | Total |
|---|---|---|---|---|---|---|---|---|---|---|
| Power (EJ/year) | 1.78 | 0.99 | 1.30 | 2.19 | 3.32 | 1.96 | 4.53 | 3.08 | 1.65 | 20.79 |
| $H_2$ (EJ/year) | 0.13 | 0.12 | 0.10 | 0.34 | 0.45 | 0.74 | 0.47 | 0.23 | 0.06 | 2.64 |
| Natural Gas (EJ/year) | 0.43 | 0.33 | 0.35 | 0.52 | 1.36 | 0.57 | 0.75 | 0.92 | 0.66 | 5.89 |
| Gasoline (EJ/year) | 0.63 | 0.26 | 0.38 | 0.49 | 0.84 | 0.50 | 1.37 | 0.86 | 0.49 | 5.84 |
| Jet Fuel (EJ/year) | 0.50 | 0.15 | 0.27 | 0.26 | 0.28 | 0.11 | 0.55 | 0.30 | 0.31 | 2.73 |
| Diesel (EJ/year) | 0.25 | 0.15 | 0.19 | 0.34 | 0.47 | 0.38 | 0.64 | 0.41 | 0.26 | 3.10 |

### S3.2. Power and $H_2$ sector modeling assumptions

Data assumptions for power and $H_2$ sectors are mainly based on those from a previous work on net-zero power-$H_2$ coupled system in similar geographical regions [5], with costs updated to 2022 USD and greenfield power generation technology cost and performance data updated to NREL Annual Technology Baseline (ATB) 2024 [6].

Table S13. Existing capacity and cost parameters in 2022 dollars for network expansion for power network transmission lines obtained from the U.S. Environmental Protection Agency (EPA) version of the Integrated Planning Model (IPM) [7].

| Network Lines | Transmission Path | Distance (Miles) | Existing Capacity (MW) | Line Reinforcement Cost ($/MW-mile) | Annualized Line Reinforcement Cost ($/MW-mile/y) |
|---|---|---|---|---|---|
| 1 | CA to NW | 622 | 6,533 | 2,089 | 128 |
| 2 | CA to SW | 490 | 11,964 | 2,090 | 128 |
| 3 | NW to SW | 577 | 4,530 | 1,286 | 79 |
| 4 | SW to CEN | 732 | 610 | 1,476 | 91 |

| | | | | | |
|---|---|---|---|---|---|
| 5 | TX to CEN | 494 | 2,525 | 1,476 | 91 |
| 6 | NCEN to CEN | 485 | 9,851 | 1,262 | 77 |
| 7 | NCEN to SE | 890 | 3,745 | 928 | 57 |
| 8 | NCEN to MIDAT | 751 | 9,083 | 1,262 | 77 |
| 9 | CEN to SE | 780 | 4,872 | 1,333 | 82 |
| 10 | SE to MIDAT | 491 | 5,552 | 1,333 | 82 |
| 11 | MIDAT to NE | 474 | 1,915 | 2,143 | 132 |

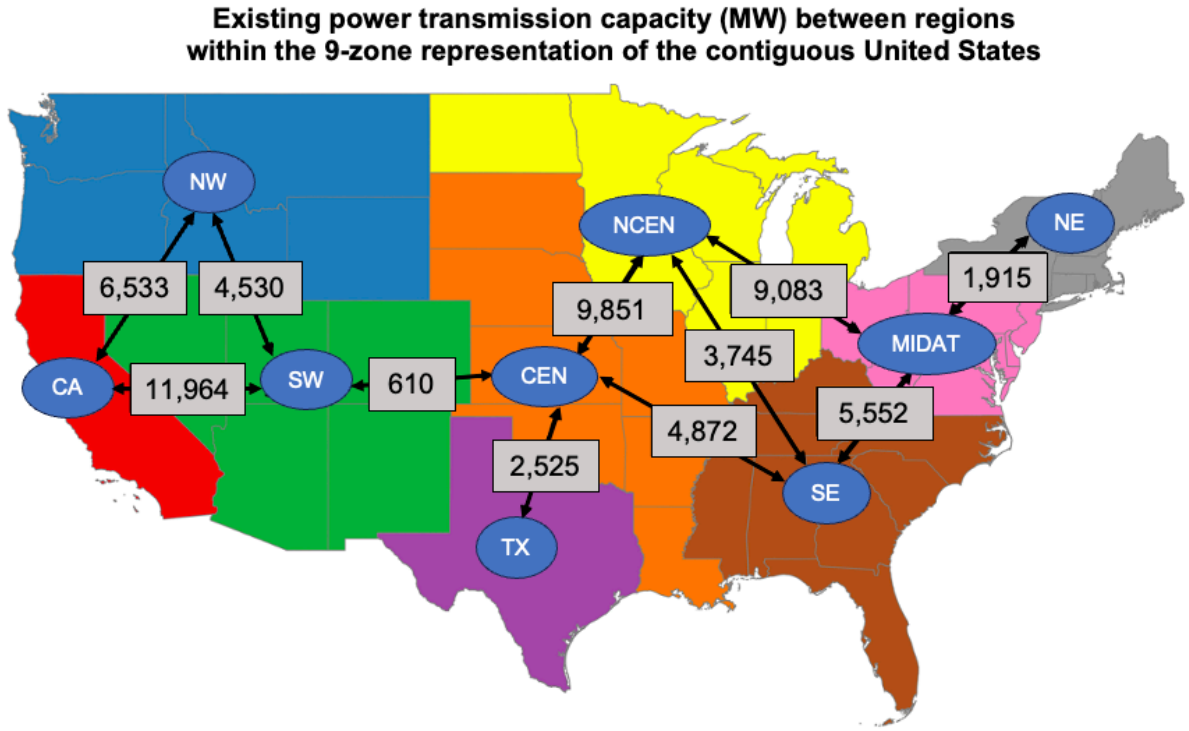


Figure S24. Existing power transmission capacity (MW) within the nine representative regions of the contiguous U.S. based on the Open Energy Outlook 2022 [8], with aggregated initial power transmission capacity between regions obtained from the U.S. Environmental Protection Agency (EPA) version of the Integrated Planning Model (IPM) [7]. “CA” = California, “NW” = Northwest, “SW” = Southwest, “TX” = Texas, “NCEN” = North Central, “CEN” = Central, “SE” = Southeast, “MIDAT” = Mid-Atlantic, “NE” = Northeast.

Table S14. Greenfield power generation technology cost and performance parameters. Data corresponds to 2045 costs (moderate) reported by the NREL Annual Technology Baseline 2024 in 2022 dollars[6], with the assumption that 2050 energy system would consist of technologies built five years earlier. A discount rate of 4.5% is used to annualize investment costs according to assumed technology lifetime and costs are converted to 2022 dollars. CC = Combined cycle, CT = Combustion turbine, CC = $CO_2$ capture and storage.

| Technology | Lifetime (year) | Investment cost | | Annualized CAPEX | | Fixed operation and maintenance (FOM) cost | | Variable operation and maintenance (VOM) cost ($/MWh) | Heat Rate (MMBtu/MWh) |
|---|---|---|---|---|---|---|---|---|---|
| | | Power ($/kW) | Energy ($/kWh) | Power ($/kW/year) | Energy ($/kWh/year) | Power ($/kW/year) | Energy ($/kWh/year) | | |
| Natural Gas (CC) | 30 | 1014 | - | 62 | - | 28 | - | 1.85 | 6.16 |
| Natural Gas (CC-CCS) | 30 | 1,792 | - | 110 | - | 48 | - | 3.76 | 6.88 |
| Natural Gas (CT) | 30 | 908 | - | 56 | - | 23 | - | 6.94 | 9.72 |
| Nuclear | 40 | 4,250 | - | 231 | - | 175 | - | 2.80 | 10.50 |
| Solar | 30 | 628 | - | 39 | - | 14 | - | - | - |
| Land Based Wind | 30 | 1,021 | - | 63 | - | 26 | - | - | - |
| Offshore Wind | 30 | 2,823 | - | 173 | - | 57 | - | - | - |
| Battery | 15 | 283 | 179 | 26 | 17 | 7 | 4 | - | - |

Table S15. $H_2$ production technology cost and performance parameters. Cost and performance parameters for electrolyzer obtained from IEA ("Long term" scenario) [9], data for natural gas reforming technologies obtained from NETL techno-economic analysis study [10], and data for tank storage obtained from Papadias & Aluwalia [11]. Feedwater cost for electrolyzers assumed to be negligible compared to the cost of electricity. The capital cost for $H_2$ storage in terms of rate of production and electricity input are associated with charging components. SMR = Steam methane reforming, ATR = Autothermal reforming, CCS = $CO_2$ capture and storage. Units of \$/MW$H_2$ are converted based on higher heating value of $H_2$. A discount rate of 4.5% is used to annualize investment costs and costs are converted to 2022 dollars.

| Technology | Lifetime (year) | Investment cost | | Annualized CAPEX | | Fixed operation and maintenance (FOM) cost | | Variable operation and maintenance (VOM) cost (\$/MWh $H_2$) | Electricity input (MWh/ MWh $H_2$) | Natural gas input (MMBtu/ MWh $H_2$) |
|---|---|---|---|---|---|---|---|---|---|---|
| | | $H_2$ production (\$/MW $H_2$) | Energy (\$/MWh $H_2$) | $H_2$ production (\$/MW $H_2$/year) | Energy (\$/MWh $H_2$/year) | $H_2$ production (\$/MW $H_2$/year) | Energy (\$/MWh $H_2$/year) | | | |
| Electrolyzer | 20 | 596,881 | - | 45,886 | - | 1,175 | - | - | 1.14 | - |
| $H_2$ Storage (tank) | 30 | 59,240 | 16,065 | 3,637 | 986 | - | 32 | - | 0.01 | - |
| SMR-CCS | 25 | 1,194,764 | - | 80,574 | - | 33,260 | - | 2.90 | 0.05 | 4.72 |
| ATR-CCS | 25 | 944,296 | - | 63,682 | - | 25,798 | - | 2.13 | 0.10 | 4.44 |

Table S16. Power generation $CO_2$ emissions and $CO_2$ captured based on a natural gas fuel emission factor of 0.054 t$CO_2$ /MMBtu [3].

| Technology | Fuel combustion emissions (t$CO_2$ /MWh) | $CO_2$ capture rate (%) | $CO_2$ captured (t$CO_2$ /MWh) |
|---|---|---|---|
| Natural Gas (CC) | 0.33 | - | - |
| Natural Gas (CC CCS) | 0.01 | 97.0 | 0.36 |
| Natural Gas (CT) | 0.52 | - | - |

Table S17. Hydrogen production $CO_2$ emissions and $CO_2$ captured based on a natural gas fuel emission factor of 0.054 $tCO_2$ /MMBtu [3].

| Technology | Fuel combustion emissions ($tCO_2/tH_2$) | $CO_2$ capture rate (%) | $CO_2$ captured ($tCO_2/tH_2$) |
|---|---|---|---|
| SMR-CCS | 0.38 | 96.2 | 9.59 |
| ATR-CCS | 0.55 | 94.5 | 9.42 |

Table S18. Cost and input assumptions for biomass to electricity and biomass to $H_2$ production technologies, from Net-Zero America study assumptions and NREL techno-economic study respectively [4], [12]. "B" – Bio, "E" – electricity, "$H_2$" – hydrogen. "$CO_2$ capture rate (CCX)" = percentage of biomass carbon content captured, "biomass energy conversion" = percentage of biomass energy converted into electricity or $H_2$ based on higher heating value basis. Amount of carbon captured and bioenergy produced would differ across biomass types and regions according to their respective carbon and energy content as shown in Table S38 and Table S39. B-$H_2$ was not modeled with $CO_2$ capture in its original reference [12], and the approximation method in Section S2.2 was used to parameterize the B-$H_2$-CC99 variant used in this study. A minimum and maximum operation output of 40% - 90%, and 85% - 90% of built capacity is enforced for B-E and B-$H_2$ respectively. Cost assumptions are scaled according to per tonne biomass input basis and converted to 2022 dollars, a technology lifetime of 30 years and discount rate of 4.5% is used to annualize investment costs.

| Technology | Lifetime (year) | Investment cost ($/(tonne biomass/h)) | Annualized Investment cost ($/(tonne biomass/h)/y) | Fixed operation and maintenance (FOM) cost ($/(tonne biomass/h)/y) | Variable operation and maintenance (VOM) cost ($/tonne biomass) | $CO_2$ capture rate (%) | Biomass energy conversion (% HHV) | Electricity input (MWh/tonne biomass) | Natural gas input (MMBtu/tonne biomass) |
|---|---|---|---|---|---|---|---|---|---|
| B-E-CC93 | 30 | 12,465,242 | 765,260 | 212,409 | 47.20 | 93.2 | 30.1 | - | - |
| B-$H_2$ | 30 | 2,814,068 | 172,760 | 190,982 | 13.35 | 0.0 | 58.6 | 0.13 | 0.46 |
| B-$H_2$-CC99 | 30 | 7,937,862 | 487,318 | 353,503 | 23.68 | 99 | 58.6 | 1.26 | 0.46 |

Table S19. Existing power generator capacity by resource in each region in 2050. The existing generation capacity in 2050 is estimated from capacity in 2021 after removing natural gas capacity that has exceeded their lifetime (40-50 years depending on natural gas plant type). Data obtained from EIA860 and Public Utility Data Liberation using PowerGenome [13]. Plant lifetimes of natural gas generators are based on NREL ReEDS model input assumption [14]. Based on the Inflation Reduction Act (IRA), second lifetime extensions were assumed for existing nuclear power generators [15]. CC = Combined Cycle. CT = Combustion Turbine.

| Technology | CA | NW | SW | TX | NCEN | CEN | SE | MIDAT | NE |
|---|---|---|---|---|---|---|---|---|---|
| Conventional Hydroelectric (GW) | 8.77 | 33.92 | 4.44 | 0.47 | 0.46 | 5.74 | 11.12 | 2.81 | 4.73 |
| Hydroelectric Pumped Storage (GW) | 3.94 | 0.31 | 0.78 | - | 2.00 | 0.94 | 6.26 | 5.24 | 3.21 |
| Natural Gas CC (GW) | 19.96 | 6.83 | 21.61 | 38.18 | 21.53 | 29.89 | 79.62 | 57.82 | 6.12 |
| Natural Gas CT (GW) | 8.32 | 1.82 | 6.53 | 4.92 | 16.80 | 13.46 | 25.62 | 15.21 | 1.41 |
| Nuclear (GW) | - | 1.16 | 4.00 | 5.02 | 14.35 | 7.26 | 35.86 | 20.21 | 5.50 |
| Onshore Wind (GW) | 6.06 | 10.85 | 5.28 | 24.93 | 22.12 | 27.69 | - | 3.23 | 3.65 |
| Small Hydroelectric (GW) | 0.34 | 0.73 | 0.15 | 0.02 | 0.48 | 0.14 | 0.25 | 0.26 | 0.83 |
| Solar Photovoltaic (GW) | 12.31 | 0.54 | 7.72 | 0.60 | 1.26 | 1.94 | 8.50 | 2.97 | 1.63 |

Table S20. Regional cost multipliers for investment cost of new power generation technologies according to region as obtained from the electricity market module in EIA's Annual Energy Outlook (AEO) 2021 [16]. CC = Combined Cycle. CT = Combustion Turbine. CCS = $CO_2$ capture and storage. The regional cost multipliers are applied to the baseline investment costs of each greenfield technology in Table S14 as model inputs for each region to account for regional variations of costs.

| Technology | CA | NW | SW | TX | NCEN | CEN | SE | MIDAT | NE |
|---|---|---|---|---|---|---|---|---|---|
| Natural Gas (CC) | 1.30 | 0.98 | 0.88 | 0.91 | 1.07 | 0.96 | 0.93 | 1.09 | 1.33 |
| Natural Gas (CC-CCS) | 1.07 | 0.95 | 0.86 | 0.95 | 1.02 | 0.96 | 0.96 | 1.01 | 1.10 |
| Natural Gas (CT) | 1.17 | 0.98 | 0.86 | 0.91 | 1.07 | 0.96 | 0.93 | 1.03 | 1.22 |
| Nuclear | 1.22 | 1.09 | 1.02 | 0.97 | 1.08 | 1.02 | 1.00 | 1.03 | 1.19 |
| Solar | 1.07 | 0.99 | 0.98 | 0.96 | 1.01 | 0.97 | 0.97 | 1.00 | 1.07 |
| Land Based Wind | 1.89 | 1.11 | 0.96 | 0.94 | 1.12 | 0.96 | 1.10 | 1.18 | 1.39 |
| Offshore Wind | 1.15 | 1.00 | - | - | - | - | - | - | 1.00 |

| | | | | | | | | | |
|---|---|---|---|---|---|---|---|---|---|
| Battery | 1.04 | 1.03 | 1.01 | 1.01 | 1.00 | 1.01 | 1.02 | 1.00 | 1.02 |

Table S21. Uranium costs in 2022 dollars for nuclear power resources from EIA's AEO 2023 [29]. Costs for fossil natural gas in Table S35.

| Fuel Cost | CA | NW | SW | TX | NCEN | CEN | SE | MIDAT | NE |
|---|---|---|---|---|---|---|---|---|---|
| Uranium ($/MMBtu) | 0.71 | 0.71 | 0.71 | 0.71 | 0.71 | 0.71 | 0.71 | 0.71 | 0.71 |

Table S22. Capacity reserve margin considered for each region based on the planning reserve margin constraint. The data sourced from IPM allocations based on electric reliability reports from NERC [7]. The planning reserve margin constraint enforces the need to procure "firm" generation capacity in excess of demand by the specified amount (i.e. reserve margin), where firm capacity contribution of each resource is calculated by either derating its installed capacity (in case of thermal plants) or available generation (in case of non-dispatchable resources like renewables and energy storage and flexible demand).

| | CA | NW | SW | TX | NCEN | CEN | SE | MIDAT | NE |
|---|---|---|---|---|---|---|---|---|---|
| Capacity Reserve Margin | 0.16 | 0.16 | 0.15 | 0.14 | 0.16 | 0.12 | 0.15 | 0.17 | 0.16 |

Table S23. Unit commitment parameters for resources. Parameters from nuclear power generators obtained from [17], [18], existing gas power generators from [13], new gas power generators from[19]. For NG-based H2 technologies, start cost and minimum up and down time not modeled, and ramping rates are assumed. Nameplate capacity contributes to the capacity reserve margin (CRM) constraint based on the respective derating factor of each technology, except for electrolyzers where its electricity consumption is the contributing factor. More information on the CRM can be found in the MACRO model documentations [20].

| Technology | Start cost ($/MW) | Min up time (h) | Min down time (h) | Max hourly ramping rate (% of nameplate capacity) | Min output (% of nameplate capacity) | Max output (% of nameplate capacity) | Derating factor for capacity reserve margin |
|---|---|---|---|---|---|---|---|
| Existing Natural Gas (CC) Power Generator | 111 | 6 | 6 | 64% | 10% - 60% | 100% | 0.93 |
| Existing Natural Gas (CT) Power Generator | 131 | 1 | 1 | 64% | 12% - 52% | 100% | 0.93 |
| Existing Nuclear Power Generator | 1,130 | 36 | 36 | 25% | 50% | 100% | 0.93 |

| | | | | | | | |
|---|---|---|---|---|---|---|---|
| New Natural Gas (CC) Power Generator | 69 | 4 | 4 | 100% | 30% | 100% | 0.93 |
| New Natural Gas (CC-CCS) Power Generator | 110 | 4 | 4 | 100% | 50% | 100% | 0.93 |
| New Natural Gas (CT) Power Generator | 158 | - | - | 100% | 25% | 100% | 0.93 |
| New Nuclear Power Generator | 1,130 | 36 | 36 | 25% | 30% | 100% | 0.93 |
| SMR-CCS H2 Resource | - | - | - | 50% | 85% | 90% | - |
| ATR-CCS Resource | - | - | - | 50% | 85% | 90% | - |
| Electrolyzer | - | - | - | 100% | 10% | 90% | 0.95 |
| Direct air capture technologies | | | | 100% | 85% | 90% | - |
| All fuels production technologies | - | - | - | 100% | 85% | 90% | - |

Table S24. $H_2$ pipeline data obtained from Hydrogen Delivery Scenario Analysis Model (HDSAM) v2 from Argonne National Laboratory for 100 km pipelines with 20 tonne $H_2$/h capacity [21]. HDSAM also provided the pipeline loss fraction, as well as the investment and operational costs, and energy requirements of 2 required compressors per 100 km that were included in the model inputs. This translates into an investment cost of $2228/MW-mile. Discount rate for annualization is 4.5%. Unless otherwise reported, all costs are in 2022 dollars. The total number of $H_2$ pipes (modeled as a continuous variable) along each line will be determined by the model based on the capacity requirement of $H_2$ transportation respectively. Candidate pipelines paths (i.e. regional source-sink pairs) and pipeline lengths are the same as power transmission network shown in Figure S24.

| Technology | Lifetime | Pipeline Investment Cost ($/MW $H_2$-mile) | Pipeline Annualized Investment Cost ($/MW $H_2$-mile/y) |
|---|---|---|---|
| $H_2$ Pipeline | 30 | 2,228 | 137 |

Table S25. Weighted regional average annual capacity factor and maximum available capacity expansion of greenfield variable renewable energy (VRE). VRE profiles were quantified using ZEPHYR (Zero-emissions Electricity system Planning with HourlY operational Resolution), a public repository where solar and wind site capacities and variability profiles were generated using historical weather data from 2011 from NREL NSRDB (National Solar Radiation Database) and WTK (WIND Toolkit) [22], [23], [24], to be consistent with the weather year in the Net-Zero America power demand profiles [4]. Together with the input of existing transmission line capacity data from NREL ReEDS (Regional Energy Development Model), the ZEPHYR model generates the available land area for solar and wind power development and determines the interconnection cost of each site (spur-line to substation and trunk-line reinforcement to urban areas) [14]. For each state, three bins (supply curves) containing hourly capacity factor, maximum capacity expansion, and interconnection transmission costs each for wind and solar resources were obtained. In ZEPHYR, state-level data was obtained by utilizing 4x4 km grids and translating hourly wind speed and irradiance into capacity factors using data from NSRDB and WTK respectively. National parks, urban areas, mountains, water bodies, and native land were excluded from the available area for greenfield VRE development, The maximum capacity expansion were obtained by multiplying the available area for VRE development by power generation density of 28 MW/km2 in wind and 1.6 MW/km2 in solar sites respectively [25]. For regions with a single state such as CA and TX, all 3 bins were utilized to represent a diverse choice of VRE availability. On the other hand, in regions with multiple states, the first bin of each state within that region was utilized (For example, NE region with 7 states modeled will have 7 bins of solar and wind resources each). The interconnection transmission cost of each bin was added onto the investment cost of greenfield wind and solar technology from NREL ATB in Table S14 as the model inputs. The weighted average capacity factor presented here are based on the 26 weeks model inputs after time domain reduction was performed on the VRE capacity factor profiles of 2011. The capacity factor in each hour of the 26 representative weeks was multiplied by their respective time weight, and weighted average across the total maximum capacity expansion of the bins utilized in each zone.

| Region | CA | NW | SW | TX | NCEN | CEN | SE | MIDAT | NE |
|---|---|---|---|---|---|---|---|---|---|
| Weighted Average Capacity Factor | | | | | | | | | |
| Solar | 0.31 | 0.25 | 0.31 | 0.30 | 0.22 | 0.26 | 0.26 | 0.22 | 0.20 |
| Land Based Wind | 0.26 | 0.39 | 0.39 | 0.46 | 0.46 | 0.47 | 0.36 | 0.40 | 0.43 |
| Maximum Capacity Expansion (GW) | | | | | | | | | |
| Solar | 5,953 | 8,913 | 9,404 | 18,172 | 10,908 | 9,021 | 8,503 | 4,328 | 2,738 |
| Land Based Wind | 340 | 945 | 736 | 1,038 | 811 | 864 | 671 | 338 | 206 |

## S3.3. $CO_2$ sector

Table S26. Cost and assumptions for DAC technologies obtained from NETL techno-economic study [26], [27]. NGCC = Natural gas combined cycle power plant, CCS = $CO_2$ capture and storage. DAC technologies with NGCC CCS are self-sufficient by producing electricity in a built-in NGCC unit and capturing natural gas combustion emissions using CCS. In the case of solvent DAC (with NGCC CCS), excess electricity is exported to grid. Investment and fixed operation and maintenance (FOM) costs are based on DAC input $CO_2$ capacity (tonne $CO_2$/h). A minimum and maximum operation output of 85% - 90% built capacity is enforced for all industrial processes. A discount rate of 4.5% is used to annualize investment costs and costs are converted to 2022 dollars.

| Technology | Lifetime (year) | Investment cost ($/($tCO_2$/h)) | Annualized CAPEX ($/($tCO_2$)/h)/y) | Fixed operation and maintenance (FOM) cost ($/($tCO_2$/h)/y) | Variable operation and maintenance (VOM) cost ($/$tCO_2$) | Electricity input (MWh/$tCO_2$) | Natural gas input (MMBtu/$tCO_2$) |
|---|---|---|---|---|---|---|---|
| Solvent DAC (with NGCC CCS) | 30 | 15,579,017 | 956,420 | 422,596 | 64 | -0.13 | 10.40 |
| Sorbent DAC (Electricity) | 30 | 17,138,793 | 1,052,177 | 837,003 | 25 | 4.38 | - |

Table S27. $CO_2$ emissions and $CO_2$ captured for DAC with built-in NGCC CCS based on a natural gas fuel emission factor of 0.0536 $tCO_2$ /MMBtu [3]. Deployment of DAC with NGCC CCS will lead to additional $CO_2$ being stored due to $CO_2$ capture of NGCC emissions.

| Technology | NGCC combustion emissions ($tCO_2$ /$tCO_2$ captured by DAC) | NGCC $CO_2$ capture rate (%) | Total $CO_2$ captured ($tCO_2$ /$tCO_2$ net removal by DAC) |
|---|---|---|---|
| Solvent DAC (with NGCC CCS) | 0.01 | 99 | 1.55 |

Table S28. $CO_2$ pipeline cost assumptions obtained from 2019 National Academies report on negative emissions technologies [28]. The report also included the pipeline loss fraction, as well as operational costs and energy requirement of 3 required pumps per 10 miles that were included in the model inputs. We assumed that investment cost of pumps is negligible. The total number of $CO_2$ pipes (modeled as a continuous variable) along each line will be determined by the model based on the capacity requirement of $CO_2$ transportation respectively. Discount rate for annualization is 4.5%. Unless otherwise reported, all costs are in 2022 dollars. Candidate pipelines paths (i.e. regional source-sink pairs) and pipeline lengths are the same as the power transmission network shown in Figure S24.

| Technology | $CO_2$ throughput (Mt CO2/y) | Lifetime | Pipeline Investment Cost ($/mile) | Pipeline Annualized Investment Cost ($/mile/y) |
|---|---|---|---|---|
| $CO_2$ Pipeline | 10 | 30 | 2,975,000 | 182,640 |

Table S29. Total number of $CO_2$ storage sites, total storage availability according to high and low sequestration scenarios as described in Figure 3A of the main text, weighted average maximum $CO_2$ injection rate, and weighted average cost of $CO_2$ injection (in 2022 dollars) in each region as shown in Figure S24. $CO_2$ geological sequestration sites in each region are obtained from NREL ReEDS (Regional Energy Development Model) [14], and represented as individual sites in each region in the MACRO model, creating a supply curve in MACRO where the cheapest sites would first be utilized, as shown in Figure S25.

| | CA | NW | SW | TX | NCEN | CEN | SE | MIDAT | NE |
|---|---|---|---|---|---|---|---|---|---|
| Number of modeled $CO_2$ storage sites in region | 19 | 37 | 39 | 24 | 15 | 9 | 11 | 1 | 0 |
| Total $CO_2$ storage availability – High sequestration (HS) scenarios (Mt $CO_2$/y) | 133.7 | 121.5 | 244.6 | 163.9 | 62.4 | 99.1 | 40.4 | 0.4 | 0 |
| Total $CO_2$ storage availability – Low sequestration (LS) scenarios (Mt $CO_2$/y) | 66.9 | 60.7 | 122.3 | 81.9 | 31.2 | 50.0 | 20.2 | 0.2 | 0 |
| Wt. average maximum $CO_2$ Injection Rate ($tCO_2$/h) | 84,089 | 25,052 | 64,450 | 41,773 | 63,993 | 84,126 | 27,980 | 1,155 | 0 |
| Wt. average cost of $CO_2$ Injection ($/$tCO_2$) | 7.35 | 11.47 | 7.76 | 6.72 | 8.19 | 7.69 | 7.57 | 7.9 | 0 |

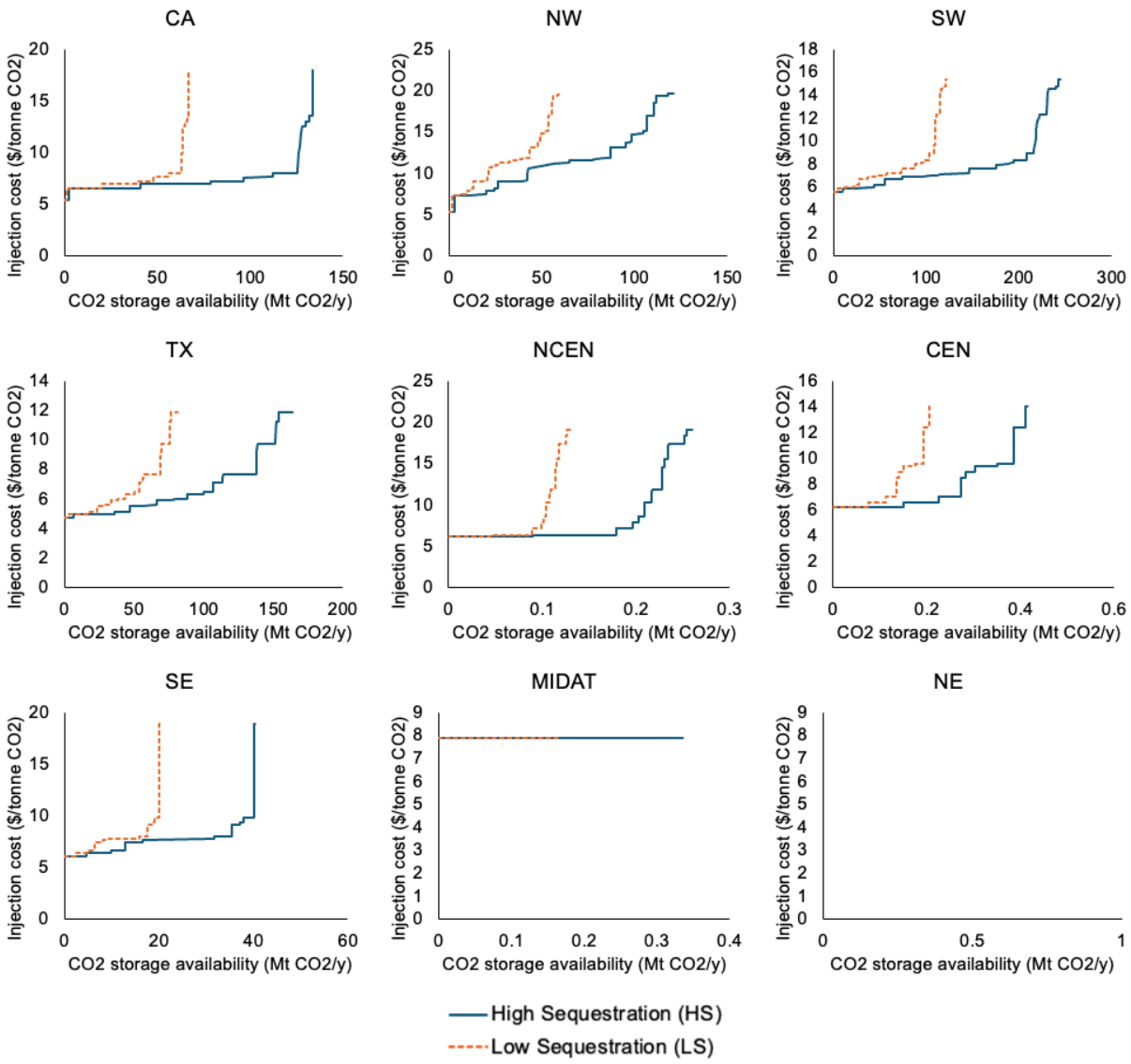


Figure S25. $CO_2$ sequestration supply curves according to regional $CO_2$ storage availability (Mt $CO_2$/y) and injection cost ($/tonne $CO_2$) using data from NREL ReEDS as described in Table S29 [14], for high sequestration (HS) and low sequestration (LS) scenarios as described in Figure 3A of the main text.

## S3.4. Liquid fuels sector

Table S30. Systemwide cost in 2022 dollars of fossil liquid fuels in 2050 based on EIA's AEO 2023 reference scenario [29].

| | Gasoline | Jet Fuel | Diesel |
|---|---|---|---|
| Fossil fuel cost ($/MMBtu) | 27.83 | 22.18 | 28.53 |

Table S31. Carbon content for fossil liquid fuels obtained from the GREET 2023 database [3].

| | Gasoline | Jet Fuel | Diesel | NG |
|---|---|---|---|---|
| Fossil fuel carbon content ($tCO_2$/MMBtu) | 0.0715 | 0.0722 | 0.0731 | 0.0536 |

Table S32. Lower and upper bounds on the fossil liquid supply distribution according to product yield of fossil gasoline, jet fuel, and diesel from U.S. refineries from 2009 – 2023 [30], used in Eq. S18 – S19 in Section S5.1 to represent realistic distributions of fossil liquid fuels in MACRO.

| | Jet Fuel/Gasoline (Min) | Diesel/Gasoline (Min) | Jet Fuel/Gasoline (Max) | Diesel/Gasoline (Max) |
|---|---|---|---|---|
| Fossil refinery constraint | 0.199 | 0.566 | 0.276 | 0.750 |

Table S33. Cost and modeling input assumptions for synthetic liquid fuel production technologies from $H_2$ and captured $CO_2$ obtained from Zang et al. as described in Section 2.2 and Figure 2B of the main text [31]. Processes are labeled as ("S" – Synthetic fuel), the dominant fuel product ( "J" – jet fuel), $CO_2$ capture rate ("CCX") if applicable, with "R" indicating the captured $CO_2$ is recycled back to the input $CO_2$ feed, effectively a high carbon conversion variant of the original process. "$CO_2$ capture rate" = rate of capture of carbon content that is not in fuels product (see Eq. S11 – S12 in Section S5.1: synthetic fuel carbon balance modeling in MACRO). Individual fuel production output is indicated (see Eq. S5 – S7 in Section S5.1: synthetic fuel energy balance modeling in MACRO). The synthetic fuel process is modeled without $CO_2$ capture in their original reference, and the approximation method elaborated in Section S2.2 was used to parameterize $CO_2$ capture variants of S-J-CC99 and S-J-CC99-R used in this study by estimating the additional costs and energy associated with capturing emissions from various flue gas streams. Input parameters might differ slightly from original references due to harmonization of energy and carbon balance for standardization for MACRO inputs as described in Section S2.3. A minimum and maximum operation output of 85% - 90% built capacity is enforced for all industrial processes. Cost assumptions are scaled according to per tonne $CO_2$ input basis and converted to 2022 dollars, a technology lifetime of 30 years and discount rate of 4.5% is used to annualize investment costs. Carbon balances of the processes are shown in Figure S35 in Section S4.

| Technology | Investment cost ($/(tonne $CO_2$ input/h)) | Annualized Investment cost ($/(tonne $CO_2$ input /h)/y) | Fixed operation and maintenance (FOM) cost ($/(tonne $CO_2$ input /h)/y) | Variable operation and maintenance (VOM) cost ($/tonne $CO_2$ input) | Electricity input (MWh/tonne $CO_2$ input) | $H_2$ input (MWh/tonne $CO_2$ input) | Gasoline output (MMbtu/ tonne $CO_2$ input) | Jet fuel output (MMbtu/ tonne $CO_2$ input) | Diesel output (MMbtu/ tonne $CO_2$ input) | $CO_2$ capture rate (%) |
|---|---|---|---|---|---|---|---|---|---|---|
| S-J | 4,522,542 | 277,646 | 240,597 | 9.66 | 0.04 | 3.68 | 1.69 | 3.06 | 1.79 | 0.0 |
| S-J-CC99 | 5,971,513 | 366,600 | 286,557 | 12.58 | 0.64 | 3.68 | 1.69 | 3.06 | 1.79 | 99.0 |
| S-J-CC99-R | 12,500,587 | 767,430 | 599,869 | 26.33 | 1.34 | 7.70 | 3.54 | 6.40 | 3.75 | 0.0 |

Table S34. Cost and modeling assumptions for biofuel technologies obtained from the literature as described in Section 2.2 and Figure 2B of the main text. Processes are labeled as ("B" - Biofuel), the dominant fuel product ("G" – gasoline [32], "J" – jet fuel [33], "D" – diesel [34]), $CO_2$ capture rate ("CCX") if applicable. "$CO_2$ capture rate" = rate of capture of biomass carbon content that is not in fuels product (see Eq. S13 – S14 in Section S5.1: biofuel carbon balance modeling in MACRO). "Biomass energy converted to fuels product" = the percentage of biomass energy converted into biofuels based on higher heating value basis with individual fuel shares indicated in the adjacent columns (see Eq. S8 – S10 in Section S5.1: biofuel energy balance modeling in MACRO). Amount of carbon captured and bioenergy produced would differ across biomass types and regions according to their respective carbon and energy content as shown in Table S38 and Table S39. Certain biofuel technologies (B-G and B-D) were not modeled with $CO_2$ capture in their original references, and the approximation method elaborated in Section S2.2 was used to parameterize $CO_2$ capture variants used in this study: B-G-CC31, B-G-CC99, B-D-CC53, B-D-CC99 by estimating the additional costs and energy associated with capturing emissions from various flue gas streams. In the case of B-J technologies, the $CO_2$ capture variants (B-J-CC75, B-J-CC84, B-J-CC99) were already parameterized in the original reference, and excess electricity is exported to grid as indicated by "Biomass energy converted to electricity" = the percentage of biomass energy converted to electricity on higher heating value basis (see Eq. S22: biofuel power balance in MACRO). Input parameters might differ slightly from original references due to harmonization of energy and carbon balance for MACRO inputs as described in Section S2.3. A minimum and maximum operation output

of 85% - 90% built capacity is enforced. Cost assumptions are scaled to per tonne biomass input basis and converted to 2022 dollars, a technology lifetime of 30 years and discount rate of 4.5% is used to annualize investment costs. Carbon balances of the processes are shown in Figure S32 to Figure S34 in Section S4.

| Technology | Investment cost ($/(tonne biomass/h)) | Annualized Investment cost ($/(tonne biomass/h)/y) | Fixed operation and maintenance (FOM) cost ($/(tonne biomass/h)/y) | Variable operation and maintenance (VOM) cost ($/tonne biomass) | Electricity input (MWh/tonne biomass) | $CO_2$ capture rate (%) | Biomass energy converted to fuels product (% HHV) | Gasoline (% fuels product) | Jet fuel (% fuels product) | Diesel (% fuels product) | Biomass energy converted to electricity (% HHV) |
|---|---|---|---|---|---|---|---|---|---|---|---|
| B-G | 5,799,717 | 356,054 | 283,503 | 22.04 | 0.00 | 0.0 | 37.90 | 100.00 | 0.00 | 0.00 | 0.00 |
| B-G-CC31 | 7,079,612 | 434,628 | 354,088 | 23.59 | 0.10 | 31.0 | 37.90 | 100.00 | 0.00 | 0.00 | 0.00 |
| B-G-CC99 | 9,618,367 | 590,486 | 434,614 | 28.74 | 1.16 | 99.3 | 37.90 | 100.00 | 0.00 | 0.00 | 0.00 |
| B-J-CC75 | 12,320,949 | 756,402 | 344,509 | 49.22 | 0.00 | 74.8 | 32.27 | 18.33 | 81.67 | 0.00 | 14.53 |
| B-J-CC84 | 12,774,703 | 784,259 | 351,017 | 50.29 | 0.00 | 83.9 | 42.47 | 18.30 | 81.70 | 0.00 | 4.63 |
| B-J-CC99 | 13,333,156 | 818,543 | 359,028 | 52.08 | 0.00 | 99.0 | 32.26 | 18.32 | 81.68 | 0.00 | 9.54 |
| B-D | 8,028,222 | 492,865 | 547,340 | 0.00 | 2.87 | 0.00 | 50.40 | 24.55 | 25.31 | 50.14 | 0.00 |
| B-D-CC53 | 8,918,107 | 547,496 | 596,415 | 1.06 | 2.94 | 52.8 | 50.40 | 24.55 | 25.31 | 50.14 | 0.00 |
| B-D-CC99 | 10,496,429 | 644,392 | 646,477 | 4.26 | 3.60 | 99.5 | 50.40 | 24.55 | 25.31 | 50.14 | 0.00 |

## S3.5. NG sector

Table S35. Regional cost in 2022 dollars of fossil natural gas based on EIA's AEO 2023 reference scenario, with modeled regions mapped to EIA's AEO fuel regions weighted by state-level demand from Net-Zero America [29].

| Region | CA | NW | SW | TX | NCEN | CEN | SE | MIDAT | NE |
|---|---|---|---|---|---|---|---|---|---|
| Fossil Natural Gas ($/MMBtu) | 8.85 | 8.11 | 6.89 | 4.89 | 6.09 | 5.62 | 6.59 | 6.33 | 7.61 |

Table S36. Cost and modeling assumptions for synthetic NG production is based on a TEA study of $CO_2$ methanation process [35], operation costs are assumed to be negligible in the methanation process, and $CO_2$ capture variant was not characterized due to high carbon conversion (96.6%). Carbon balance in Figure S37 in Section S4.

| Technology | Investment cost ($/(tonne $CO_2$ input/h)) | Annualized Investment cost ($/(tonne $CO_2$ input /h)/y) | Electricity input (MWh/tonne $CO_2$ input) | $H_2$ input (MWh/tonne $CO_2$ input) | NG output (MMbtu/ tonne $CO_2$ input) |
|---|---|---|---|---|---|
| S-NG | 1,485,773 | 91,214 | 0.29 | 7.17 | 18.01 |

Table S37. Cost and modeling input assumptions for bio-NG production technologies [36]. Processes are labeled as ("B" - Biofuel), the dominant fuel product ("NG" – natural gas), $CO_2$ capture rate ("CCX") if applicable. "$CO_2$ capture rate" = rate of capture of biomass carbon content that is not in fuels product. "Biomass energy converted to NG" = the percentage of biomass energy converted into NG based on higher heating value basis. Amount of carbon captured and bioenergy produced would differ across biomass types and regions according to their respective carbon and energy content as shown in Table S38 and Table S39. The original reference contains the B-NG and B-NG-CC40 (partial $CO_2$ capture) variant, and the approximation method elaborated in Section S2.2 was used to parameterize B-NG-CC99 by estimating the additional costs and energy associated with capturing emissions from the remaining flue gas stream in the B-NG-CC40 variant. Input parameters might differ slightly from original references due to harmonization of energy and carbon balance for standardization for MACRO inputs as described in Section S2.3. A minimum and maximum operation output of 85% - 90% built capacity is enforced for all industrial processes. Cost assumptions are scaled according to per tonne biomass input basis and converted to 2022 dollars, a technology lifetime of 30 years and discount rate of 4.5% is used to annualize investment costs. Carbon balances of the processes are shown in Figure S36 in Section S4.

| Technology | Investment cost ($/(tonne biomass/h)) | Annualized Investment cost ($/(tonne biomass/h)/y) | Fixed operation and maintenance (FOM) cost ($/(tonne biomass/h)/y) | Variable operation and maintenance (VOM) cost ($/tonne biomass) | Electricity input (MWh/tonne biomass) | $CO_2$ capture rate (%) | Biomass energy converted to NG (% HHV) |
|---|---|---|---|---|---|---|---|
| B-NG | 14,138,646 | 867,993 | 500,251 | 9.04 | 0.21 | 0.00 | 51.60 |
| B-NG-CC40 | 16,534,444 | 1,015,075 | 586,131 | 9.76 | 0.25 | 39.51 | 51.20 |
| B-NG-CC99 | 18,327,293 | 1,125,141 | 646,258 | 14.86 | 0.98 | 99.11 | 51.20 |

## S3.6. Biomass sector

Table S38. Total biomass availability weighted average costs (in 2022 dollars) and properties (energy and carbon content) for biomass types (herbaceous, woody, and agricultural residue) in each region as shown in Figure S24 for high biomass (HB) scenarios as described in Figure 3A of the main text. Biomass availability, cost, and energy content are quantified using projected county-level 2040 biomass availabilities from the high mature market scenario in the 2023 Billion Ton Study [37]. The carbon content of each biomass type in each region was estimated by mapping the county-level biomass resources to similar feedstocks primarily from the GREET 2023 database as shown in Table S40 [3]. Biomass of the same type and costs within the same region were aggregated together and modeled as individual regional-level resources in MACRO, effectively creating regional supply curves for each biomass type in MACRO as shown in Figure S26 to Figure S28, where the cheapest biomass would be first purchased. The weighted average energy and carbon content of biomass types are used as MACRO inputs to model the energy and carbon balance of bioenergy processes built for a specific biomass type in a specific region (e.g. B-G-CC99 process consuming herbaceous biomass in NCEN region). according to Eq. S8 – S10 and Eq. S13 – S14 respectively.

| **High biomass availability (HB) scenarios** | **CA** | **NW** | **SW** | **TX** | **NCEN** | **CEN** | **SE** | **MIDAT** | **NE** |
|---|---|---|---|---|---|---|---|---|---|
| Total herbaceous biomass availability (Mt biomass /y) | 0.00 | 2.17 | 15.55 | 131.57 | 56.97 | 195.08 | 69.76 | 11.96 | 2.61 |
| Wt. avg. herbaceous biomass cost ($/t biomass) | 77.16 | 77.16 | 77.16 | 77.16 | 77.16 | 77.16 | 77.16 | 77.16 | 77.16 |
| Wt. avg. herbaceous biomass energy content (MMBtu/t biomass) | 18.19 | 18.23 | 18.11 | 18.15 | 18.34 | 18.23 | 18.20 | 18.30 | 18.37 |
| Wt. avg. herbaceous biomass carbon content ($tCO_2$/t biomass) | 1.72 | 1.73 | 1.71 | 1.71 | 1.74 | 1.72 | 1.72 | 1.74 | 1.75 |
| Total woody biomass availability (Mt/y) | 0.69 | 6.25 | 6.97 | 8.20 | 23.88 | 29.40 | 39.51 | 26.37 | 9.53 |
| Wt. average woody biomass cost ($/t) | 52.11 | 67.44 | 74.96 | 73.41 | 73.55 | 74.08 | 69.10 | 74.00 | 73.07 |
| Wt. avg. woody biomass energy content (MMBtu/t biomass) | 19.36 | 19.32 | 19.14 | 18.99 | 19.06 | 19.07 | 19.14 | 19.01 | 18.89 |
| Wt. avg. woody biomass carbon content ($tCO_2$/t biomass) | 1.84 | 1.82 | 1.80 | 1.82 | 1.80 | 1.80 | 1.82 | 1.81 | 1.83 |
| Total agricultural residue availability (Mt/y) | 4.89 | 6.30 | 2.42 | 4.01 | 111.61 | 50.03 | 7.63 | 6.19 | 1.79 |
| Wt. average agricultural residue cost ($/t) | 52.64 | 74.43 | 75.70 | 67.79 | 77.12 | 76.05 | 70.56 | 76.51 | 73.77 |
| Wt. avg. agricultural residue energy content (MMBtu/t biomass) | 18.29 | 16.72 | 17.03 | 16.59 | 17.30 | 17.17 | 17.23 | 17.28 | 17.48 |
| Wt. avg. agricultural residue carbon content ($tCO_2$/t biomass) | 1.72 | 1.66 | 1.69 | 1.63 | 1.71 | 1.70 | 1.69 | 1.71 | 1.72 |

Table S39. Total biomass availability weighted average costs (in 2022 dollars) and properties (energy and carbon content) for biomass types (herbaceous, woody, and agricultural residue) in each region as shown in Figure S24 for low biomass (LB) scenarios as described in Figure 3A of the main text. Biomass availability, cost, and energy content are quantified using projected county-level 2040 biomass availabilities from the low mature market scenario in the 2023 Billion Ton Study [37]. The carbon content of each biomass type in each region was estimated by mapping the county-level biomass resources to similar feedstocks primarily from the GREET 2023 database as shown in Table S40 [3]. Biomass of the same type and costs within the same region were aggregated together and modeled as individual regional-level resources in MACRO, effectively creating regional supply curves for each biomass type in MACRO as shown in Figure S29 to Figure S31, where the cheapest biomass would be first purchased. The weighted average energy and carbon content of biomass types are used as MACRO inputs to model the energy and carbon balance of bioenergy processes built for a specific biomass type in a specific region according to Eq. S8 – S10 and Eq. S13 – S14 respectively.

| **Low biomass availability (LB) scenarios** | **CA** | **NW** | **SW** | **TX** | **NCEN** | **CEN** | **SE** | **MIDAT** | **NE** |
|---|---|---|---|---|---|---|---|---|---|
| Total herbaceous biomass availability (Mt biomass /y) | - | 1.11 | 7.39 | 82.94 | 14.45 | 105.02 | 38.82 | 7.04 | 0.88 |
| Wt. avg. herbaceous biomass cost ($/t biomass) | - | 77.16 | 77.16 | 77.16 | 77.16 | 77.16 | 77.16 | 77.16 | 77.16 |
| Wt. avg. herbaceous biomass energy content (MMBtu/t biomass) | - | 18.10 | 18.10 | 18.12 | 18.35 | 18.20 | 18.16 | 18.16 | 18.35 |
| Wt. avg. herbaceous biomass carbon content ($tCO_2$/t biomass) | - | 1.71 | 1.71 | 1.71 | 1.74 | 1.72 | 1.72 | 1.72 | 1.75 |
| Total woody biomass availability (Mt/y) | 0.69 | 3.65 | 2.36 | 3.72 | 11.82 | 12.38 | 28.72 | 15.92 | 8.64 |
| Wt. average woody biomass cost ($/t) | 52.11 | 60.50 | 70.68 | 68.91 | 69.88 | 69.86 | 66.07 | 71.93 | 72.64 |
| Wt. avg. woody biomass energy content (MMBtu/t biomass) | 19.36 | 19.5 | 19.3 | 19.11 | 19.06 | 19.16 | 19.18 | 18.99 | 18.87 |
| Wt. avg. woody biomass carbon content ($tCO_2$/t biomass) | 1.84 | 1.84 | 1.82 | 1.83 | 1.82 | 1.81 | 1.83 | 1.82 | 1.83 |
| Total agricultural residue availability (Mt/y) | 4.76 | 5.27 | 1.76 | 3.44 | 76.84 | 42.34 | 7.62 | 7.82 | 1.74 |
| Wt. average agricultural residue cost ($/t) | 51.95 | 73.90 | 75.15 | 66.25 | 77.10 | 75.85 | 70.56 | 76.65 | 73.69 |
| Wt. avg. agricultural residue energy content (MMBtu/t biomass) | 18.33 | 16.76 | 16.97 | 16.48 | 17.28 | 17.14 | 17.23 | 17.30 | 17.51 |
| Wt. avg. agricultural residue carbon content ($tCO_2$/t biomass) | 1.72 | 1.67 | 1.68 | 1.62 | 1.71 | 1.70 | 1.69 | 1.71 | 1.72 |

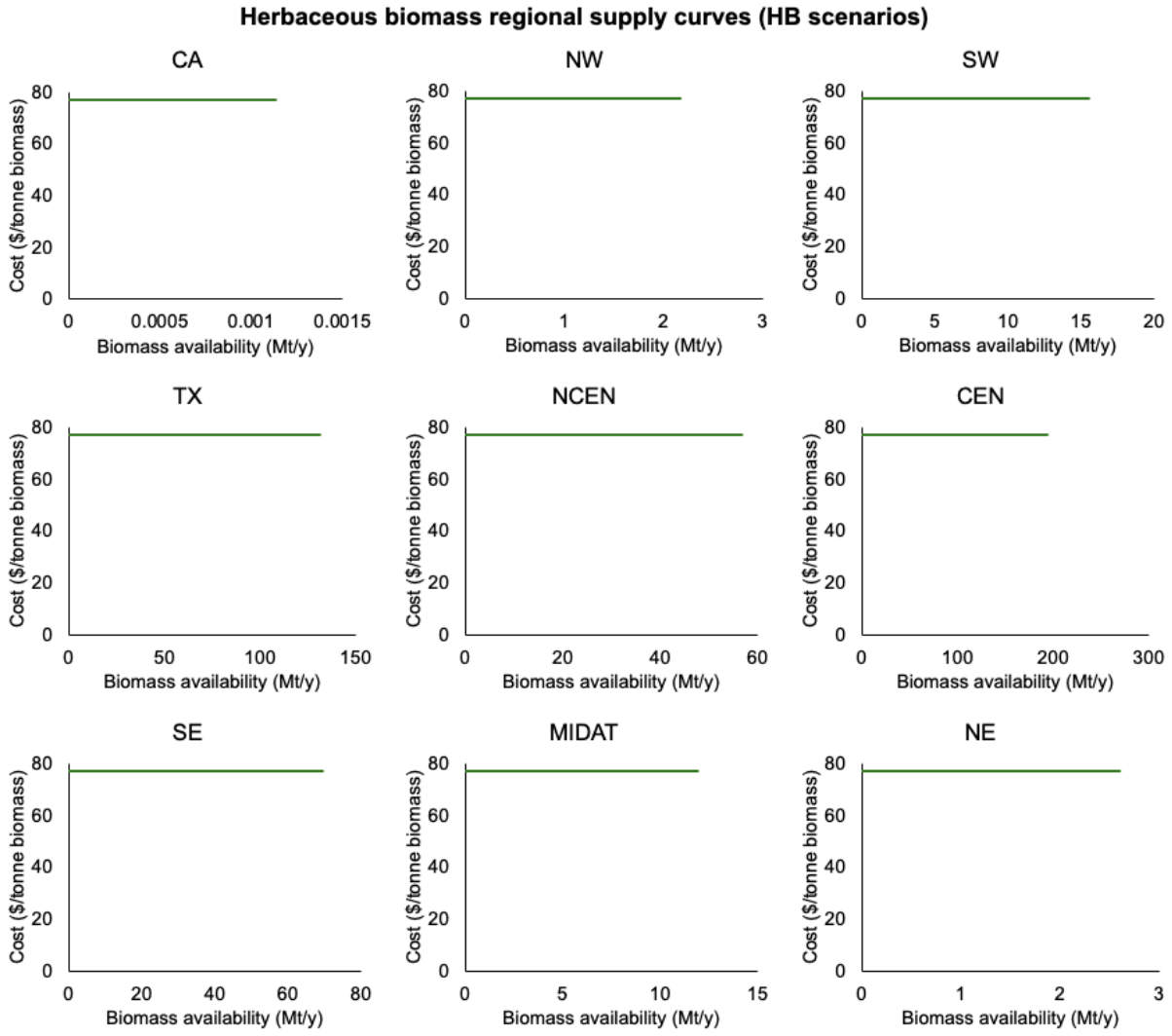


Figure S26. Supply curves for herbaceous biomass type according to biomass availability (Mt/y) and purchase cost ($/tonne biomass) as described in Table S38 for high biomass availability (HB) scenarios as described in Figure 3A of the main text, obtained from the 2023 Billion Ton Study [37].

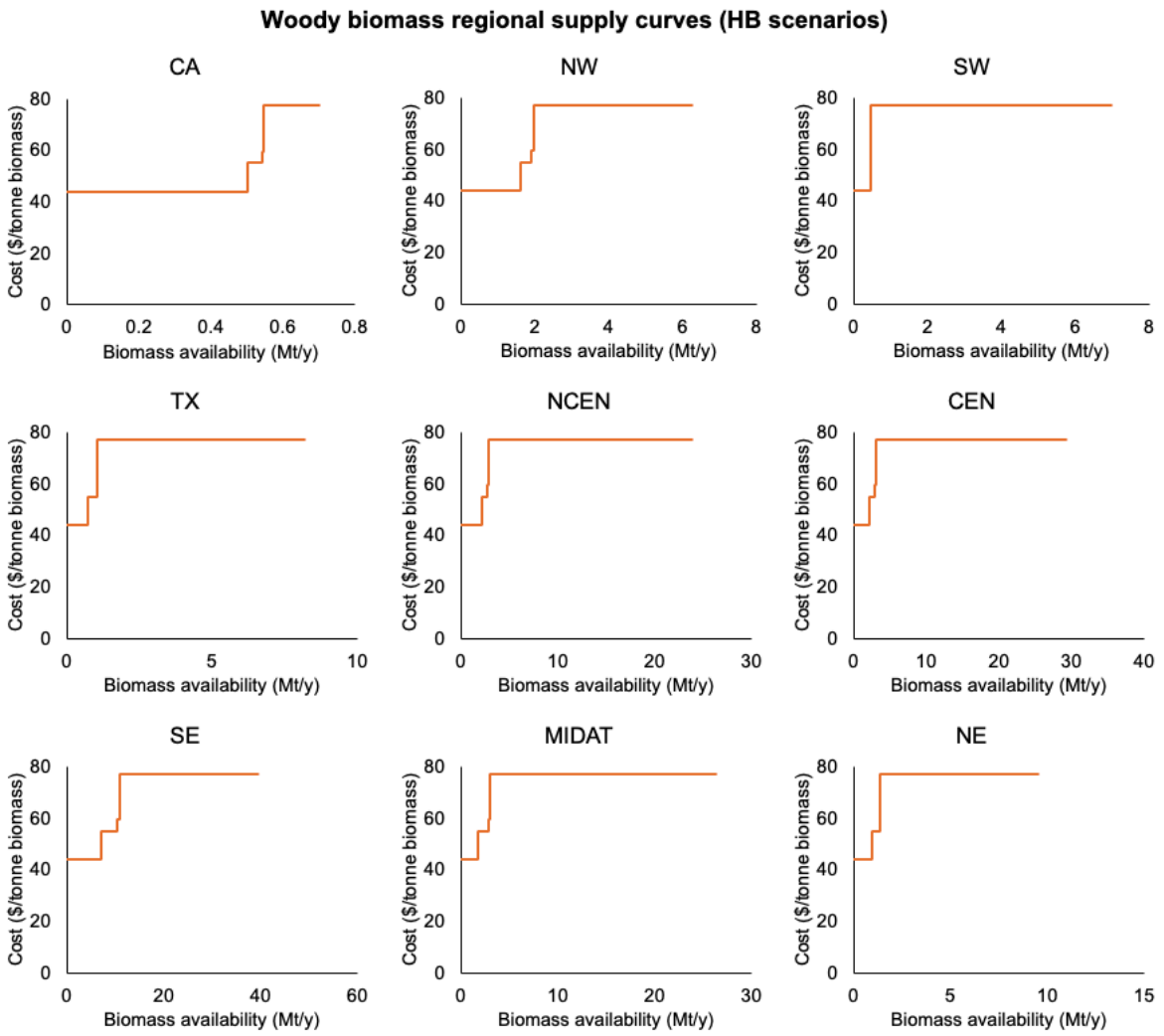


Figure S27. Supply curves for woody biomass type according to biomass availability (Mt/y) and purchase cost ($/tonne biomass) as described in Table S38 for high biomass availability (HB) scenarios as described in Figure 3A of the main text, obtained from the 2023 Billion Ton Study [37].

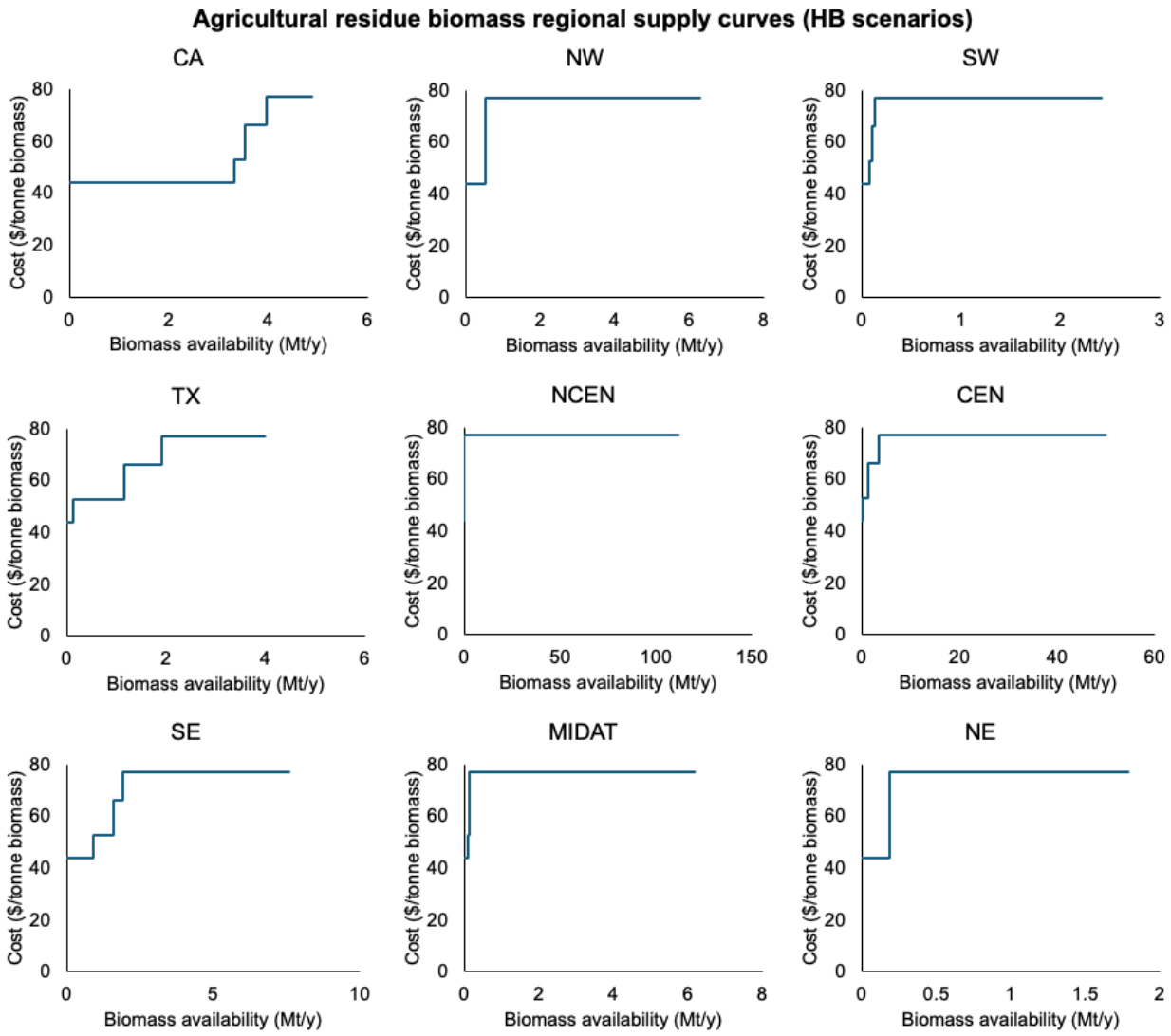


Figure S28. Supply curves for agricultural residue biomass type according to biomass availability (Mt/y) and purchase cost ($/tonne biomass) as described in Table S38 for high biomass availability (HB) scenarios as described in Figure 3A of the main text, obtained from the 2023 Billion Ton Study [37].

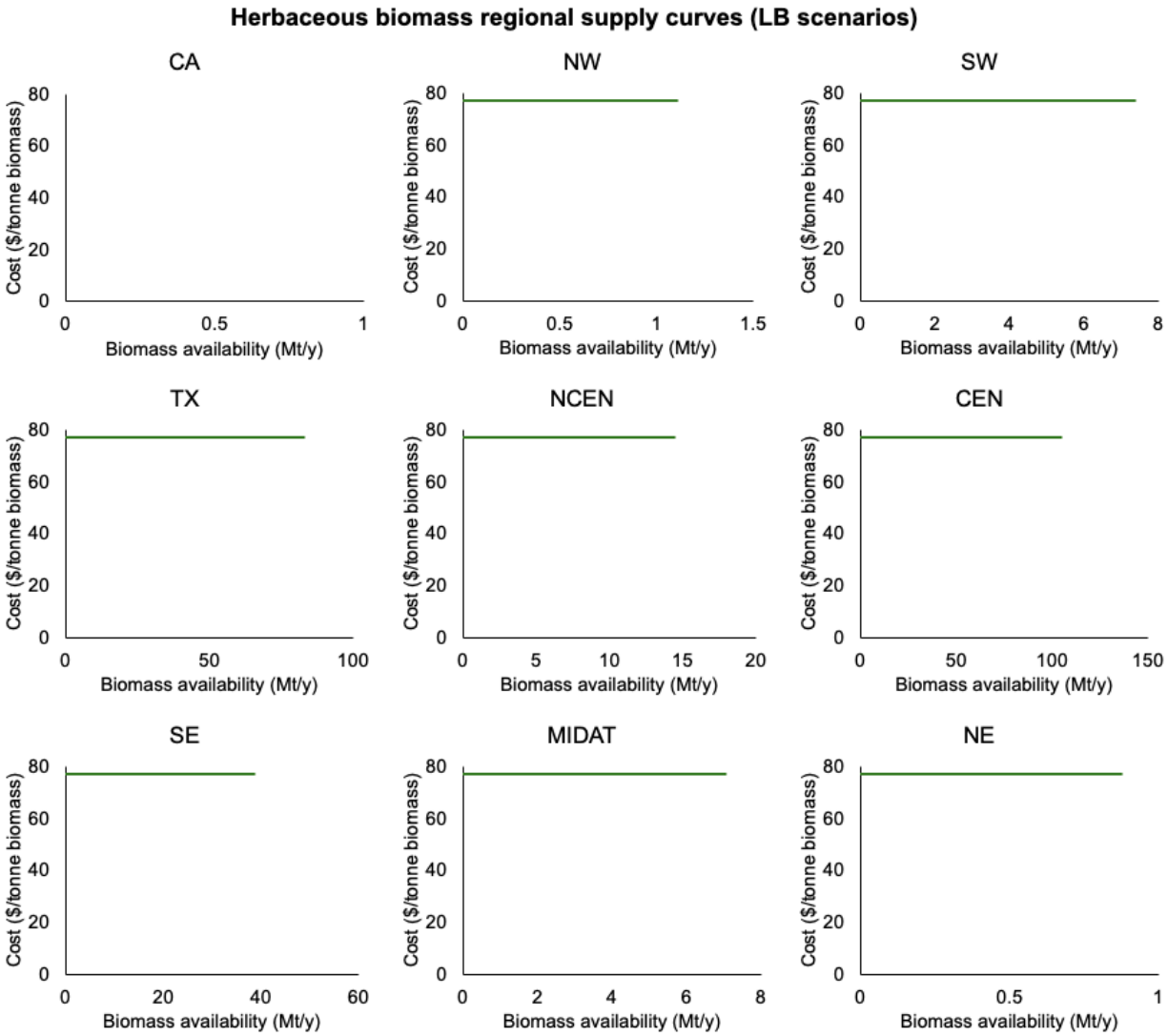


Figure S29. Supply curves for herbaceous biomass type according to biomass availability (Mt/y) and purchase cost ($/tonne biomass) as described in Table S39 for low biomass availability (LB) scenarios as described in Figure 3A of the main text, obtained from the 2023 Billion Ton Study [37].

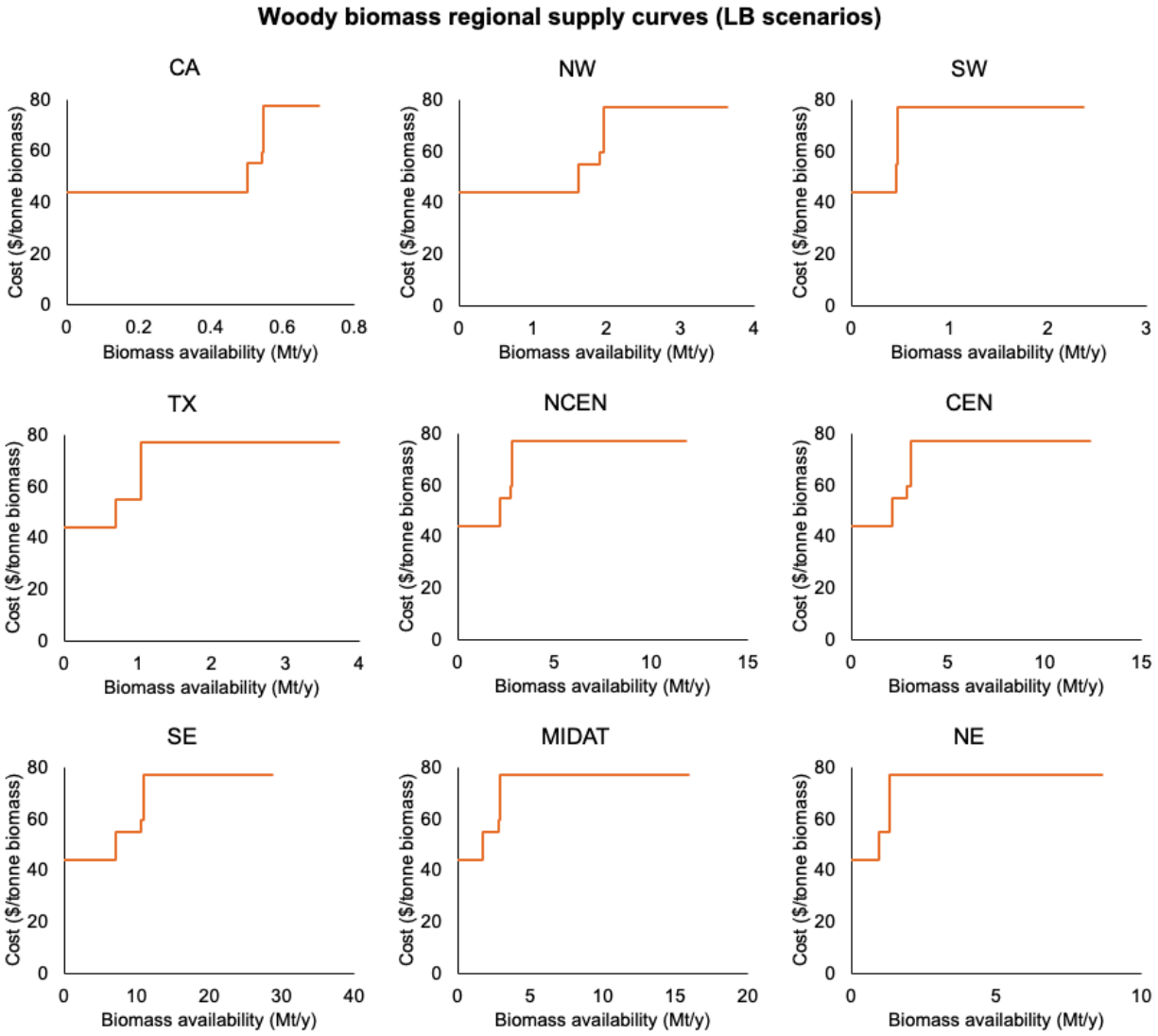


Figure S30. Supply curves for woody biomass type according to biomass availability (Mt/y) and purchase cost ($/tonne biomass) as described in Table S39 for low biomass availability (LB) scenarios as described in Figure 3A of the main text, obtained from the 2023 Billion Ton Study [37].

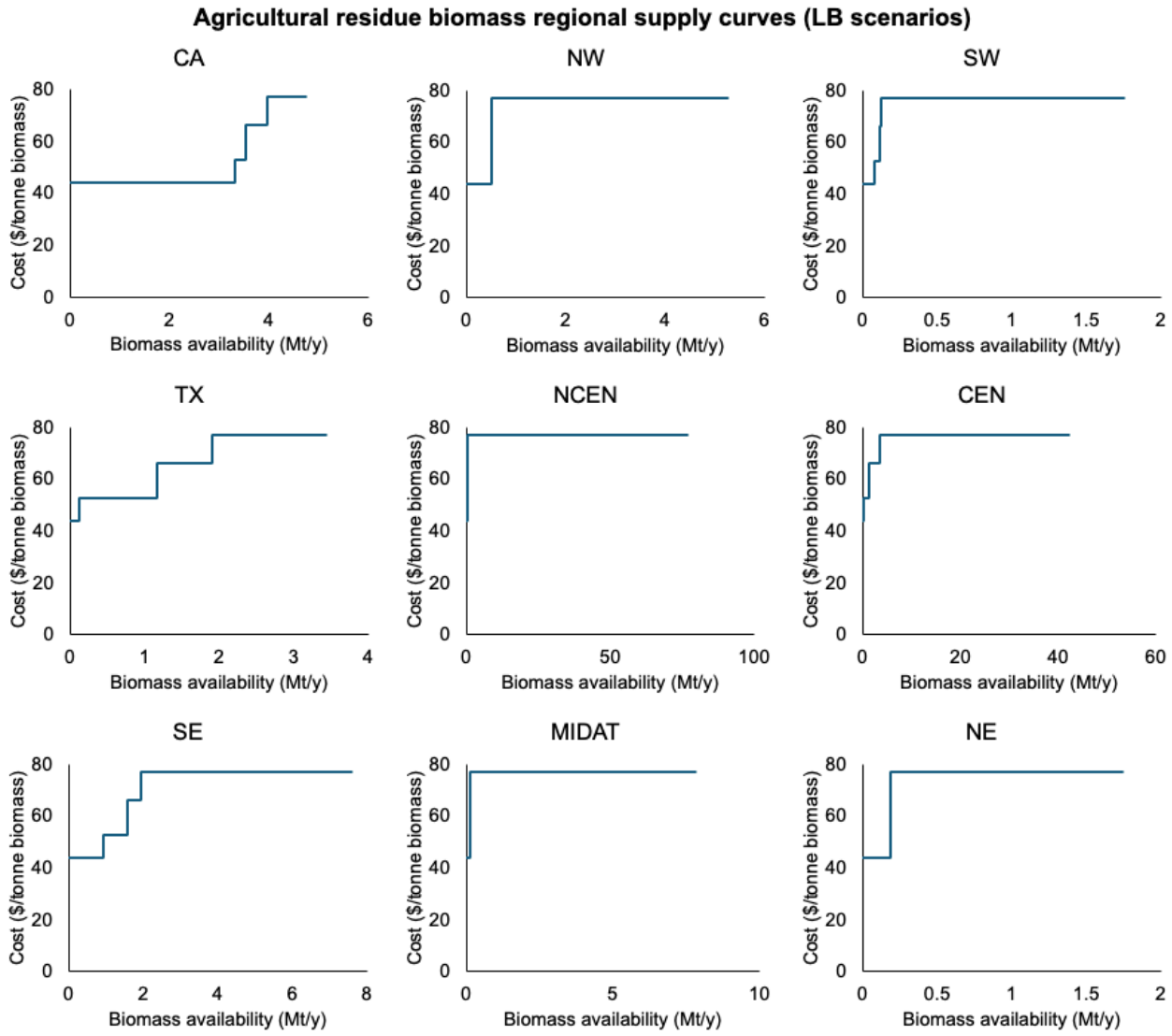


Figure S31. Supply curves for agricultural residue biomass type according to biomass availability (Mt/y) and purchase cost ($/tonne biomass) as described in Table S39 for low biomass availability (LB) scenarios as described in Figure 3A of the main text, obtained from the 2023 Billion Ton Study [37].

Table S40. Biomass carbon content (% wt.) according to species in various biomass types. County-level biomass data from the 2023 Billion-Ton Study contain information about these species-level biomass availabilities, which could be used to estimate regional weighted average carbon content of each biomass types for MACRO inputs. When possible, individual biomass species are mapped to an analogous feedstock in the GREET 2023 database to obtain their respective carbon contents as shown in the "Represented by" column. If no suitable representations are available in GREET 2023, values are taken from other cited literature in the "Reference" column.

| Biomass type | Individual biomass species | Represented by | Reference | Carbon % wt. |
|---|---|---|---|---|
| Herbaceous | Biomass sorghum | Sorghum | Bioenergy Feedstock Library [38] | 0.456 |
| | Miscanthus | Miscanthus | GREET 2023 [3] | 0.476 |
| | Energy cane | Energy cane | | 0.463 |
| | Switchgrass | Switchgrass | | 0.466 |
| Woody | Eucalyptus | Eucalyptus | | 0.492 |
| | Willow | Willow | | 0.487 |
| | Pine | Pine | | 0.501 |
| | Poplar | Poplar | | 0.501 |
| | Logging residual | Forest Residues | | 0.503 |
| | Forest processing waste | | | |
| | Fire reduction thinning | | | |
| | Other forest waste | | | |
| | Small diameter trees | Poplar | | 0.501 |
| Agricultural residue | Corn stover | Corn stover | | 0.467 |
| | Sorghum stubble | Forage sorghum bagasse | | 0.420 |
| | Pruning Residuals | Yard Trimming Waste | | 0.478 |
| | Wheat Straw | Wheat Straw | Bioenergy Feedstock Library [38] | 0.450 |
| | Oats Straw | | | |
| | Rice Straw | | | |
| | Cotton field residue | Cotton Stalk | Tao et al. [39] | 0.460 |
| | Cotten gin trash | Cotton gin | Subramani et al. [40] | 0.410 |
| | Rice hulls | Rice husk | AboDalam et al. [41] | 0.419 |

## S4. Carbon balance of biofuel and synthetic fuels technologies

This section shows carbon balances of biofuel and synthetic fuels production processes used in this study. For biofuel technologies, the carbon balances are calculated using biomass properties of 47.3% carbon content per biomass weight and 18.15 MMBtu/tonne energy content, which are the weighted average values from the high biomass (HB) scenario. The carbon content of fuel products are harmonized to those obtained from the GREET 2023 database shown in Table S31 as described in Section S2.3 [3], and might differ from carbon balances from their original reference TEAs.

Carbon conversion is not a technology input parameter in the MACRO model. Instead, biofuel production technologies are modeled using energy conversion efficiency and product distribution inputs as described in Section S5.1 (see Eq. S8 – S10) using energy conversion efficiency of individual biofuel technologies shown in Table S34. As such, the actual carbon conversion might differ according to biomass type consumed as shown in Table S38 and Table S39.

Dashed boxes in the carbon balance indicate $CO_2$ capture units estimated by applying the approximation method of matching the $CO_2$ concentrations of the flue gas stream(s) in each pathway to analogous industrial point sources $CO_2$ capture units as described in Section S2.2, and applying the corresponding capture rate to quantify the amount of $CO_2$ captured and emitted.

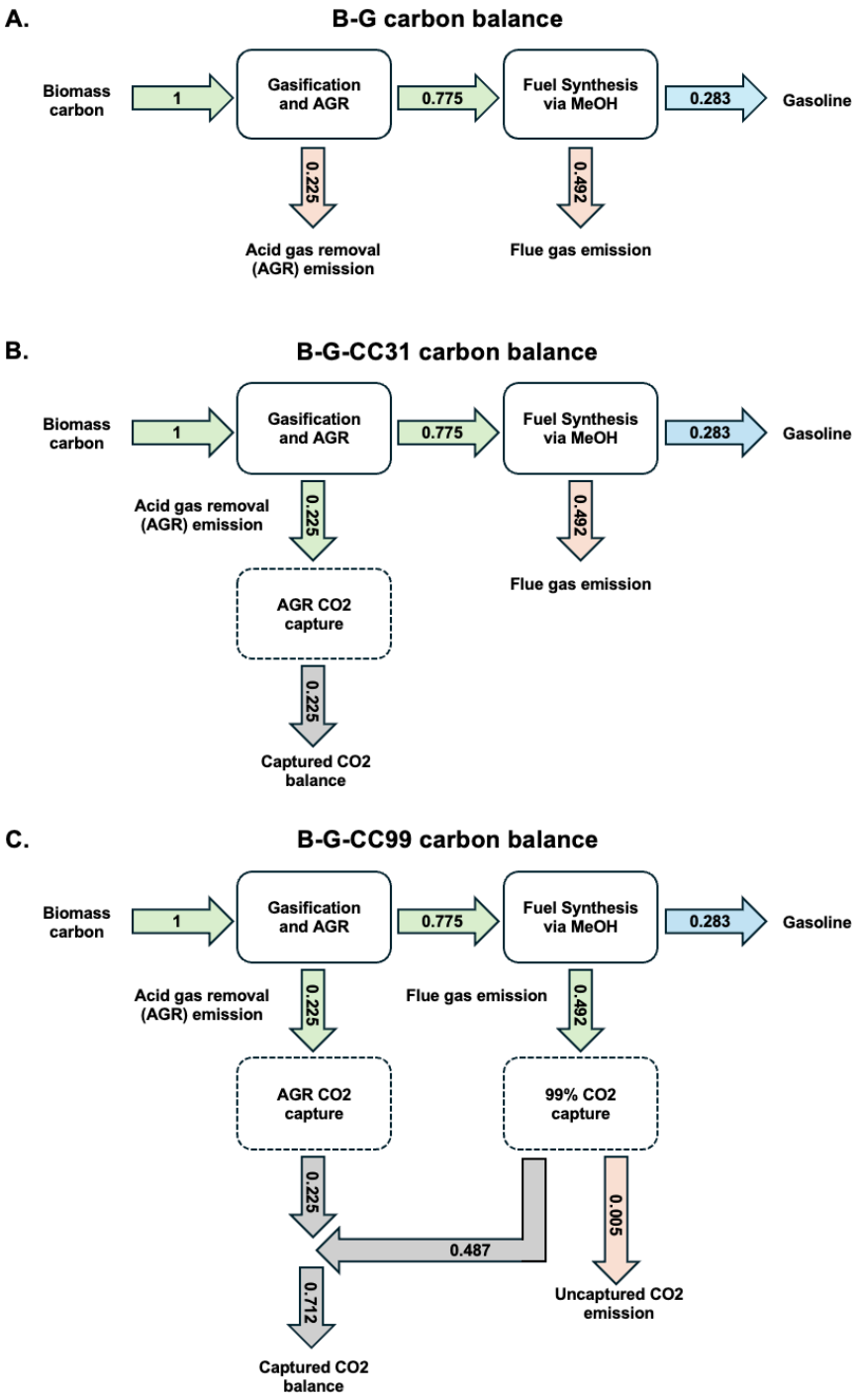


Figure S32. Carbon balance of B-G biofuel production technologies in Table S34, with box diagrams showing simplified process and carbon flows (normalized to % wt. basis). B-G is based on the SOT (state-of-technology) process configuration in the reference TEA by NREL for gasoline production from biomass gasification followed by methanol synthesis [32]. B-G-CC31 and B-G-CC99 are characterized by using the approximation method described in Section S2.2 by matching the $CO_2$ concentrations of various flue gas stream to analogous industrial point sources $CO_2$ capture units (represented by dashed boxes) from the original B-G configuration – The AGR $CO_2$ capture and 99% $CO_2$ capture units are based on ethanol and cement production $CO_2$ capture units respectively as shown in Table S11. Biomass properties of 47.3% carbon content per biomass weight and 18.15 MMBtu/tonne energy content were used to obtain this carbon balance.

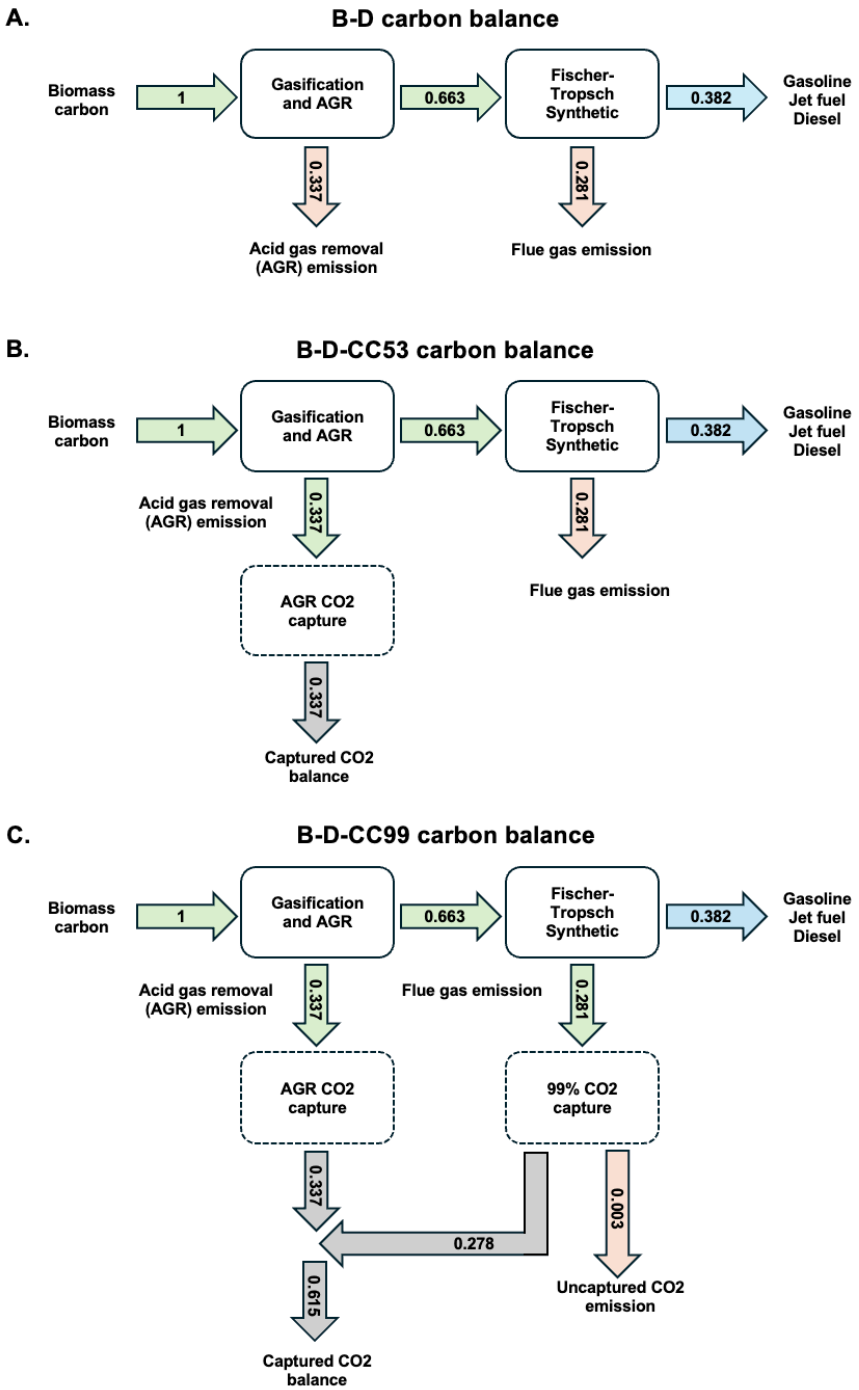


Figure S33. Carbon balance of B-D biofuel production technologies in Table S34, with box diagrams showing simplified process and carbon flows (normalized to % wt. basis). B-D is based on the CFB-FT (circulating fluidized bed Fischer-Tropsch) process configuration in the reference TEA by Dimitriou et al. for production of diesel (dominant product), jet fuel and gasoline (both side product) from biomass gasification followed by FT process [34]. B-D-CC53 and B-D-CC99 are characterized by using the approximation method described in Section S2.2 by matching the $CO_2$ concentrations of various flue gas stream to analogous industrial point sources $CO_2$ capture units (represented by dashed boxes) from the original B-D configuration – The AGR $CO_2$ capture and 99% $CO_2$ capture units are based on ethanol and cement production $CO_2$ capture units respectively as shown in Table S11. Biomass properties of 47.3% carbon content per biomass weight and 18.15 MMBtu/tonne energy content were used to obtain this carbon balance.

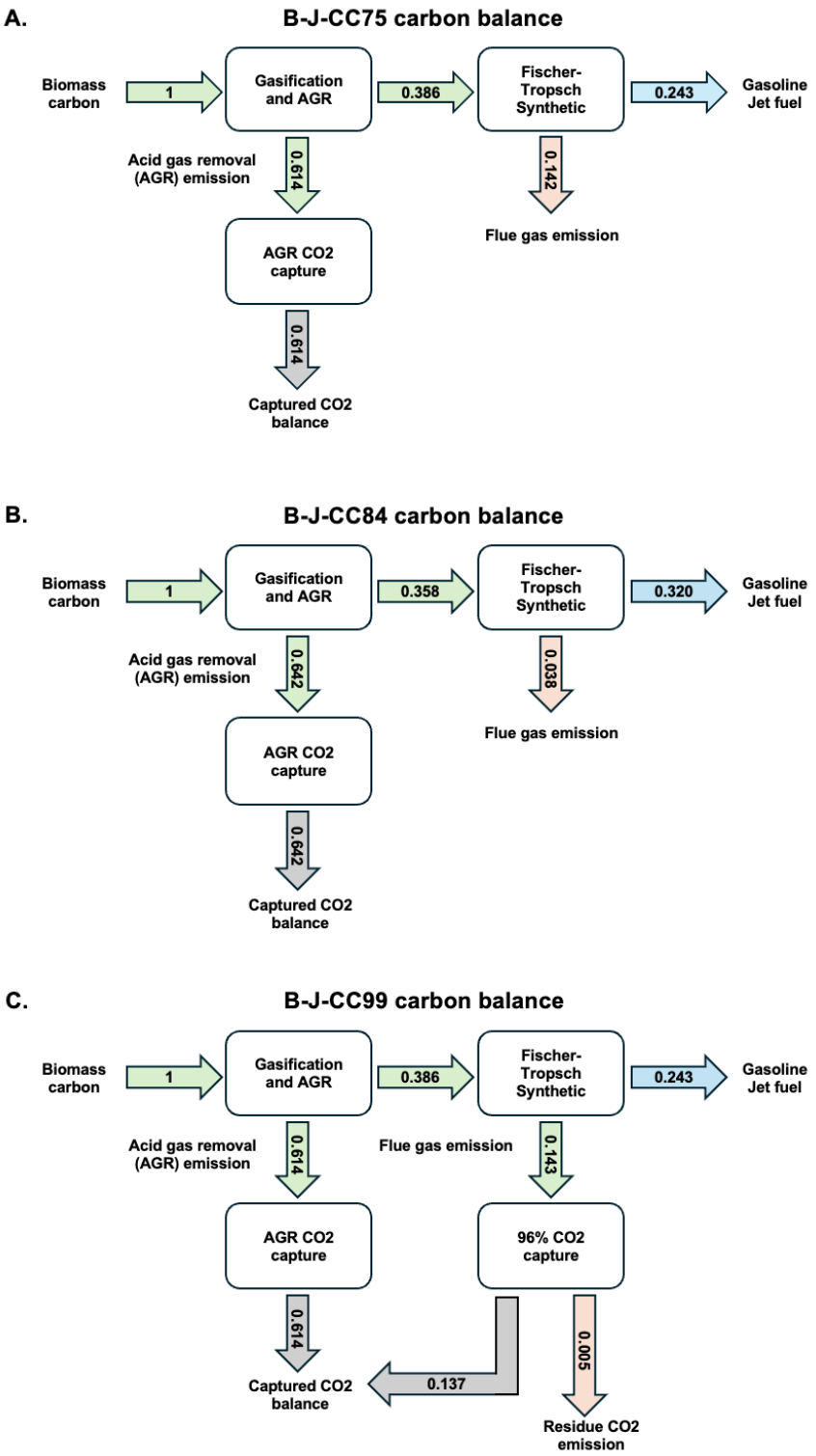


Figure S34. Carbon balance of B-J biofuel production technologies in Table S34, with box diagrams showing simplified process and carbon flows (normalized to % wt. basis). B-J-CC75, B-J-CC84 and B-J-CC99 are obtained from the original process configurations of OT-B, RC-B, and OTA-B in the reference TEA by Kreutz et al. for production of jet fuel (dominant product) and gasoline (side product) from biomass gasification followed by FT process [33]. Biomass properties of 47.3% carbon content per biomass weight and 18.15 MMBtu/tonne energy content were used to obtain this carbon balance.

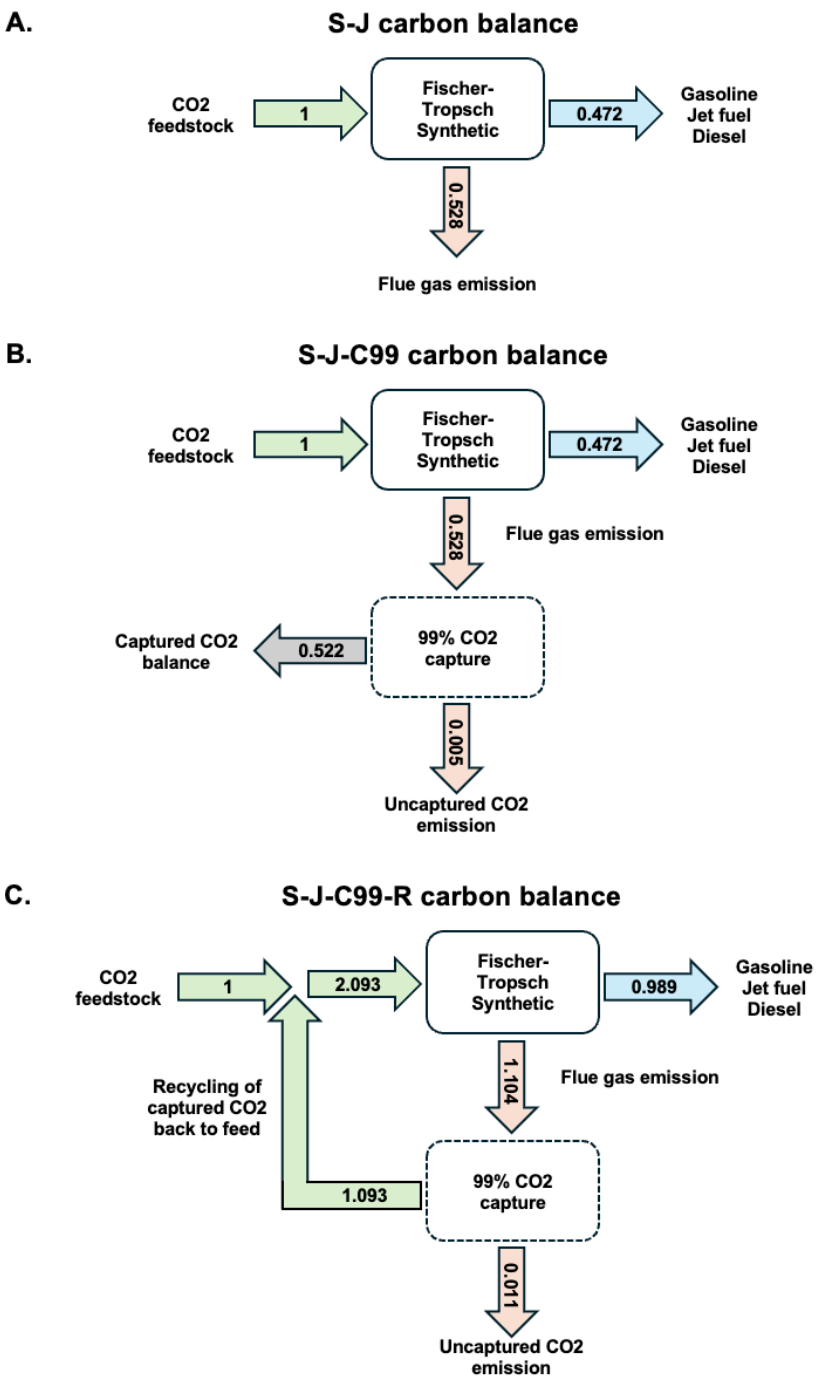


Figure S35. Carbon balance of S-J synthetic fuel production technologies in Table S33, with box diagrams showing simplified process and carbon flows (normalized to % wt. basis). S-J is based on the FT process in the reference TEA by Zang et al. for production of jet fuel (dominant product), gasoline and diesel (both side product) from $H_2$ and $CO_2$ feedstocks [31]. S-J-CC99 is characterized by using the approximation method described in Section S2.2 by matching the flue gas stream to an analogous industrial point source (represented by dashed box) from the original S-J configuration – The 99% $CO_2$ capture unit is based on a cement production $CO_2$ capture unit as shown in Table S11. The S-J-CC99-R configuration is characterized by assuming the recycling of captured $CO_2$ stream from S-J-CC99 into the input feedstock of the synthetic fuel production process, resulting in a high carbon conversion variant with additional $H_2$ and electricity inputs, and high fuels product output.

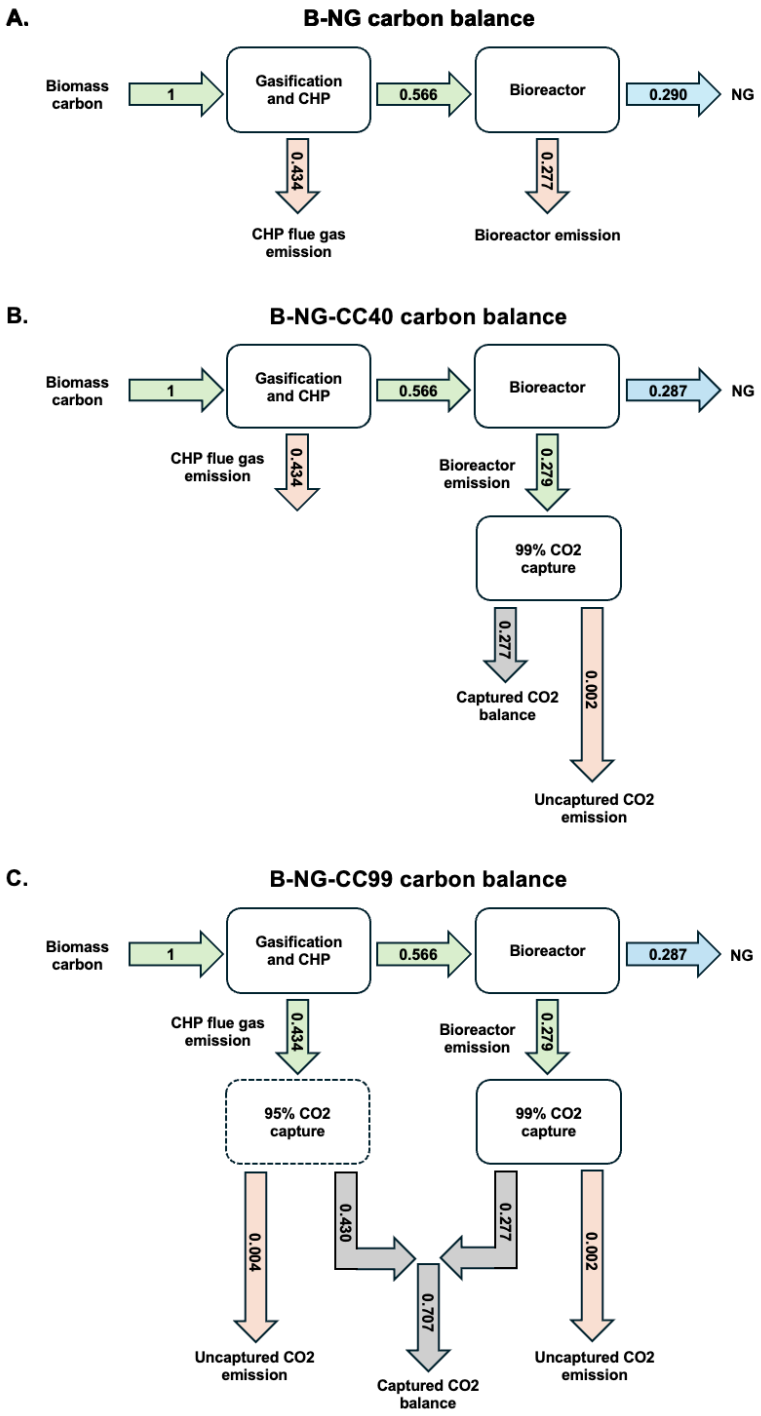


Figure S36. Carbon balance of B-NG production technologies in Table S37, with box diagrams showing simplified process and carbon flows (normalized to % wt. basis). B-NG and B-NG-CC40 is based on the process configurations with and without bioreactor flue gas $CO_2$ capture in the reference TEA by Michailos et al. for NG production from biomass gasification followed by fermentation [36]. B-NG-CC99 is characterized by using the approximation method described in Section S2.2 by matching the $CO_2$ concentrations of the CHP flue gas stream to an analogous industrial point source (represented by dashed box) from the original B-NG-CC40 configuration – The 95% $CO_2$ capture unit is based on a NGCC $CO_2$ capture unit as shown in Table S11. Biomass properties of 47.3% carbon content per biomass weight and 18.15 MMBtu/tonne energy content were used to obtain this carbon balance.

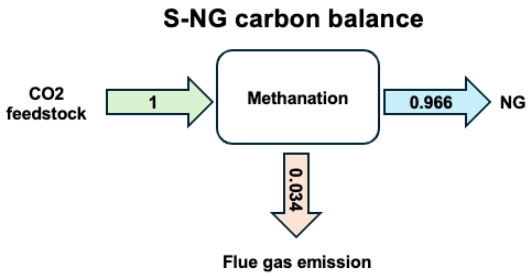


Figure S37. Carbon balance of S-NG production technology in Table S36 with box diagrams showing simplified process and carbon flows (normalized to % wt. basis). S-NG is based on the methanation process in the reference TEA by Kiani et al. for production NG from $H_2$ and $CO_2$ feedstocks [35]. Due to the high carbon conversion of 96.6%, $CO_2$ capture variants of S-NG were not necessary to be developed.

## S5. MACRO model

The documentations of the electricity, $H_2$, $CO_2$, and biomass sectors of the MACRO model are available in a public GitHub repository [20]. Existing bioenergy modeling in MACRO includes electricity generation and H2 production from biomass. The liquid fuels and natural gas supply chains add the modeling of liquid fuels (S5.1 and S5.2) and natural gas (S5.3) production from synthetic (electricity, $H_2$, and captured $CO_2$ as inputs) and biomass pathways, as well as the option of purchasing fossil fuels. S5.4 and S5.5 describe the changes made to the captured $CO_2$ balance constraint and $CO_2$ emission policy constraint in MACRO.

### S5.1 Liquid fuels supply chains modeling in MACRO

The liquid fuels supply chain in MACRO is modeled such that gasoline, jet fuel, and diesel can be produced by synthetic fuel and biofuel processes, as well as purchased fossil fuel options. Each synthetic and biofuel processes follow fixed product distribution as specified per input parameters, with the option of introducing user specified flexibility in product distribution as described in S5.2. Individual liquid fuels balance is enforced at the system level, assuming low cost of transportation of liquid fuels across regions.

#### Notation

Table S41. Notation of various supply chains in MACRO.

| Notation | Description |
|---|---|
| $z \in Z$ | Zone z in set of all zones in the system |
| $t \in T$ | Time step t in set of all modeled time steps |
| $p \in P$ | Index and set of power generation resource p |
| $h \in H$ | Index and set of H2 production resource h |
| $d \in D$ | Index and set of DAC resource d |
| $s \in S$ | Index and set of synthetic fuel resources s |
| $b \in B$ | Index and set of bioenergy resources b |

#### Parameters

Table S42. Input parameters of liquid fuels supply chain modeling in MACRO.

| | |
|---|---|
| **Liquid fuel demands** | |
| $d_t^G$ | Systemwide gasoline demand in MMBtu at time step t |
| $d_t^J$ | Systemwide jet fuel demand in MMBtu at time step t |
| $d_t^D$ | Systemwide diesel demand in MMBtu at time step t |
| **Synthetic fuel resources** | |
| $\eta_s^{H_2}$ | Tonne H2 per tonne $CO_2$ input to resource s |
| $\eta_s^{Elec}$ | MWh electricity per tonne $CO_2$ input to resource s |
| $\epsilon_s^{G,Syn}$ | MMBtu gasoline output per tonne $CO_2$ input from resource s |
| $\epsilon_s^{J,Syn}$ | MMBtu jet fuel output per tonne $CO_2$ input from resource s |
| $\epsilon_s^{D,Syn}$ | MMBtu diesel output per tonne $CO_2$ input from resource s |
| $\gamma_s$ | % capture of input $CO_2$ not converted to fuels in resource s |
| $\overline{\Omega_s}$ | Maximum operating factor of built capacity of resource s |

| | |
|---|---|
| $\underline{\Omega_s}$ | Minimum operating factor of built capacity of resource s |
| $c_s^{Inv}$ | Annualized investment cost of resource s ($/(tonne $CO_2$ input/h)/y) |
| $c_s^{FOM}$ | Annual fixed operation cost of resource s ($/(tonne $CO_2$ input/h)/y) |
| $c_s^{VOM}$ | Variable operation cost of resource s ($/tonne $CO_2$ input) |
| $\alpha^{G,Syn}$ | Emission factor of synthetic gasoline (tonne $CO_2$/MMBtu) |
| $\alpha^{J,Syn}$ | Emission factor of synthetic jet fuel (tonne $CO_2$/MMBtu) |
| $\alpha^{D,Syn}$ | Emission factor of synthetic diesel (tonne $CO_2$/MMBtu) |
| **Biofuel resources** | |
| $E_z^{Bio}$ | Energy content of biomass in zone z (MMBtu/tonne biomass) |
| $C_z^{Bio}$ | Carbon content of biomass in zone z (tonne biogenic $CO_2$/tonne biomass) |
| $\eta_b^{Elec}$ | MWh electricity per tonne biomass input to resource b |
| $\xi_b$ | % of biomass energy converted into biofuels |
| $f_b^{G,Bio}$ | % of gasoline in biofuel produced by resource b |
| $f_b^{J,Bio}$ | % of jet fuel in biofuel produced by resource b |
| $f_b^{D,Bio}$ | % of diesel in biofuel produced by resource b |
| $\gamma_b$ | % capture of biogenic CO2 not converted to fuels in resource b |
| $P_b$ | % of biomass energy converted into electricity by resource b |
| $\overline{\Omega_b}$ | Maximum operating factor of built capacity of resource b |
| $\underline{\Omega_b}$ | Minimum operating factor of built capacity of resource b |
| $c_b^{Inv}$ | Annualized investment cost of resource b ($/(tonne biomass/h)/y) |
| $c_b^{FOM}$ | Annual fixed operation cost of resource b ($/(tonne biomass/h)/y) |
| $c_b^{VOM}$ | Variable operation cost of resource b ($/tonne biomass) |
| $\alpha^{G,Bio}$ | Emission factor of bio gasoline (tonne $CO_2$/MMBtu) |
| $\alpha^{J,Bio}$ | Emission factor of bio jet fuel (tonne $CO_2$/MMBtu) |
| $\alpha^{D,Bio}$ | Emission factor of bio diesel (tonne $CO_2$/MMBtu) |
| **Fossil liquid fuels** | |
| $\min^{J:G,Fossil}$ | Min fraction of fossil jet fuel to fossil gasoline |
| $\max^{J:G,Fossil}$ | Max fraction of fossil jet fuel to fossil gasoline |
| $\min^{D:G,Fossil}$ | Min fraction of fossil diesel to fossil gasoline |
| $\max^{D:G,Fossil}$ | Max fraction of fossil diesel to fossil gasoline |
| $c^{G,Fossil}$ | Cost of purchasing fossil gasoline ($/MMBtu) |
| $c^{J,Fossil}$ | Cost of purchasing fossil jet fuel ($/MMBtu) |
| $c^{D,Fossil}$ | Cost of purchasing fossil diesel ($/MMBtu) |
| $\alpha^{G,Fossil}$ | Emission factor of fossil gasoline (tonne $CO_2$/MMBtu) |
| $\alpha^{J,Fossil}$ | Emission factor of fossil jet fuel (tonne $CO_2$/MMBtu) |
| $\alpha^{D,Fossil}$ | Emission factor of fossil diesel (tonne $CO_2$/MMBtu) |

### Decision Variables

Table S43. Decision variables in liquid fuels supply chain modeling in MACRO.

| | |
|---|---|
| **Synthetic fuel resources** | |
| $y_s^{CO_2,in}$ | Invested capacity of resource s (tonne $CO_2$ input/h) |
| $x_{s,t}^{CO_2,in}$ | Tonne $CO_2$ input to resource s in zone z in time step t |
| **Biofuel resources** | |
| $y_b^{Bio,in}$ | Invested capacity of b (tonne biomass input/h) |
| $x_{b,t}^{Bio,in}$ | Tonne biomass input to biofuel resource b in zone z in time step t |
| **Fossil fuel purchase** | |
| $\theta_t^{G,Fossil}$ | MMBtu fossil gasoline purchased in time step t |
| $\theta_t^{J,Fossil}$ | MMBtu fossil jet fuel purchased in time step t |
| $\theta_t^{D,Fossil}$ | MMBtu fossil diesel purchased in time step t |

### Expressions

Table S44. Model expressions in liquid fuels supply chain in MACRO.

| | |
|---|---|
| **Synthetic fuel resources** | |
| $\theta_{s,t}^{G,Syn}$ | MMBtu synthetic gasoline produced in resource s in time step t |
| $\theta_{s,t}^{J,Syn}$ | MMBtu synthetic jet fuel produced in resource s in time step t |
| $\theta_{s,t}^{D,Syn}$ | MMBtu synthetic diesel produced in resource s in time step t |
| $\theta_{s,t}^{CO2,emi}$ | $CO_2$ emitted from resource s in time step t |
| $\theta_{s,t}^{CO2,capt}$ | $CO_2$ captured by resource s in time step t |
| **Biofuel resources** | |
| $\theta_{b,t}^{G,Bio}$ | MMBtu bio gasoline produced in resource b in time step t |
| $\theta_{b,t}^{J,Bio}$ | MMBtu bio jet fuel produced in resource b in time step t |
| $\theta_{b,t}^{D,Bio}$ | MMBtu bio diesel produced in resource b in time step t |
| $\theta_{b,t}^{CO2,emi}$ | $CO_2$ emitted from resource b in time step t |
| $\theta_{b,t}^{CO2,capt}$ | $CO_2$ captured by resource b in time step t |

The following expressions represent the amount of individual synthetic and biofuel types produced by respective resources.

$$\theta_{s,t}^{G,Syn} = x_{s,t}^{CO_2,in} \cdot \epsilon_s^{G,Syn} \quad \text{(Eq. S5)}$$

$$\theta_{s,t}^{J,Syn} = x_{s,t}^{CO_2,in} \cdot \epsilon_s^{J,Syn} \quad \text{(Eq. S6)}$$

$$\theta_{s,t}^{D,Syn} = x_{s,t}^{CO_2,in} \cdot \epsilon_s^{D,Syn} \quad \text{(Eq. S7)}$$

$$\theta_{b,t}^{G,Bio} = E_z^{Bio} \cdot x_{b\in z,t}^{Bio,in} \cdot \xi_b \cdot f_b^{G,Bio} \quad \text{(Eq. S8)}$$

$$\theta_{b,t}^{J,Bio} = E_z^{Bio} \cdot x_{b\in z,t}^{Bio,in} \cdot \xi_b \cdot f_b^{J,Bio} \quad \text{(Eq. S9)}$$

$$\theta_{b,t}^{D,Bio} = E_z^{Bio} \cdot x_{b\in z,t}^{Bio,in} \cdot \xi_b \cdot f_b^{D,Bio} \quad \text{(Eq. S10)}$$

The following expressions represent the $CO_2$ emissions and $CO_2$ capture by synthetic and biofuel resources, according to the carbon capture rates of carbon not converted to fuels.

$$\theta_{s,t}^{CO2,emi} = \left(x_{s,t}^{CO2,in} - \theta_{s,t}^{G,Syn} \cdot \alpha^{G,Syn} - \theta_{s,t}^{J,Syn} \cdot \alpha^{J,Syn} - \theta_{s,t}^{D,Syn} \cdot \alpha^{D,Syn}\right) \cdot (1 - \gamma_s) \quad \text{(Eq. S11)}$$

$$\theta_{s,t}^{CO2,capt} = \left(x_{s,t}^{CO2,in} - \theta_{s,t}^{G,Syn} \cdot \alpha^{G,Syn} - \theta_{s,t}^{J,Syn} \cdot \alpha^{J,Syn} - \theta_{s,t}^{D,Syn} \cdot \alpha^{D,Syn}\right) \cdot \gamma_s \quad \text{(Eq. S12)}$$

$$\theta_{b,t}^{CO2,emi} = \left(x_{b\in z,t}^{Bio,in} \cdot C_z^{Bio} - \theta_{b,t}^{G,Bio} \cdot \alpha^{G,Bio} - \theta_{b,t}^{J,Bio} \cdot \alpha^{J,Bio} - \theta_{b,t}^{D,Bio} \cdot \alpha^{D,Bio}\right) \cdot (1 - \gamma_b) \quad \text{(Eq. S13)}$$

$$\theta_{b,t}^{CO2,capt} = \left(x_{b\in z,t}^{Bio,in} \cdot C_z^{Bio} - \theta_{b,t}^{G,Bio} \cdot \alpha^{G,Bio} - \theta_{b,t}^{J,Bio} \cdot \alpha^{J,Bio} - \theta_{b,t}^{D,Bio} \cdot \alpha^{D,Bio}\right) \cdot \gamma_b \quad \text{(Eq. S14)}$$

**Constraints**

The liquid fuels balance constraints are formulated with a “greater or equal” than demand, as having fixed product distribution in synthetic and biofuel processes might result in cases with mismatch in product-demand distribution, thus causing excess production of individual fuel types. In addition, systemwide demand for each time step is implemented to reflect the interconnectedness of the liquid fuels supply chain, with assumption of low cost of transportation of liquid fuels across regions.

**Gasoline balance**

$$\sum_{z\in Z} \theta_{z,t}^{G,Fossil} + \sum_{z\in Z}\sum_{s\in z} \theta_{s,t}^{G,Syn} + \sum_{z\in Z}\sum_{b\in z} \theta_{b,t}^{G,Bio} \geq d_t^G \quad \text{(Eq. S15)}$$

**Jet fuel balance**

$$\sum_{z\in Z} \theta_{z,t}^{J,Fossil} + \sum_{z\in Z}\sum_{s\in z} \theta_{s,t}^{J,Syn} + \sum_{z\in Z}\sum_{b\in z} \theta_{b,t}^{J,Bio} \geq d_t^J \quad \text{(Eq. S16)}$$

**Diesel balance**

$$\sum_{z\in Z} \theta_{z,t}^{D,Fossil} + \sum_{z\in Z}\sum_{s\in z} \theta_{s,t}^{D,Syn} + \sum_{z\in Z}\sum_{b\in z} \theta_{b,t}^{D,Bio} \geq d_t^D \quad \text{(Eq. S17)}$$

**Fossil fuels ratio bounds**

Enforcing constraints on ratio bounds between fossil fuels allow users to represent a realistic distribution of fossil fuels produced from oil refineries, instead of allowing the model to purchase fossil liquid fuels in any distribution ratios (i.e. all fossil liquids purchased in the form of jet fuel if fossil jet fuel is the cheapest among all fossil fuels). This reflects the realistic operation of oil refineries where there is a range of distribution of various fossil fuel types. In this study, historical distribution bounds were used based on data from EIA[30] (Refer to Table S32).

$$\min^{J:G,Fossil} \cdot \theta_{z,t}^{G,Fossil} \leq \theta_{z,t}^{J,Fossil} \leq \max^{J:G,Fossil} \cdot \theta_{z,t}^{G,Fossil} \quad \text{(Eq. S18)}$$

$$\min^{D:G,Fossil} \cdot \theta_{z,t}^{G,Fossil} \leq \theta_{z,t}^{D,Fossil} \leq \max^{D:G,Fossil} \cdot \theta_{z,t}^{G,Fossil} \quad \text{(Eq. S19)}$$

**Operation constraints**

The hourly operation of each synthetic and biofuel resources is constrained to maximum and minimum operating factors of their built capacities.

$$y_s^{CO_2,in} \cdot \underline{\Omega_s} \leq x_{s,t}^{CO_2,in} \leq y_s^{CO_2,in} \cdot \overline{\Omega_s} \quad \text{(Eq. S20)}$$

$$y_b^{Bio,in} \cdot \underline{\Omega_b} \leq x_{b,t}^{Bio,in} \leq y_b^{Bio,in} \cdot \overline{\Omega_b} \quad \text{(Eq. S21)}$$

**Contribution to power balance**

The following terms are the total electricity consumption of synthetic and biofuel resources, and excess electricity produced by biofuel resources (if applicable) of each zone z, which are accounted to their respective regional power balance.

$$\text{Power Balance}_z -= \sum_{s \in z} x_{s,t}^{CO_2,in} \cdot \eta_s^{Elec} + \sum_{b \in z} x_{b,t}^{Bio,in} \cdot \eta_b^{Elec} - \sum_{b \in z} x_{b,t}^{Bio,in} \cdot E_z^{Bio} \cdot P_b \quad \text{(Eq. S22)}$$

**Contribution to H2 balance**

The following terms are the total H2 consumption of each zone, which are deducted from respective regional H2 balance.

$$H_2 \text{ Balance}_z -= \sum_{s \in z} x_{s,t}^{CO_2,in} \cdot \eta_s^{H_2} \quad \text{(Eq. S23)}$$

**Addition to objective function**

The following terms representing the total cost (investment, fixed operating costs, and variable operating costs of synthetic and biofuel resources, as well as purchase costs of fossil liquid fuels) of the liquid fuels supply chain are added to the overall objective function (Obj). $\omega_t$ is the time weight of each modeled time step that sums up to 8760 hours when representative periods are used in the model instead of modeling an entire full year for computational tractability.

$$\begin{aligned} \text{Obj} += & \sum_{z \in Z} \sum_{s \in z} y_s^{CO_2,in} \cdot (c_s^{Inv} + c_s^{FOM}) + \sum_{z \in Z} \sum_{b \in z} y_b^{Bio,in} \cdot (c_b^{Inv} + c_b^{FOM}) + \sum_{z \in Z} \sum_{t \in T} \sum_{s \in z} \omega_t \cdot x_{s,t}^{CO_2,in} \cdot c_s^{VOM} \\ & + \sum_{z \in Z} \sum_{t \in T} \sum_{b \in z} \omega_t \cdot x_{b,t}^{Bio,in} \cdot c_b^{VOM} + \sum_{t \in T} c^{G,Fossil} \theta_t^{G,Fossil} + \sum_{t \in T} c^{J,Fossil} \theta_t^{J,Fossil} \\ & + \sum_{t \in T} c^{D,Fossil} \theta_t^{D,Fossil} \end{aligned} \quad \text{(Eq. S24)}$$

## S5.2 Modeling flexibility in synthetic and biofuels production in MACRO

MACRO allows the choice of operating synthetic and biofuel resources with flexibility in fuel product distribution, instead of following strictly the specified product distribution of processes. This is done by producing a certain percentage of originally produced liquid fuel type (gasoline, jet fuel, diesel) as another type, with the assumption that all costs and energy requirement remains the same. This gives the model

flexibility to produce individual synthetic and biofuel types according to the optimal distribution of gasoline, jet fuel and diesel instead of adhering to specified fixed product distributions.

These parameters and variables are only activated when synthetic and biofuels production are chosen by the user to operate flexibly.

**Parameters**

Table S45. Parameters for flexible synthetic and biofuels production in MACRO.

| **Synthetic fuel resources** | |
|---|---|
| $\max^{G\to J,Syn}$ | Max % of original gasoline produced as jet fuel in resource s in time step t |
| $\max^{G\to D,Syn}$ | Max % of original gasoline produced as diesel in resource s in time step t |
| $\max^{J\to G,Syn}$ | Max % of original jet fuel produced as gasoline in resource s in time step t |
| $\max^{J\to D,Syn}$ | Max % of original jet fuel produced as diesel in resource s in time step t |
| $\max^{D\to G,Syn}$ | Max % of original diesel produced as gasoline in s in time step t |
| $\max^{D\to J,Syn}$ | Max % of original diesel produced as jet fuel in s in time step t |
| **Biofuel resources** | |
| $\max^{G\to J,Bio}$ | Max % of original gasoline produced as jet fuel in resource b in time step t |
| $\max^{G\to D,Bio}$ | Max % of original gasoline produced as diesel in resource b in time step t |
| $\max^{J\to G,Bio}$ | Max % of original jet fuel produced as gasoline in resource b in time step t |
| $\max^{J\to D,Bio}$ | Max % of original jet fuel produced as diesel in resource b in time step t |
| $\max^{D\to G,Bio}$ | Max % of original diesel produced as gasoline in resource b in time step t |
| $\max^{D\to J,Bio}$ | Max % of original diesel produced as jet fuel in resource b in time step t |

**Variables**

Table S46. Variables for flexible synthetic and biofuels production in MACRO.

| **Synthetic fuel resources** | |
|---|---|
| $\theta_{s,t}^{G\to J,Syn}$ | MMBtu original gasoline produced as jet fuel in resource s in time step t |
| $\theta_{s,t}^{G\to D,Syn}$ | MMBtu original gasoline produced as diesel in resource s in time step t |
| $\theta_{s,t}^{J\to G,Syn}$ | MMBtu original jet fuel produced as gasoline in resource s in time step t |
| $\theta_{s,t}^{J\to D,Syn}$ | MMBtu original jet fuel produced as diesel in resource s in time step t |
| $\theta_{s,t}^{D\to G,Syn}$ | MMBtu original diesel produced as gasoline in resource s in time step t |
| $\theta_{s,t}^{D\to J,Syn}$ | MMBtu original diesel produced as jet fuel in resource s in time step t |
| **Biofuel resources** | |
| $\theta_{b,t}^{G\to J,Bio}$ | MMBtu original gasoline produced as jet fuel in resource b in time step t |
| $\theta_{b,t}^{G\to D,Bio}$ | MMBtu original gasoline produced as diesel in resource b in time step t |
| $\theta_{b,t}^{J\to G,Bio}$ | MMBtu original jet fuel produced as gasoline in resource b in time step t |
| $\theta_{b,t}^{J\to D,Bio}$ | MMBtu original jet fuel produced as diesel in resource b in time step t |
| $\theta_{b,t}^{D\to G,Bio}$ | MMBtu original diesel produced as gasoline in resource b in time step t |
| $\theta_{b,t}^{D\to J,Bio}$ | MMBtu original diesel produced as jet fuel in resource b in time step t |

**Expressions**

The expressions representing the amount of individual synthetic and biofuel types produced by respective resources are thus modified to account for flexibility in liquid fuels production.

$$\theta_{s,t}^{G,Syn} = x_{s,t}^{CO_2,in} \cdot \epsilon_s^{G,Syn} - \theta_{s,t}^{G\to J,Syn} - \theta_{s,t}^{G\to D,Syn} + \theta_{s,t}^{J\to G,Syn} + \theta_{s,t}^{D\to G,Syn} \quad \text{(Eq. S25)}$$

$$\theta_{s,t}^{J,Syn} = x_{s,t}^{CO_2,in} \cdot \epsilon_s^{J,Syn} - \theta_{s,t}^{J\to G,Syn} - \theta_{s,t}^{J\to D,Syn} + \theta_{s,t}^{G\to J,Syn} + \theta_{s,t}^{D\to J,Syn} \quad \text{(Eq. S26)}$$

$$\theta_{s,t}^{D,Syn} = x_{s,t}^{CO_2,in} \cdot \epsilon_s^{D,Syn} - \theta_{s,t}^{D\to G,Syn} - \theta_{s,t}^{D\to J,Syn} + \theta_{s,t}^{G\to D,Syn} + \theta_{s,t}^{J\to D,Syn} \quad \text{(Eq. S27)}$$

$$\theta_{b,t}^{G,Bio} = E_z^{Bio} \cdot x_{b,t}^{Bio,in} \cdot \xi_b \cdot f_b^{G,Bio} - \theta_{b,t}^{G\to J,Bio} - \theta_{b,t}^{G\to D,Bio} + \theta_{b,t}^{J\to G,Bio} + \theta_{b,t}^{D\to G,Bio} \quad \text{(Eq. S28)}$$

$$\theta_{b,t}^{J,Bio} = E_z^{Bio} \cdot x_{b,t}^{Bio,in} \cdot \xi_b \cdot f_b^{J,Bio} - \theta_{b,t}^{J\to G,Bio} - \theta_{b,t}^{J\to D,Bio} + \theta_{b,t}^{G\to J,Bio} + \theta_{b,t}^{D\to J,Bio} \quad \text{(Eq. S29)}$$

$$\theta_{b,t}^{D,Bio} = E_z^{Bio} \cdot x_{b,t}^{Bio,in} \cdot \xi_b \cdot f_b^{D,Bio} - \theta_{b,t}^{D\to G,Bio} - \theta_{b,t}^{D\to J,Bio} + \theta_{b,t}^{G\to D,Bio} + \theta_{b,t}^{J\to D,Bio} \quad \text{(Eq. S30)}$$

**Constraints**

These constraints control the flexibility in liquid fuel production by synthetic or biofuel technologies according to specified maximum fraction of originally produced fuel types.

$$\theta_{s,t}^{G\to J,Syn} \le max^{G\to J,Syn} \cdot x_{s,t}^{CO_2,in} \cdot \epsilon_s^{G,Syn} \quad \text{(Eq. S31)}$$

$$\theta_{s,t}^{G\to D,Syn} \le max^{G\to D,Syn} \cdot x_{s,t}^{CO_2,in} \cdot \epsilon_s^{G,Syn} \quad \text{(Eq. S32)}$$

$$\theta_{s,t}^{J\to G,Syn} \le max^{J\to G,Syn} \cdot x_{s,t}^{CO_2,in} \cdot \epsilon_s^{J,Syn} \quad \text{(Eq. S33)}$$

$$\theta_{s,t}^{J\to D,Syn} \le max^{J\to D,Syn} \cdot x_{s,t}^{CO_2,in} \cdot \epsilon_s^{J,Syn} \quad \text{(Eq. S34)}$$

$$\theta_{s,t}^{D\to G,Syn} \le max^{D\to G,Syn} \cdot x_{s,t}^{CO_2,in} \cdot \epsilon_s^{D,Syn} \quad \text{(Eq. S35)}$$

$$\theta_{s,t}^{D\to J,Syn} \le max^{D\to J,Syn} \cdot x_{s,t}^{CO_2,in} \cdot \epsilon_s^{D,Syn} \quad \text{(Eq. S36)}$$

$$\theta_{b,t}^{G\to J,Bio} \le max^{G\to J,Bio} \cdot E_z^{Bio} \cdot x_{b,t}^{Bio,in} \cdot \xi_b \cdot f_b^{G,Bio} \quad \text{(Eq. S37)}$$

$$\theta_{b,t}^{G\to D,Bio} \le max^{G\to D,Bio} \cdot E_z^{Bio} \cdot x_{b,t}^{Bio,in} \cdot \xi_b \cdot f_b^{G,Bio} \quad \text{(Eq. S38)}$$

$$\theta_{b,t}^{J\to G,Bio} \le max^{J\to G,Bio} \cdot E_z^{Bio} \cdot x_{b,t}^{Bio,in} \cdot \xi_b \cdot f_b^{J,Bio} \quad \text{(Eq. S39)}$$

$$\theta_{b,t}^{J\to D,Bio} \le max^{J\to D,Bio} \cdot E_z^{Bio} \cdot x_{b,t}^{Bio,in} \cdot \xi_b \cdot f_b^{J,Bio} \quad \text{(Eq. S40)}$$

$$\theta_{b,t}^{D\to G,Bio} \le max^{D\to G,Bio} \cdot E_z^{Bio} \cdot x_{b,t}^{Bio,in} \cdot \xi_b \cdot f_b^{D,Bio} \quad \text{(Eq. S41)}$$

$$\theta_{b,t}^{D\to J,Bio} \le max^{D\to J,Bio} \cdot E_z^{Bio} \cdot x_{b,t}^{Bio,in} \cdot \xi_b \cdot f_b^{D,Bio} \quad \text{(Eq. S42)}$$

The following constraints control the flexibility in liquid fuel production such that it does not exceed total amount of original production of liquid fuel types.

$$\theta_{s,t}^{G\to J,Syn} + \theta_{s,t}^{G\to D,Syn} \le x_{s,t}^{CO_2,in} \cdot \epsilon_s^{G,Syn} \quad \text{(Eq. S43)}$$

$$\theta_{s,t}^{J\to G,Syn} + \theta_{s,t}^{J\to D,Syn} \le x_{s,t}^{CO_2,in} \cdot \epsilon_s^{J,Syn} \quad \text{(Eq. S44)}$$

$$\theta_{s,t}^{D\to G,Syn} + \theta_{s,t}^{D\to J,Syn} \le x_{s,t}^{CO_2,in} \cdot \epsilon_s^{D,Syn} \quad \text{(Eq. S45)}$$

$$\theta_{b,t}^{G\to J,Bio} + \theta_{b,t}^{G\to D,Bio} \le E_z^{Bio} \cdot x_{b,t}^{Bio,in} \cdot \xi_b \cdot f_b^{G,Bio} \quad \text{(Eq. S46)}$$

$$\theta_{b,t}^{J\to G,Bio} + \theta_{b,t}^{J\to D,Bio} \le E_z^{Bio} \cdot x_{b,t}^{Bio,in} \cdot \xi_b \cdot f_b^{J,Bio} \quad \text{(Eq. S47)}$$

$$\theta_{b,t}^{D\to G,Bio} + \theta_{b,t}^{D\to J,Bio} \le E_z^{Bio} \cdot x_{b,t}^{Bio,in} \cdot \xi_b \cdot f_b^{D,Bio} \quad \text{(Eq. S48)}$$

### S5.3 Natural gas supply chains modeling in MACRO

The natural gas (NG) supply chain in MACRO is modeled in a similar way to the liquid fuels supply chain in S5.1 such that NG can be produced by synthetic and bio processes, as well as purchased fossil natural gas options. One key difference between synthetic and bio-NG technologies compared to their liquid fuels counterparts is that only one product of NG is produced. Similarly, regional electricity and $H_2$ balance are modified to account for the consumption of these commodities in the natural gas supply chain.

#### Constraints

Apart from the NG balance constraint, the operational constraints are similar to that of synthetic and bio liquid fuels production, and NG production does not have any product flexibility since there is only one product.

#### NG balance

The NG balance constraints are formulated as regional demand for each time step, as the prices of fossil NG in each region already include any NG transportation costs from sources to respective regions. The NG balance consists of purchased fossil NG, synthetic and bio-NG produced by respective technologies, NG consumed by the power and $H_2$ sectors, and NG utilized in direct air capture (DAC) as a fuel, that must be equal to the NG demand in each region.

$$\theta_{z,t}^{NG,Fossil} + \sum_{s\in z} \theta_{s,t}^{NG,Syn} + \sum_{b\in z} \theta_{b,t}^{NG,Bio} - \sum_{p\in P} \theta_{p,t}^{NG,Power} - \sum_{h\in H} \theta_{h,t}^{NG,H_2} - \sum_{d\in D} \theta_{d,t}^{NG,DAC} = d_{z,t}^{NG} \quad \text{(Eq. S49)}$$

### S5.4 Captured $CO_2$ balance constraint in MACRO

Captured $CO_2$ terms from the liquid fuels and natural gas supply chains are added to the existing captured $CO_2$ balance constraint in MACRO.

#### Expressions

Table S47. Expressions for existing sectors in $CO_2$ balance constraint in MACRO.

| **Captured $CO_2$ balance** | |
|---|---|
| $\theta_{d,t}^{CO_2,DAC,atm}$ | Tonne atmospheric $CO_2$ captured by DAC from resource d in time step t |
| $\theta_{d,t}^{CO_2,DAC\ fuel,capt}$ | Tonne $CO_2$ captured from DAC fuel combustion from resource d in time step t |
| $\theta_{p,t}^{CO_2,capt}$ | Tonne $CO_2$ captured by power generation resource p in time step t |

| | |
|---|---|
| $\theta_{h,t}^{CO_2,capt}$ | Tonne $CO_2$ captured by $H_2$ generation resource h in time step t |
| $\theta_{z,t}^{CO_2,export}$ | Tonne $CO_2$ exported by pipelines from zone z in time step t |
| $\theta_{z,t}^{CO_2,seq}$ | Tonne $CO_2$ sequestered in zone z in time step t |

The captured $CO_2$ balance accounts for the capture, utilization, export, and sequestration of all captured $CO_2$ by technologies with $CO_2$ capture in each region. These technologies include NG-based power and $H_2$ generation with $CO_2$ capture, synthetic and biofuel technologies, as well as atmospheric $CO_2$ and capture of combustion emissions from fuel utilization in DAC technologies.

$$\sum_{h\in z}\theta_{h,t}^{CO_2,capt}+\sum_{p\in z}\theta_{p,t}^{CO_2,capt}+\sum_{s\in z}\theta_{s,t}^{CO_2,capt}+\sum_{b\in z}\theta_{b,t}^{CO_2,capt}+\sum_{d\in z}\left(\theta_{d,t}^{CO_2,DAC,atm}+\theta_{d,t}^{CO_2,DAC\ fuel,capt}\right)-\sum_{s\in z}x_{s,t}^{CO_2,in}-\theta_{z,t}^{CO_2,export}=\theta_{z,t}^{CO_2,seq} \quad (Eq.\ S50)$$

## S5.5 $CO_2$ emission policy constraint

$CO_2$ emission terms from the liquid fuels and natural gas supply chains have to be added to the existing $CO_2$ emission policy constraint in MACRO. This constraint accounts for emissions from all sectors across all regions and time steps, including emissions from fossil fuel power and $H_2$ production, uncaptured $CO_2$ from DAC fuel combustion, all liquid and gaseous fuels combustion, as well as negative emissions from biogenic $CO_2$ intake and DAC atmospheric capture, which have to be lesser than the system $CO_2$ emission cap.

### Expressions

Table S48. Expressions for $CO_2$ emission policy constraint in MACRO.

| **$CO_2$ emissions** | |
|---|---|
| $\theta_{p,t}^{CO_2,emi}$ | Tonne $CO_2$ emitted by power generation resource p in time step t |
| $\theta_{h,t}^{CO_2,emi}$ | Tonne $CO_2$ emitted by $H_2$ generation resource h in time step t |
| $\theta_{d,t}^{CO_2,DAC\ fuel,emi}$ | Tonne $CO_2$ emitted from DAC fuel combustion from resource d in time step t |

$$\omega\cdot\sum_{t\in T}\left(\sum_{p\in P}\theta_{p,t}^{CO_2,emi}+\sum_{h\in H}\theta_{h,t}^{CO_2,emi}+\sum_{s\in S}\theta_{s,t}^{CO_2,emi}+\sum_{b\in B}\theta_{b,t}^{CO_2,emi}+\sum_{d\in D}\theta_{d,t}^{CO_2,DAC\ fuel,emi}+\theta_t^{G,Fossil}\cdot\alpha^{G,Fossil}+\theta_t^{J,Fossil}\cdot\alpha^{J,Fossil}+\theta_t^{D,Fossil}\cdot\alpha^{D,Fossil}+\theta_t^{NG,Fossil}\cdot\alpha^{NG,Fossil}+\sum_{s\in S}\left(\theta_{s,t}^{G,Syn}\cdot\alpha^{G,Syn}+\theta_{s,t}^{J,Syn}\cdot\alpha^{J,Syn}+\theta_{s,t}^{D,Syn}\cdot\alpha^{D,Syn}+\theta_{s,t}^{NG,Syn}\cdot\alpha^{NG,Syn}\right)+\sum_{b\in B}\left(\theta_{b,t}^{G,Bio}\cdot\alpha^{G,Bio}+\theta_{b,t}^{J,Bio}\cdot\alpha^{J,Bio}+\theta_{b,t}^{D,Bio}\cdot\alpha^{D,Bio}+\theta_{b,t}^{NG,Bio}\cdot\alpha^{NG,Bio}\right)-\sum_{d\in D}\theta_{d,t}^{CO_2,DAC,atm}-\sum_{b\in B}\sum_{b\in z}C_z^{Bio}x_{b,t}^{Bio,in}\right)\leq CO_2\ Cap \quad (Eq.\ S51)$$

## S6. Model implementation details

The MACRO model used in this study is formulated as a linear program (LP). Across the case studies, each instance has a problem size of approximately 2,300,000 constraints and 1,400,000 continuous decision variables for scenarios with "IA-PF" and "IA-FF" modeling assumptions, and approximately 3,350,000 constraints and 2,100,000 continuous decision variables for "FA-PF" and "FA-FF" modeling assumptions. The implementation uses Julia 1.10 and JuMP 1.20, and we solve the instances with Gurobi 10.0 on 8 CPU cores on MIT SuperCloud [42]. Typical runtimes per instance are 78–93 minutes for scenarios with "IA-PF" and "IA-FF" modeling assumptions, and 124–286 minutes for "FA-PF" and "FA-FF" modeling assumptions. The codebase for this analysis is available in the MACRO GitHub repository on the "MACRO-Liquid-Fuels-Net-Zero" branch [20].

## S7. References


[1] S. Hughes, A. Zoelle, M. Woods, S. Henry, S. Homsy, S. Pidaparti, N. Kuehn, H. Hoffman, K. Forrest, A. Sheriff, T. Fout, W. Summers, and S. Herron, "Cost of Capturing CO2 from Industrial Sources," DOE/NETL-2022/3319, 1887586, Jul. 2022. doi: 10.2172/1887586.

[2] T. Schmitt, S. Leptinsky, M. Turner, A. Zoelle, C. W. White, S. Hughes, S. Homsy, M. Woods, H. Hoffman, T. Shultz, and R. E. James III, "Cost and Performance Baseline for Fossil Energy Plants Volume 1: Bituminous Coal and Natural Gas to Electricity," National Energy Technology Laboratory (NETL), Pittsburgh, PA, Morgantown, WV, and Albany, OR (United States), DOE/NETL-2023/4320, Oct. 2022. doi: 10.2172/1893822.

[3] M. Wang, A. Elgowainy, U. Lee, K. Baek, S. Balchandani, P. Benavides, A. Burnham, H. Cai, P. Chen, Y. Gan, U. Gracida-Alvarez, T. Hawkins, T.-Y. Huang, R. Iyer, S. Kar, J. Kelly, T. Kim, C. Kolodziej, K. Lee, X. Liu, Z. Lu, F. Masum, M. Morales, C. Ng, L. Ou, T. Poddar, K. Reddi, S. Shukla, U. Singh, L. Sun, P. Sun, P. Vyawahare, and J. Zhang, "Summary of Expansions and Updates in R&D GREET® 2023," ANL/ESIA--23/10, 2278803, 185721, Dec. 2023. doi: 10.2172/2278803.

[4] E. Larson, C. Greig, J. Jenkins, E. Mayfield, A. Pascale, C. Zhang, J. Drossman, R. Williams, S. Pacala, R. Socolow, E. Baik, R. Birdsey, R. Duke, R. Jones, B. Haley, E. Leslie, K. Paustian, and A. Swan, "Net-Zero America: Potential Pathways, Infrastructure, and Impacts," Princeton University, Princeton, NJ, Oct. 2021.

[5] J. W. Law, B. K. Mignone, and D. S. Mallapragada, "Role of Technology Flexibility and Grid Coupling on Hydrogen Deployment in Net-Zero Energy Systems," *Environ. Sci. Technol.*, vol. 59, no. 10, pp. 4974–4988, Mar. 2025, doi: 10.1021/acs.est.4c12166.

[6] B. Mirletz, L. Vimmerstedt, T. Stehly, D. Stright, S. Cohen, W. Cole, P. Duffy, D. Feldman, P. Kurup, V. Ramasamy, J. Zuboy, G. Oladosu, J. Hoffmann, A. Eberle, O. Roberts, D. Mulas Hernando, G. Avery, E. Rosenlieb, A. Schleifer, D. Akindipe, E. Witter, B. Fuchs, G. Zuckerman, A. Zolan, A. Abou Jaoude, L. Larson, C. Lohse, N. Guaita, I. Trivedi, F. Joseck, T. Hedalen, B. Rakov, and A. Sekar, "2024 Annual Technology Baseline (ATB) Cost and Performance Data for Electricity Generation Technologies." DOE Open Energy Data Initiative (OEDI); National Renewable Energy Laboratory (NREL), p. 9 files, 2024. doi: 10.25984/2377191.

[7] U.S. EPA, "Documentation for EPA's Power Sec- tor Modeling Platform v6 Using the Integrated Planning Model," EPA, Washington, D.C., 2018.

[8] A. Venkatesh, K. Jordan, A. Sinha, J. Johnson, and P. Jaramillo, "An Open Energy Outlook: Decarbonization Pathways for the USA," Carnegie Mellon University & North Carolina State University, 2022.

[9] IEA, "The Future of Hydrogen," IEA, Paris, 2019. [Online]. Available: https://www.iea.org/reports/the-future-of-hydrogen

[10] E. Lewis, S. McNaul, M. Jamieson, M. Henriksen, H. Matthews, L. Walsh, J. Grove, T. Shultz, T. Skone, and R. Stevens, "Comparison of Commercial, State-of-the-Art, Fossil-Based Hydrogen Production Technologies," DOE/NETL-2022/3241, 1862910, Apr. 2022. Accessed: Jun. 11, 2024. [Online]. Available: https://www.osti.gov/servlets/purl/1862910/

[11] D. D. Papadias and R. K. Ahluwalia, "Bulk storage of hydrogen," *International Journal of Hydrogen Energy*, vol. 46, no. 70, pp. 34527–34541, Oct. 2021, doi: 10.1016/j.ijhydene.2021.08.028.

[12] P. Spath, A. Aden, T. Eggeman, M. Ringer, B. Wallace, and J. Jechura, “Biomass to Hydrogen Production Detailed Design and Economics Utilizing the Battelle Columbus Laboratory Indirectly-Heated Gasifier,” NREL/TP-510-37408, 15016221, May 2005. doi: 10.2172/15016221.
[13] G. Schivley, E. Welty, N. Patankar, A. Jacobson, Q. Xu, Aneesha Manocha, B. Pecora, R. Bhandarkar, and J. D. Jenkins, *PowerGenome/PowerGenome: v0.6.1*. (Sep. 08, 2023). Zenodo. doi: 10.5281/ZENODO.8329515.
[14] ReEDS Modeling and Analysis Team, J. Ho, J. Becker, M. Brown, P. Brown, I. Chernyakhovskiy, S. Cohen, W. Cole, S. Corcoran, K. Eurek, W. Frazier, P. Gagnon, N. Gates, D. Greer, P. Jadun, S. Khanal, S. Machen, M. Macmillan, T. Mai, M. Mowers, C. Murphy, A. Rose, A. Schleifer, B. Sergi, D. Steinberg, Y. Sun, and E. Zhou, “Regional Energy Deployment System (ReEDS) Model Documentation (Version 2020),” NREL/TP-6A20-78195, 1788425, MainId:32104, Jun. 2021. doi: 10.2172/1788425.
[15] The White House, “Inflation Reduction Act Guidebook - Clean Energy,” 2022. [Online]. Available: https://bidenwhitehouse.archives.gov/cleanenergy/inflation-reduction-act-guidebook/
[16] U.S. EIA, “Annual Energy Outlook 2021,” 2021.
[17] N. A. Sepulveda, J. D. Jenkins, F. J. De Sisternes, and R. K. Lester, “The Role of Firm Low-Carbon Electricity Resources in Deep Decarbonization of Power Generation,” *Joule*, vol. 2, no. 11, pp. 2403–2420, Nov. 2018, doi: 10.1016/j.joule.2018.08.006.
[18] J. D. Jenkins, Z. Zhou, R. Ponciroli, R. B. Vilim, F. Ganda, F. De Sisternes, and A. Botterud, “The benefits of nuclear flexibility in power system operations with renewable energy,” *Applied Energy*, vol. 222, pp. 872–884, Jul. 2018, doi: 10.1016/j.apenergy.2018.03.002.
[19] MIT Energy Initiative, “The Future of Energy Storage,” MITEI, Cambridge, MA, 2022.
[20] G. He, D. S. Mallapragada, R. Macdonald, J. W. Law, Y. Shaker, Y. Zhang, and A. Cybulsky, *DOLPHYN: Decision Optimization for Low-Carbon Power and Hydrogen Networks*. (2024). [Online]. Available: https://github.com/macroenergy/Dolphyn.jl
[21] M. Mintz, J. Gillette, A. Elgowainy, M. Paster, M. Ringer, D. Brown, and J. Li, “Hydrogen Delivery Scenario Analysis Model for Hydrogen Distribution Options,” *Transportation Research Record*, vol. 1983, no. 1, pp. 114–120, Jan. 2006, doi: 10.1177/0361198106198300116.
[22] M. Sengupta, Y. Xie, A. Lopez, A. Habte, G. Maclaurin, and J. Shelby, “The National Solar Radiation Data Base (NSRDB),” *Renewable and Sustainable Energy Reviews*, vol. 89, pp. 51–60, Jun. 2018, doi: 10.1016/j.rser.2018.03.003.
[23] C. Draxl, A. Clifton, B.-M. Hodge, and J. McCaa, “The Wind Integration National Dataset (WIND) Toolkit,” *Applied Energy*, vol. 151, pp. 355–366, Aug. 2015, doi: 10.1016/j.apenergy.2015.03.121.
[24] P. Brown, *ZEPHYR*. (2022). [Online]. Available: https://github.com/patrickbrown4/zephyr
[25] P. R. Brown and A. Botterud, “The Value of Inter-Regional Coordination and Transmission in Decarbonizing the US Electricity System,” *Joule*, vol. 5, no. 1, pp. 115–134, Jan. 2021, doi: 10.1016/j.joule.2020.11.013.
[26] J. Valentine, A. Zoelle, S. Homsy, H. Mantripragada, A. Kilstofte, M. Sturdivan, M. Steutermann, and T. Fout, “Direct Air Capture Case Studies: Solvent System,” DOE/NETL-2021/2864, 1893369, Aug. 2022. doi: 10.2172/1893369.
[27] J. Valentine, A. Zoelle, S. Homsy, H. Mantripragada, M. Woods, N. Roy, A. Kilstofte, M. Sturdivan, M. Steutermann, and T. Fout, “Direct Air Capture Case Studies: Sorbent System,” DOE/NETL-2021/2865, 1879535, Jul. 2022. doi: 10.2172/1879535.
[28] Committee on Developing a Research Agenda for Carbon Dioxide Removal and Reliable Sequestration, Board on Atmospheric Sciences and Climate, Board on Energy and Environmental Systems, Board on Agriculture and Natural Resources, Board on Earth Sciences and Resources, Board on Chemical Sciences and Technology, Ocean Studies Board, Division on Earth and Life Studies, and National Academies of Sciences, Engineering, and Medicine, *Negative Emissions Technologies and Reliable Sequestration: A Research Agenda*. Washington, D.C.: National Academies Press, 2019, p. 25259. doi: 10.17226/25259.
[29] U.S. EIA, “Annual Energy Outlook 2023,” 2023.
[30] U.S. EIA, “Petroleum & Other Liquids, Refinery Yield,” 2025. [Online]. Available: https://www.eia.gov/dnav/pet/pet_pnp_pct_dc_nus_pct_m.htm
[31] G. Zang, P. Sun, A. A. Elgowainy, A. Bafana, and M. Wang, “Performance and cost analysis of liquid fuel production from H2 and CO2 based on the Fischer-Tropsch process,” *Journal of CO2 Utilization*, vol. 46, p. 101459, Apr. 2021, doi: 10.1016/j.jcou.2021.101459.

[32] K. Harris, C. Nash, D. Ruddy, A. Dutta, D. Dupuis, E. Christensen, A. Rein, E. Tan, D. Hartley, H. Cai, and L. Ou, “High-Octane Gasoline from Lignocellulosic Biomass via Syngas and Methanol/Dimethyl Ether Intermediates (2021 State of Technology),” NREL/TP-5100-81178, 1842283, MainId:80953, Jan. 2022. doi: 10.2172/1842283.
[33] T. G. Kreutz, E. D. Larson, C. Elsido, E. Martelli, C. Greig, and R. H. Williams, “Techno-economic prospects for producing Fischer-Tropsch jet fuel and electricity from lignite and woody biomass with CO2 capture for EOR,” *Applied Energy*, vol. 279, p. 115841, Dec. 2020, doi: 10.1016/j.apenergy.2020.115841.
[34] I. Dimitriou, H. Goldingay, and A. V. Bridgwater, “Techno-economic and uncertainty analysis of Biomass to Liquid (BTL) systems for transport fuel production,” *Renewable and Sustainable Energy Reviews*, vol. 88, pp. 160–175, May 2018, doi: 10.1016/j.rser.2018.02.023.
[35] A. Kiani, M. Lejeune, C. Li, J. Patel, and P. Feron, “Liquefied synthetic methane from ambient CO2 and renewable H2 - A technoeconomic study,” *Journal of Natural Gas Science and Engineering*, vol. 94, p. 104079, Oct. 2021, doi: 10.1016/j.jngse.2021.104079.
[36] S. Michailos, O. Emenike, D. Ingham, K. J. Hughes, and M. Pourkashanian, “Methane production via syngas fermentation within the bio-CCS concept: A techno-economic assessment,” *Biochemical Engineering Journal*, vol. 150, p. 107290, Oct. 2019, doi: 10.1016/j.bej.2019.107290.
[37] M. Langholtz, “2023 Billion-Ton Report.” Oak Ridge National Laboratory (ORNL), Oak Ridge, TN (United States), Bioenergy Knowledge Discovery Framework (BEKDF); Oak Ridge National Laboratory (ORNL), Oak Ridge, TN (United States), Bioenergy Knowledge Discovery Framework (BEKDF), 2024. doi: 10.23720/BT2023/2316165.
[38] R. Emerson, A. Hoover, M. Cortez, and R. Kinoshita, “Bioenergy Feedstock Library 2023 Annual Summary Report,” INL/RPT--23-75339-Rev000, 2204843, Oct. 2023. doi: 10.2172/2204843.
[39] Y. Tao, W. Feng, Z. He, B. Wang, F. Yang, A. I. Nafsun, and Y. Zhang, “Utilization of cotton byproduct-derived biochar: a review on soil remediation and carbon sequestration,” *Environ Sci Eur*, vol. 36, no. 1, p. 79, Apr. 2024, doi: 10.1186/s12302-024-00908-7.
[40] V. B. Subramani, L. Atanda, W. O. S. Doherty, D. Rackemann, and L. Moghaddam, “Co-liquefaction of cotton gin trash and low-density polyethylene wastes via supercritical ethanolysis for hydrocarbon-rich oil,” *Energy Conversion and Management*, vol. 290, p. 117216, Aug. 2023, doi: 10.1016/j.enconman.2023.117216.
[41] H. AboDalam, V. Devra, F. K. Ahmed, B. Li, and K. A. Abd-Elsalam, “Rice wastes for green production and sustainable nanomaterials: An overview,” in *Agri-Waste and Microbes for Production of Sustainable Nanomaterials*, Elsevier, 2022, pp. 707–728. doi: 10.1016/B978-0-12-823575-1.00009-3.
[42] A. Reuther, J. Kepner, C. Byun, S. Samsi, W. Arcand, D. Bestor, B. Bergeron, V. Gadepally, M. Houle, M. Hubbell, M. Jones, A. Klein, L. Milechin, J. Mullen, A. Prout, A. Rosa, C. Yee, and P. Michaleas, “Interactive Supercomputing on 40,000 Cores for Machine Learning and Data Analysis,” in *2018 IEEE High Performance extreme Computing Conference (HPEC)*, Sep. 2018, pp. 1–6. doi: 10.1109/HPEC.2018.8547629.